SOME ASPECTS OF CHARGE TRANSPORT IN ORGANIC SEMICONDUCTORS: MOTION OF A BIPOLARON IN HETEROCYCLIC POLYMERS AND CHARGE MOBILITY IN CONJUGATED POLYMERS WITH APPLICATIONS TO SOLAR CELLS

YAPING LI

Some Aspects of Charge Transport in Organic Semiconductors: Motion of a Bipolaron in Heterocyclic Polymers and Charge Mobility in Conjugated Polymers with Applications to Solar Cells

by

© Yaping Li
M. Sc. (Physics) Northeast Normal University
B. Sc. (Physics) Northeast Normal University

A thesis submitted to the
School of Graduate Studies
in partial fulfillment of the
requirements for the degree of
Doctor of Philosophy.

Department of Physics and Physical Oceanography
Memorial University of Newfoundland

February 2011

St. John's Newfoundland

Contents

Abstract

Organic semiconducting materials such as conjugated polymers have many important industrial applications. Understanding the process of charge transport is crucial in order to improve their overall efficiency. The transport of charges in devices made of organic conjugated polymers is a complex process. For example, in organic photovoltaic cells (commonly called solar cells), many steps are involved between the points of absorbing light energy and of ultimately generating a photocurrent; they include the exciton formations followed by their dissociations leading to charge-separated states where the holes and electrons are free to move along the polymer chains (forming polarons or bipolarons) and/or between molecular constituents of the device and finally the collection of charges at the electrodes. The part of the process where the hole and electrons are free to move independently of each other is typically referred to as charge mobility. In this thesis we focus primarily on two aspects of charge mobility. Namely, in the first part of the thesis we study the motion of a bipolaron as a function of the electric field strength since this subject is still relatively controversial and unresolved. In the second part of the thesis we propose a multi-step approach that allows for a calculation of charge mobility (that is primarily due to polarons hopping from site to site) as a function of molecular and morphological structure of the organic materials.

The motion of a bipolaron is investigated in heterocyclic conjugated polymers

such as polythiophene (PT) (Part I of the thesis). In their intrinsic state, heterocyclic conjugated polymers form organic semiconducting materials. When doped, they can become conductors. One of the main goals of studies involving doped conjugated polymers is to describe the transport mechanisms of their charge species when an electric field is applied. We employ the extended Su-Schrieffer-Heeger (SSH) theoretical model to study the transport properties of bipolarons in conjugated polymers in the presence of an electric field. This model involves the solution of coupled equations which include the time-dependent Schrödinger equation and the classical motion equation for the lattice displacement which are solved numerically in a self-consistent way. Our theoretical investigation finds that the bipolaron (when formed in polymers such as PT) moves with little change of its shape along the chain backbone in a weak electric field. However, in the presence of a strong electric field, the bipolaron dissolves and free charges become the main charge carriers. The energy trends of the doped polymer with increasing strength of the electric field provide further support for this conclusion. In addition, we apply the SSH model with electron-electron (e-e) interactions to PT. The parameters employed in the computations are determined by requiring a good agreement between the theoretical and experimental values for PT band gap and bond lengths. We find that, within the extended SSH model, e-e interactions in comparison to electron-phonon coupling do not significantly affect the nature of bipolaron transport in polymers such as PT.

Recently, organic solar cells, because of their light weight, low cost and processing flexibility, have attracted considerable attention in the field of photovoltaic cells. In Part II of the thesis, the charge mobility of conjugated organic polymers (mostly fluorene and carbazole based) primarily used in the construction of the organic solar cells is investigated using a multi-step computational approach. The proposed approach employs the use of the density functional theory (DFT), semiempirical (ZINDO) and

Monte Carlo (MC) theoretical methods to determine transfer integrals, reorganization energies, transfer rates and mobilities of conjugated organic polymers. We find that, in organic polymers, the transfer integrals and the reorganization energies are equally important factors in determining charge transport rates and that the one dimensional (1D) approach to estimating trends in mobilities gives reasonable results, i.e. is in good agreement with experimental trends, provided their relative intermolecular distances can be obtained with some accuracy. However, a greater understanding of the mobilities must take into account the three dimensional (3D) structure and/or the inherent disorder that is present in the organic thin films. We illustrate this requirement with some calculations, for example, the computation of an electron mobility in poly(9,9-di-n-octylfluorene-alt-benzothiadiazole)'s (F8BT's) where their 3D structure is known from x-ray diffraction experiments. The proposed approach illustrates that theoretical computations/simulations based on chemical structure and known morphology of organic semiconductors is an important and reliable approach to studying charge mobility in organic materials used in devices such as solar cells.

Acknowledgements

First, I would like to give a million thanks to my supervisor, Prof. Lagowski. From my application for Ph.D. study to now, my supervisor teaches and helps me much much more than what a professor does, more like a parent educating and caring for her own children, which makes me really enjoy my research and life. Her serious attitude in science and optimism for life will affect me forever. From the bottom of my heart, I would like to say: " thank you so much, my dear professor, I am so lucky to meet you in my life, I appreciate you for everything in all of my life."

Second, I would like to thank my Ph.D. committee members: Dr. Booth and Dr. Curnoe for annual evaluations and instructions. In the Department of Physics and Physical Oceanography, I will especially thank Dr. Plumer for his excellent lectures and Dr. Poduska for her instructions on Graduate Program in Teaching. I also would like to thank Dr. Chen, Dr. Lewis, Dr. Morrow, Dr. Whitehead, Dr. Yethiraj, Dr. Andrews, Dr. de Young, Daphne Corbett, Joy Simmons, Maureen Wade and Brenda Burke for their help. For the teaching assistant work, I would like to thank John Jerrett, John Wells, William Kavanagh, Krystyna Pawlowska, Dr. Shorlin and Dr. Goulding. I really enjoy the work with them.

Third, I really appreciate these people for helping me in computers. I can't work without their help. They are Fred Perry, Michelle Shaw, Jason Mercer and Mark Staveley. I also appreciate financial support from the School of Graduate Studies

in Memorial University of Newfoundland and the Natural Science and Engineering Council of Canada (NSERC). I would like to thank the Atlantic Computational Excellence Network (ACEnet), and Memorial University of Newfoundland (St. Johns, NL, Canada) for the use of their computational resources.

Fourth, I would like to thank my Ph.D thesis examiners: Drs. M. Côte, Q. Chen and I. Saika-Voivod for their valuable comments and careful reviews of the thesis.

Last but not least, I would like to give huge thanks to my parents, my husband, brother and sisters for their support. They always do their best to let me have a good life. I feel very happy because of them. I also would like to thank all of my teachers, friends and relatives.

Abbreviations

- **1D** One dimensional
- **3D** Three dimensional
- **BHJ** Bulk heterojunctions
- **BT** Benzothiadiazole
- **CD** Carbazole dimer
- **CDM** Correlated disorder model
- **CF** Cofacial
- **CM** Carbazole monomer
- **CT** Carbazole trimer
- **DFT** Density function theory
- **e-e** Electron-electron
- **e-ph** Electron-phonon
- **EA's** Electron affinities
- **ESR** Electron spin resonance

- **F8BT** Poly(9,9-di-n-octylfluorene-alt-benzothiadiazole)
- **FD** Fluorene dimer
- **FET** Field effect transistor
- **FM** Fluorene monomer
- **fs** femtosecond
- **FT** Fluorene trimer
- **GDM** Gaussian disorder model
- **HF** Hartree-Fock
- **HOMO** Highest occupied molecular orbital
- **HX** Hexagonal
- **IP's** Ionization potentials
- **IR** Infrared
- **LUMO** Lowest unoccupied molecular orbital
- **MA** Miller-Abrahams
- **MC** Monte Carlo
- **MD** Molecular dynamics
- **MDMO-PPV** Poly[2-methoxy-5-(3',7'-dimethyloctyloxy)-p -phenylenevinylene]
- **MM** Molecular mechanics

- **MO** Molecular orbital
- **MOO** Molecular orbital overlap
- **OFETs** Organic field effect transistors
- **OLEDs** Organic light emitting diodes
- **OPV** Organic photovoltaic
- **OPVs** Organic photovoltaic devices
- **OPVCs** Organic photovoltaic Cells
- **P3HT** Poly(3-hexythiophene)
- **PA** Polyacetylene
- **PC** Poly(2,7-carbazole)
- **$PC_{61}BM$** [6,6]-phenyl C_{61} butyric acid methyl
- **PCDTBT** Poly(N-9'-heptadecanyl-2-7-carbazole-alt-5, 5-(4',7'-di-2-thienyl-2',1',3'-benzothiadiazole)
- **PCE** Power conversion efficiency
- **PF** Poly(9,9'-dioctylfluorene)
- **PFB** Poly(9,9'-di-n-octylfluorene-alt-bis-N-N'-(4-butylphenyl)bis-N,N'-phenyl-1,4-phenylene diamine)
- **PPP** Pariser-Parr-Pople
- **PT** Polythiophene

- **PV** Photovoltaic
- **QM** Quantum mechanical
- **RW** Random walk
- **SAW** Acousto-electric traveling wave
- **SCF** Self-consistent field
- **SCLC** Space-charge-limited-current
- **SS** Side-by-side
- **SSH** Su-Schrieffer-Heeger
- **TDDFT** Time-dependent DFT
- **TOF** Time-of-flight
- **TW** Terawatts
- **UV-vis** Ultraviolet-visible
- **ZINDO** Zerner's intermediate neglect of differential overlap

List of Tables

List of Figures

Chapter 1

Introduction

1.1 Organic Semiconducting Polymers

In the past decades, organic conjugated polymers (also called conducting polymers) aroused great interests among physicists and chemists alike because of their special conductivity, optical and magnetic properties. Conjugated (organic) polymers are semiconductors or insulators with band gaps ranging between less than 1 eV to a few electron volts. We briefly trace the development of organic material conductivity studies. In the late 1950s, polyacetylene (PA) was first synthesized and viewed as a wide band gap semiconductor with a low intrinsic conductivity. [1, 2] In 1977, a team led by A. J. Heeger, A. G. MacDiarmid and H. Shirakawa found that doped PA can form a new class of conducting polymers in which the electrical conductivity can be systematically and continuously varied over a range of eleven orders of magnitude. [3] This discovery opened the new field of conducting polymers. In 1987, H. Naarmann and coworkers [4] performed a milestone contribution to conducting polymers. They made the conductivity of PA as high as that of copper metal. In 2000, A. Heeger, A. MacDiarmid and H. Shirakawa were awarded Nobel Prize in chemistry "for the

discovery and development of conductive polymers," which further confirmed the importance of conducting polymers. Another milestone step was the discovery (in 1990) of electroluminescence in phenylene-based polymers. [5]

Many applications have been proposed for conducting polymers and some have already been commercially implemented. [6] The most important applications involve the devices such as the organic light emitting diodes (OLEDs), [5, 6, 7] organic field-effect transistors (OFETs) [6, 7, 8, 9] and organic photovoltaic cells (OPVCs) [7, 10]. For example, in future, it is possible that the patterns and colors of wallpapers can be altered by clicking a switch, the contents of newspapers and books can be updated or changed on demand etc. [8, 11, 12] Currently, in all cases, better performance of these devices is continually being sought. This effort typically requires better knowledge of their optoelectronic properties such as band gaps and band widths, excitation energies, energy levels, binding energies, density-of-states, and others. At the same time there is a great effort to understand their dynamic properties, such as charge and energy transport, which is essential information for the improvement of the efficiency of these devices. While great progress has been made, there are still many questions left to investigate and a lot of room for improvement.

There are many excellent recent reviews that summarize the latest theories, synthesis methods and characterization results of organic semiconductors. [6, 7, 9, 13] It remains true however, that understanding the process of charge transport is a crucial and challenging step in the effort of improving the overall efficiency of organic devices. In general, the transport of charge in devices made of organic conjugated polymers is a complex process that involves a variety of time and length scales. That is, the process involves many stages as described in many recent reviews that also summarize the latest methodologies used in investigating charge transport. [14, 15, 16] As an example, in OPVC (commonly called solar cell), charge takes the following steps

between the points of light absorption and photocurrent generation: exciton formation and dissociation leading to intermolecular charge-transfer states (electron and holes are on different molecules but are still bound to each other), eventually reaching charge-separated states where the holes and electrons are free from one another and can move along the polymer chains and/or hop between molecular constituents of the device material until they reach their respective electrodes (this part of the process is typically referred to as charge mobility) and finally charges are collected at the electrodes. In this case the rate of intermolecular charge transfer occurs on the ps-ns time scale while the charge transit across the device occurs on the ns-ms time scale. The corresponding lengths range from intermolecular distances (10^{-10} m) to device thickness ($10^{-7} \sim 10^{-5}$ m). [16]

The inherent complexity of the charge transport in organic semiconductors means that no single method can model all aspects of this process. Different theories and methodologies must be used. In this thesis we focus primarily on two aspects of charge mobility (that is, when holes on donors and electrons on acceptors are separated and are essentially "free" to move along or between molecular systems). In organic semiconductors charges that move along the polymer chains typically form charged species such as polarons or bipolarons due to relatively strong electron-phonon coupling. In the first part of the thesis we study the motion of a bipolaron as a function of the electric field strength since this subject is still relatively unresolved. In the second part of the thesis we propose a multi-step approach that allows for a calculation of charge mobility (that is primarily due to polarons hoping from site to site) as a function of molecular and morphological structure of the organic materials.

In order to test the computational approach (as proposed in Part II), reliable experimental mobility data are required. A number of experimental methods are available for mobility measurements. [17, 15] They are: (a) the time-of-flight (TOF)

method [18, 19]; (b) the xerographic discharge method [20]; (c) the equilibrium charge carrier extraction method [21, 22, 23, 24]; (d) drift current methods under limited range conditions [25, 26, 27]; (e) the space-charge-limited-current (SCLC) method [28]; (f) the conductivity /concentration method [29, 30]; (g) the field effect transistor (FET) method [31, 32, 33]; and(h) the surface acousto-electric traveling wave (SAW) method. [19, 34] Here, we just briefly describe the typical features of the most widely used TOF and FET methods. In the TOF method, an organic semiconductor material is irradiated by a laser pulse to generate charges. An electric field typically of the order of $10^4 \cong 10^6$ V/cm is then applied and the photogenerated holes or electrons are collected at the electrodes. The mobility, μ, of the holes or electrons is calculated as:

$$\mu = \frac{v}{E} = \frac{d}{Et} = \frac{d^2}{Vt}$$

where d is the distance between the electrodes, E is the electric field, t is the averaged transit time, and V is the applied voltage. It should be noted that the above equation for mobility can be modified to include dielectric constant of the medium, ϵ,

$$\mu = \frac{d^2\epsilon}{Vt}$$

since $E = D/\epsilon$ where D is an applied field. [35] TOF mobility measurements are sensitive to the structure and the presence of defects in the materials. [15] In the FET method, the I-V (current-voltage) expressions as shown, for example, in reference [33] depend, amongst number of parameters, on charge mobility μ and therefore can be used to obtain carrier mobilities.

In summary, in light of the fact that there are potential numerous applications of organic polymer material in devices, it is necessary to understand the underlying mechanism to make these devices operate more efficiently. Charge transport is one of the main factors to determine their efficiency, hence we study some important aspects

of charge transport in conjugated polymers.

1.2 Charged Species in Organic Semiconducting Polymers: Polarons and Bipolarons

Conducting polymers have an unusual inherent mechanism of electrical conductivity and charge transport along the chains. Even though doped organic polymers display electrical conductivity similar to the conventional doped inorganic semiconductors, physics involved in the process is very different. The charge transfer processes along the chain result in significant local modification of the chain geometry in organic materials and the local geometry modifications of the chain, in turn, markedly affect their electronic structure by inducing localized electronic states in the gap. The formation of inter band states complicates significantly the charge transport phenomena in organic polymers. We can begin to understand this from the simplest of conducting polymers, PA.

In PA the chemically relevant valance electrons can be classified as σ and π bonding electrons (the core electrons are not involved in most of the chemical processes and their effect can be neglected). The σ electrons form the strong covalent bond between two bonded nuclei. In trans-PA polymer, the σ bonds form sp^2 hybridized bonds. The π electrons are less localized and form weaker bonds. The π bonds are delocalized over the whole length of the polymer chain. They are responsible for the bond alternation or conjugation (i.e. the formation of alternating shorter than single and longer than double bond structure) in trans-PA. [36]

Highly mobile neutral magnetic defects have been observed in undoped trans-PAs with the use of magnetic resonance experiments. [37, 38] Su et al. [38] suggested that

these defects are generated by kinks, often referred to as solitons and characterized by unpaired spins, in the alternating bond structure of the neutral trans-PA. They also suggested that doping may give rise to the creation of charged domain walls (i.e. charged solitons). These studies of (neutral or charged) solitons formation and their dynamic properties eventually led to the development of new class of materials such as organic conducting polymers.

Su, Schrieffer and Heeger (SSH) [37, 38] developed a theoretical model for PA that showed the existence of bond alternation along the polymer chain backbone (i.e., alternating "single" and "double" bonds). They assumed a relatively weak coupling between chains. That is, PA was treated as a quasi one-dimensional system. σ electrons were treated in the adiabatic approximation. In this model, a is defined as the equilibrium spacing between the x coordinates of successive CH groups in the undimerized (all bonds are equal) structure. a is approximately $1.4 \times \sqrt{3}/2$ Å=1.22 Å. It is assumed that π electrons (p_z) can be treated in the tight-biding or Huckel-type approximation with a transfer integral. The Hamiltonian for the system was taken as:

$$H = -\sum_n \sum_s [t_0 - \alpha(u_{n+1} - u_n)](c^+_{n+1s} c_{ns} + h.c.) + (K/2)\sum_n (u_{n+1} - u_n)^2 + (M/2)\sum_n \dot{u}_n^2 \tag{1.1}$$

where u_n is the displacement of the ion group on the n-th site from its equilibrium position, c^+_{ns} and c_{ns} are the creation and annihilation operators of an electron with spin s on the n-th site, they satisfy Fermi anticommutation relation, $h.c.$ stands for hermitian conjugate, t_0 is the equilibrium value of the nearest-neighbor transfer integral, α denotes the electron-lattice displacement (phonon) coupling constant, K is the spring constant and M is the mass of an ionic group. Missing from H are the explicit Coulomb interactions between π electrons.

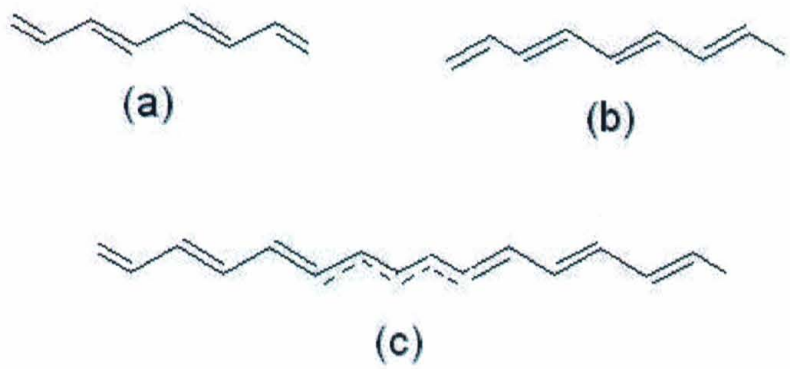

Figure 1.1: Two degenerate structures of trans-polyacetylene (a) A phase, (b) B phase and (c) soliton.

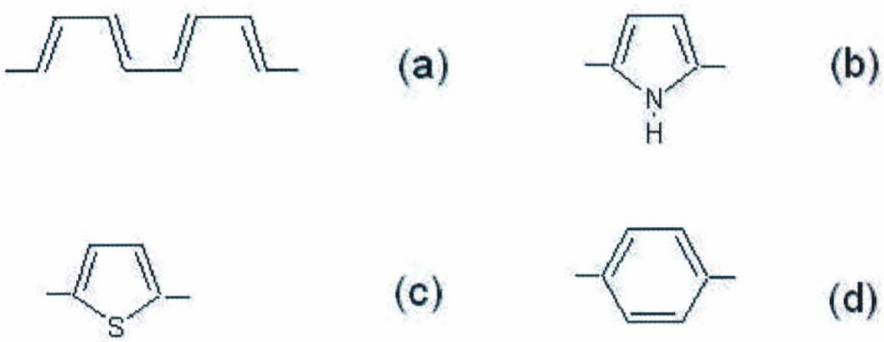

Figure 1.2: Configurations for (a) cis - PA, (b) polypyrrole, (c) polythiophene, and (d) polyparaphenylene.

The original SSH Hamiltonian was developed to describe trans-PA that has a doubly degenerate ground state and hence can form solitons (see Fig. 1.1). Most conducting polymers such as (a) cis - PA (b) polypyrrole (c) polythiophene (d) poly-parapheneylene (see Fig. 1.2) have non-degenerate ground states and can not form neutral solitons. [36] When doped, their charge carriers are polarons or bipolarons. Polarons or bipolarons can be formed through electrons or holes coupling with the lattice (often referred as phonon-electron (ph-e) coupling). The charge of a polaron is $\pm e$ and the spin is $\pm\frac{1}{2}$. A bound pair of polarons is called a bipolaron, its charge is twice that of an electron or a hole and it has no spin. [39]

An extended SSH model was developed to study the properties of nondegenerate conducting polymers. The extended SSH model (with and without electron-electron (e-e) interactions) is described in Part I (Chapter 3). The model is then applied to studying the motion of a bipolaron in heterocyclic polymers such as polythiophenes (PTs). Amongst the conjugated polymers, PTs because of their environmental and thermal stability [40], are widely used in many applications. Experimental and theoretical evidence [41, 42, 43, 44, 45, 46, 47, 48] indicates that the main charge carriers in PT are bipolarons at an intermediate level of doping. At very low doping concentrations, polarons are believed to be more stable. [39, 41, 43] Their relative stability is affected by many factors such as the strength of e-e interactions versus lattice confinement, the strength of an electric field and level of dopant concentration. [39, 49] In particular, the motion of polarons and bipolarons under the influence of an electric field has been investigated [50, 51, 52] for poly(p-phenylene). We examine more closely how the electric field affects the bipolaron motion in PT using the tight-binding approximation (that is, the extended SSH model). The results of the investigation of a bipolaron motion in PT are presented in Part I (Chapter 4) of this thesis.

1.3 Modelling Charge Mobilities in Organic Semiconductors

The SSH model can be applied to an isolated single polymer chain, or to highly ordered and stretch-oriented polymer systems, but it is well known that common conjugated polymer systems have a disordered nature and that disorder plays a very important role in the charge transport. Also, because of their relatively weak intermolecular interactions, bulk transport of charge involves hopping mechanism and not band transport that is observed in covalently bonded inorganic crystals. [7]

The hopping transport in disordered molecular films has commonly been analyzed within the context of the Gaussian Disorder Model (GDM) [53] and its improvement such as Correlated Disorder Model (CDM). [54] The GDM made the assumption that a Gaussian density of states with a width σ can describe the energy disorder in conjugated polymers. Also Miller-Abrahams (MA) intersite hopping rate, defined as the jump rate among sites i and j is the product of a prefactor ν_o, an electronic wave function overlap factor, and a Boltzmann factor for jumps upward in energy,

$$\nu_{i,j} = \left\{ \begin{array}{ll} \nu_o \exp(-\alpha \Delta R_{ij} - \beta(\varepsilon_j - \varepsilon_i)) & \varepsilon_j > \varepsilon_i \\ \nu_o \exp(-\alpha \Delta R_{ij}) & \varepsilon_j < \varepsilon_i \end{array} \right\}$$

where α is the inverse localization length, ΔR_{ij} is the distance between the localized states, $\beta = 1/kT$, and ε_i is the energy at state i, is used in the GDM. Then performing Monte Carlo (MC) simulations of a biased random walk (RW) on disordered cubic lattices, some results (such as the $\sqrt{E}$ dependence of the mobility, also called Poole-Frenkel dependence, and photocurrent transition from non-dispersive to dispersive regimes) compared well with experimental data. However, GDM can't predict charge-transport properties from the physical and chemical structure of real molecular materials because the MA rate parameters cannot be calculated directly from

chemical structure and because no details of the relative positions of charge transport units are included.

A first attempt to use quantum chemical methods to calculate the effect of chemical structure on the hopping rate distributions is given in the reference [55]. They proposed a model to describe electrical transport in dense films of conjugated polymers in which thermal fluctuations changed the molecular geometries of the polymers which led to modifications in the energy levels of the localized (polaronic) electronic states. The main restoring force for these geometry fluctuations is due to intermolecular interactions (intramolecular contributions are neglected), which results in spatial correlation in the molecular distortions which, in turn, leads to a spatial correlation in the energies of the localized states. The model explains the experimentally observed field and carrier density dependence of the mobility.

More recently, Athanasopoulos and co-workers [56] use the actual chemical structure of organic polymers to simulate their mobility. They also employ MC simulations of a biased RW to model charge transport but they overcome the limitations of the GDM by first employing an arrangement of charge transporting units that is based on the observed structure of organic material and, second, using small-polaron hopping rates calculated directly from the electronic structure of the units. That is, the intermolecular hole transfer rate, Γ, is obtained using the Marcus-Hush theory,

$$\Gamma_{ij} = \frac{t_{ij}^2}{\hbar}\sqrt{\frac{\pi}{\lambda k_B T}}\exp\{-\frac{(\Delta G_{ij} - \lambda)^2}{4\lambda k_B T}\}.$$

Γ_{ij} depends on the electronic transfer integral (t_{ij}), the molecular reorganization energy (λ), and the temperature (T) (k_B, $\hbar$, and ΔG_{ij} are Boltzmann's constant, Planck's constant divided by 2π and the free energy difference between initial and final sites, respectively). Thus, through calculation of electronic properties from first principles using an empirical morphology, their method includes the influences of

morphology and chemical structure on mobility.

Athanasopoulos and co-workers [56] model a film of aligned poly-(9,9′-dioctylfluorene) (PF) chains as a hexagonal lattice of lattice constant a where the chains are parellel both to each other and to the substrate. A fluorene trimer is the charge transporting unit in all cases. The relaxed geometry of the trimer is calculated in Gaussian 03 using density functional theory (DFT) with the B3LYP hybrid function and Pople's double-ζ split basis set with added polarization functions 6-31 G^*. All the trimers are in the neutral state. The trimers are arranged coaxially in columns, aligned with the z direction, as a model of a continuous chain. The trimer position is determined by the midpoint of the trimer relative to the (x,y) axes and the torsion angle, ϕ, by the angle between the plane of the central fluorene unit and the x-z plane. The simulation cell consists of 20×20 chains, where each chain consists of 10 trimers and periodic boundary conditions are applied in the y and z directions. The hopping transport parameters are calculated as follows: λ is calculated from the method in reference [57] and the transfer integral t_{ij} is calculated with Molecular Orbital Overlap (MOO) method. [58] Then a MC simulation is executed on the chosen morphology. The waiting time from site i to j is τ_{ij} and is related to the transfer rate Γ_{ij}, that is $\tau_{ij} = -\ln(X)/\Gamma_{ij}$, where X is a random number uniformly distributed between 0 and 1. The hop with the smallest waiting time is chosen. They follow the trajectory of a hole randomly placed on a trimer in the film and calculated the time for the hole travel a fixed distance d. A transit time averaged over several hundred trajectories, $\langle\tau\rangle$, is obtained. The field-dependent mobility μ is computed from $\mu = d/(\langle\tau\rangle E)$. They obtain mobilities in the range of $2 - 9 \times 10^{-4}$ cm^2/Vs for ordered PF (with hexagonal symmetry) systems and a value of 8×10^{-3} cm^2/Vs for a torsionally disordered system which compares well with the experimental result of $8.5 \pm 1 \times 10^{-3}$ cm^2/Vs. Another result that they obtain is that for a certain ordered configuration

of the system the mobility (2×10^{-2} cm^2/Vs) can be made higher than the mobility for a torsionally disordered system. [56]

Recently, Nelson et.al. [16] extended the above approach to include Molecular Dynamics (MD) method to simulate the molecular packing better which makes this approach more powerful. However, it increases the computational complexity of calculating the mobility. Moreover, the accurate simulation of molecular packing structures with MD requires reliable structural information, both for validation of results and for the definition of suitable starting configurations, which is still difficult to obtain from experiments. A number of case studies [59, 60, 61, 62] that involved materials that have high symmetry or well-defined structures have been recently investigated with the above method that uses the MD calculations as its initial step. In this thesis the aim is to propose an approach that is expedient and reliable enough to reproduce experimental trends in charge mobility in organic conjugated polymers. The MD simulations have not been employed in the proposed method. The future work may include the MD computations to obtain more information about the three-dimensional (3D) structure of the polymer systems.

Part I

Bipolaron Motion in Heterocyclic Polymers

Chapter 2

Introduction

Beginning in the late 1970's, conjugated organic polymers emerged and continue to emerge as new materials that could be used in electronic and optical devices such as conductors, polymer light emitting diodes, field effect transistors, solar cells, sensors and many others. Their main advantages are the low cost, ease of processability and relatively high efficiency. [40, 63] Amongst the conjugated polymers, heterocyclic polymers such as PTs, because of their environmental and thermal stability [40], are the most widely used in many applications. When doped, many conjugated organic polymers can become good conductors. PTs and other conjugated polymers have the flexibility, broad spectral range, and can be easily patterned which make them competitive with their inorganic counterparts. [63]

To improve the efficiency of the above devices, it is necessary to understand their underlying transport mechanisms. Many early theories and experiments demonstrated that, in organic conjugated molecular systems, the main charge carriers are solitons, polarons and/or bipolarons. [38, 41, 64, 65, 66] These species are different from the conventional charge carriers such as electrons or holes which are present in inorganic semiconductors and conductors. Solitons, which form as a result of

the lattice distortion, can only exist in materials such as trans-polyacetylene which has a two-fold degenerate ground state. [67, 68] In most conjugated polymers with non-degenerate ground states, the prevalent charge carriers are polarons and/or bipolarons. There are many intrinsic and extrinsic factors that determine the formation and the stability of polarons and bipolarons. These factors include the strengths of lattice confinement e-ph coupling, e-e interactions and an electric field, and the level of dopant concentration. [39, 49, 69]

Earlier (prior to approximately mid 1990s) experimental and theoretical studies [39, 41, 42, 43, 44, 45, 46, 47, 48] predominantly indicated that the main charge carriers in polymers such as PTs [70, 71] are bipolarons at some (possibly intermediate) level of doping. At other doping concentrations (possibly very low), polarons were believed to be more stable. [39, 41, 43] The main evidence for these assignments came from the empirical theoretical approaches (such as those involving model Hamiltonian of SSH and its extensions or of Pariser-Parr-Pople (PPP)) or low level ab initio theories (at a restricted Hartree-Fock, RHF/STO-3G level) that were used to interpret the ultraviolet-visible (UV-vis) and near infrared (IR) absorption spectra and the electron spin resonance (ESR) signals.

More recently, other interpretations were proposed to explain the experimental results [72, 73, 74, 75, 76, 77, 78, 79, 80, 81] of doped (mostly thiophene) oligomer studies. It was suggested that two strong subgap (also referred to as intra-gap) transitions in the photoinduced absorption spectra are indicative of the formation of a polaron (radical cation) or two separate polarons (biradicals) on a single oligomer not bipolarons (dications) as was previously believed. Bipolarons, if formed, would give rise only to one strong subgap transition. Theoretically, the main support for these interpretations comes from predominantly DFT including the time-dependent DFT (TDDFT) investigations [82, 83, 84, 85, 86, 87, 88, 89, 90, 91, 92] as applied

to oligomers. Some of these studies also proposed that the disappearance of ESR signal in some case was indicative of the formation of π-dimers instead of bipolarons. The results of these alternative interpretations have been summarized in Chapters 16 and 17 of reference [93] and extensive references are given in the most recent DFT study. [92]

The above mentioned oligomer investigations seem to suggest that bipolaron formation is possible on shorter chains (say less than ten rings) or in a very heavily doped materials. There continues to be a controversy surrounding the polaron versus bipolaron issue. For example, relatively recent experimental [94, 95] and theoretical [96, 97, 98] works suggest that under certain conditions bipolarons are formed and are stable in thiophene based systems. It would seem reasonable to suggest that bipolarons could be formed (either due to confinement or to intrinsic binding) in a highly disordered (amorphous) PT or at a high level of doping. This is because the effective conjugation length of PT is known to be less than ten rings and effectively the amorphous PT could be thought of as consisting of short oligomers verses linear ordered chains. Other effects such as intermolecular interactions of the polymers with the solvent molecules or counterions could also have a stabilizing effect on the bipolaron. In this work, we are assuming that under certain conditions, bipolarons are formed. We study the motion of bipolarons with the extended SSH model. The SSH model is relatively simple compared to the higher level theoretical approaches such as say, TDDFT, however, it allows us to investigate the effect of an external field such as an electric field on the motion of the bipolaron in a straightforward way. Also, the effects due to e-ph and e-e interactions can be both included in the model and their relative importance can be studied.

In most materials, charge transport or conductivity normally occurs under the influence of an electric field. It should be noted that electric field will also act on

or induce charge distributions such as dipoles which are often present in neutral or doped conjugated polymers such PT [99] and which are key to the understanding of their optical properties (i.e. their optical spectra). In this work we are primarily interested in the effects of an electric field on the transport of a bipolaron once it has been formed. The properties and dynamics of solitons and polarons in conjugated polymers in the presence of an electric field have been extensively studied. [50, 51, 52, 100, 101, 102, 103, 104, 105, 106] It has been found that a soliton in doped PA moves like a Brownian particle in the presence of an electric field and at some point, its velocity reaches a maximum value that is independent of the strength of an applied electric field. [100] The evolution of a polaron in an electric field depends on the magnitude of the field. For example, in PA, [102, 103] if the electric field is $\geq 10^6$ V/cm, the polaron dissociates into a moving free charge carrier and phonon-like lattice deformation (provided the polaron was formed before the field is switched on). The motion of polarons and bipolarons under the influence of an electric field has also been investigated in poly(p-phenylene). [50, 51, 52]

As stated above, in this work we examine more closely how the electric field affects the bipolaron motion in heterocyclic conjugated polymers using the tight-binding approximation. The magnitude of the applied electric fields varies from weak 2.6×10^5 V/cm to very strong 7×10^6 V/cm. In a typical organic semiconducting device the charges are injected under fields up to 10^6 V/cm. [102] Application of higher electric fields is possible with high-voltage pulses with pulsewidths between 250 ns and 5 μs. [107] Chayet et al. [107] showed that an application of fields higher than 7×10^7 V/cm leads to material degradation. It is expected that with high electric field, just as in the case of the polaron, the bipolaron will dissolve into free charge carriers and independent lattice distortion (again provided that the bipolaron was formed before the field is applied). The material degradation at fields higher than

7×10^7 V/cm also indicates that anharmonic phonons and by extension anharmonic electron-phonon interactions (not included in this study) may play an increasingly important role at fields of the order of 10^7 V/cm. Hence at very high fields, a path integral approach to the SSH model as proposed by M. Zol [108, 109, 110] (instead of the SSH model as used in this work) should probably be employed to study the charge transport.

The simulations in this thesis use the extended theoretical model SSH. [38, 51, 52] It should be pointed out that this model contains no dissipation (damping) mechanism and hence in the presence of an electric field the energy of the system will increase continuously with time. We also point out that we follow the dynamics of the order of 100 fs which is a very short time. During this time the dissipative effects may not be significant. [105] We evaluate the effect of viscous damping by introducing an additional term in the SSH Hamiltonian and show that its effect is indeed negligible when using the damping constant as suggested in reference [105]. In Part A of Chapter 4, we use the extended SSH model (with the symmetry breaking term) and analyze how the strength of an electric field affects bipolaron transport in heterocyclic conjugated polymers. In Part B of Chapter 4, we include e-e interactions in the SSH Hamiltonian and modify the model parameters to better reproduce the structure and band gap of PT. That is, we investigate the effect of a strength of an electric field on bipolaron transport in PT in the presence of e-ph and e-e interactions. First, in Chapter 3, we describe in details the theory employed in simulations. Conclusions are given in Chapter 4. The results presented in Chapter 4 have been published. [111]

Chapter 3

Theoretical Model

3.1 Original SSH Model

The original Su-Schrieffer-Heeger's model Hamiltonian [37, 38] as given in Chapter 1 (Eq. (1.1)) was used to study solitons and polarons in degenerate conjugated polymers such as PA. In the first part of this section, a short outline is given that describes the procedure that uses the solution to the stationary Schrödinger equation and Hellmann-Feynman theorem to obtain the ionic displacements and charge distribution that are created when solitons or polarons are formed in the polymer. In the second part of this section, the electric field is introduced into the original SSH Hamiltonian to study the dynamics of the solitons and polarons in degenerate polymers. This necessitates the solution of two coupled equations: the time-dependent Schrödinger equation and the classical motion equation for the lattice displacement in order to obtain ionic displacements and charge distribution as functions of time. The details are given below.

For the stationary case, first, the Hellmann-Feynman theorem is applied to the

SSH Hamiltonian (see Eq. (1.1)) and the following is obtained [37, 38],

$$\langle \frac{\partial H}{\partial u_n} \rangle = -\alpha(c_{n+1}^{+}c_n + h.c.) + \alpha(c_n^{+}c_{n-1} + h.c.) - K(u_{n+1} - u_n) + K(u_n - u_{n-1}). \quad (3.1)$$

Minimizing the energy of the system requires that the above equation equals to zero, that is,

$$u_n = (u_{n+1} + u_{n-1})/2 + \alpha/(2K)[(c_{n+1}^{+}c_n + h.c.) - (c_n^{+}c_{n-1} + h.c.)]. \quad (3.2)$$

Then, using the field operator [112]

$$c_{ns} = \sum_{\nu} \phi_\nu(n) c_{\nu s}$$

where $\phi_\nu(n)$ is the n-th component of the eigenvector ϕ_ν, and Fermi anticommutation relation

$$c_\nu^{+}c_\nu + c_\nu c_\nu^{+} = 1$$

we obtain

$$u_n = (u_{n+1} + u_{n-1})/2 - (\alpha/K)\sum_{\nu,s}{}' \phi_\nu(n)[\phi_\nu(n-1) - \phi_\nu(n+1)] \quad (3.3)$$

where the prime indicates that the summations are restricted to the occupied electronic states. Next, we define

$$y(n) = u_{n+1} - u_n$$

with the constraint that

$$\sum y(n) = 0$$

which results in $y(n)$ given as

$$y(n) = -2(\alpha/K)\sum_{\nu,s}{}' \phi_\nu(n)\phi_\nu(n+1) + 2(\alpha/KN)\sum_{n}\sum_{\nu,s}{}' \phi_\nu(n)\phi_\nu(n+1) \quad (3.4)$$

where ϕ_ν's diagonalize the first term on the r.h.s. of Eq. (1.1), that is,

$$\varepsilon_\nu \phi_\nu(n) = -[t_0 - \alpha y(n-1)]\phi_\nu(n-1) - [t_0 - \alpha y(n)]\phi_\nu(n+1). \tag{3.5}$$

Eqs. (3.4) and (3.5) are coupled equations. They are solved using the iterative method. One can obtain a soliton or a polaron in the excited state.

In order to study the dynamics of a single soliton, A. Terai and Y. Ono [100] introduced an external electric field in the model, then the SSH Hamiltonian becomes

$$\begin{aligned} H = &-\sum_n \sum_s [t_0 - \alpha(u_{n+1} - u_n)](e^{-i\gamma A} c^+_{n+1s} c_{ns} + h.c.) \\ &+ (K/2)\sum_n (u_{n+1} - u_n)^2 + (M/2)\sum_n \dot{u}_n^2 \end{aligned} \tag{3.6}$$

where $\gamma = ea/\hbar c$, e is the absolute value of the electronic charge, a is the lattice constant, c is the light velocity and A is a vector potential. The electric field is given by $E = -(1/c)\dot{A}$. Using Hamiltonian given in Eq. (3.6), the time-dependent Schrödinger equation becomes

$$i\hbar \frac{\partial \psi_\nu(n,t)}{\partial t} = -(t_0 - \alpha y_n)e^{-i\gamma A}\psi_\nu(n+1,t) - (t_0 - \alpha y_{n-1})e^{i\gamma A}\psi_\nu(n-1,t). \tag{3.7}$$

The solution to Eq. (3.7) can be written as

$$\psi_\nu(t_{j+1}) = \sum_\mu C_{\mu\nu} e^{-i\varepsilon_\mu \Delta t/\hbar}\phi_\mu(t_j) \tag{3.8}$$

where ϕ_μ is a single particle eigenfunction and $C_{\mu\nu} =< \phi_\mu(t_j)|\psi_\nu(t_j) >$, which means the $(j+1)^{\text{th}}$ instant wave function can be obtained from j^{th} one. In order to obtain the force, the electronic potential energy is calculated first

$$\begin{aligned} E_{el} &= < \psi_\nu | H_{el} | \psi_\nu > \\ &= \sum_n [-(t_0 - \alpha y_n)e^{-i\gamma A}\sum_\nu \psi^*_\nu(n,t)\psi_\nu(n+1,t) \\ &\quad -(t_0 - \alpha y_{n-1})e^{i\gamma A}\sum_\nu \psi^*_\nu(n,t)\psi_\nu(n-1,t)] \end{aligned} \tag{3.9}$$

and using

$$-\frac{dE_{el}}{du_n} = F_{el}(n)$$

the electronic force is given by

$$\begin{aligned} F_{el} &= \alpha \sum_{\nu}{}' e^{-i\gamma A}[\psi_\nu^*(n,t)\psi_\nu(n+1,t) - \psi_\nu^*(n-1,t)\psi_\nu(n,t)] \\ &\quad +\alpha \sum_{\nu}{}' e^{i\gamma A}[\psi_\nu^*(n+1,t)\psi_\nu(n,t) - \psi_\nu^*(n,t)\psi_\nu(n-1,t)]. \end{aligned} \tag{3.10}$$

Adding the elastic force, the total force is given by

$$\begin{aligned} F_n(t) &= -K(2u_n(t) - u_{n+1}(t) - u_{n-1}(t)) \\ &\quad +\alpha \sum_{\nu}{}' e^{-i\gamma A}[\psi_\nu^*(n,t)\psi_\nu(n+1,t) - \psi_\nu^*(n-1,t)\psi_\nu(n,t)] \\ &\quad +\alpha \sum_{\nu}{}' e^{i\gamma A}[\psi_\nu^*(n+1,t)\psi_\nu(n,t) - \psi_\nu^*(n,t)\psi_\nu(n-1,t)] \end{aligned} \tag{3.11}$$

where the last two terms correspond to the force exerted by all electrons on the atom on the n^{th} site. Then, the equation of motion for the lattice,

$$M\ddot{u} = F_n(t) \tag{3.12}$$

can be solved, that is,

$$\begin{aligned} u_n(t_{j+1}) &= u_n(t_j) + \dot{u}_n(t_j)\Delta t \\ \dot{u}_n(t_{j+1}) &= \dot{u}_n(t_j) + \frac{F_n(t_j)}{M}\Delta t. \end{aligned} \tag{3.13}$$

The electron density is defined as,

$$\rho_n = \sum_{\nu} \psi_\nu^*(n) f_\nu \psi_\nu(n) \tag{3.14}$$

where the f_ν is the time-independent distribution function determined by initial occupation (being 0, 1 or 2). For completeness, we include expressions for the bond variable $\bar{y}_n$ and its time derivative $\dot{\bar{y}}_n$

$$\bar{y}_n = (-1)^n(1/4)(-y_{n-1} + 2y_n - y_{n+1}) \tag{3.15}$$

$$\bar{\dot{y}}_n = (-1)^n(1/4)(-\dot{y}_{n-1} + 2\dot{y}_n - \dot{y}_{n+1}) \tag{3.16}$$

since they are often used in other works (see for example [100]). By numerically solving the coupled equations Eq. (3.8) for the electric wave function and Eq. (3.13) for the motion of the lattice displacement, one can simulate the movement of the soliton in the presence of an electric field

3.2 Extended SSH Model

Because PA is not a stable material, scientist were more interested in heterocyclic conjugated polymers. The structure of heterocyclic conjugated polymers can be viewed as consisting of a backbone of sp^2 hybridized carbon atoms analogous to that of cis-PA, and is stabilized by a heteroatom covalently bonded to carbon atoms. [71] The Hamiltonian [38, 51, 52] used to describe this system has the following form:

$$\begin{aligned} H &= -\sum_n [t_0 - \alpha(u_{n+1} - u_n) - t_1 \cos\frac{n\pi}{2}] \\ &\quad \times (e^{-i\gamma A} c^+_{n+1,s} c_{n,s} + e^{i\gamma A} c^+_{n,s} c_{n+1,s}) \\ &\quad + \frac{1}{2} K \sum_n (u_{n+1} - u_n)^2 + \frac{M}{2} \sum_n \dot{u}_n^2 \end{aligned} \tag{3.17}$$

where the symmetry-breaking term $t_1 \cos\frac{n\pi}{2}$ simulates the effects of the heteroatom (such as S) since it generates four bond lengths (three of which are unequal): 1.307 Å, 1.468 Å, 1.307 Å and 1.554 Å. The inequality of "single" bonds suggests the presence of heteroatom in polymer backbone. This pattern can be compared, for example, to the experimental bond lengths for PT: 1.357 Å, 1.433 Å, 1.357 Å and 1.480 Å. [70] t_1 is typically smaller than t_0 and is often referred to as the polymerization parameter. The following parameters were selected for heterocyclic polymers [52]: $a = 1.22$ Å, $t_0 = 2.5$ eV, $t_1 = 0.27t_0$, $K = 21$ eV/Å^2 and $\alpha = 4.5$ eV/Å. Each electronic state

is described by the wave function, $\psi_\nu(n,t)$, where the index ν labels the electronic energy level. The time evolution of the electron state is found by integrating the following time-dependent Schrödinger equation:

$$\begin{aligned} i\hbar\frac{\partial\psi_\nu(n,t)}{\partial t} &= -[t_0-\alpha(u_{n+1}-u_n)-t_1\cos\frac{n\pi}{2}]e^{-i\gamma A}\psi_\nu(n+1,t) \\ &\quad -[t_0-\alpha(u_n-u_{n-1})-t_1\cos\frac{(n-1)\pi}{2}]e^{i\gamma A}\psi_\nu(n-1,t). \end{aligned} \tag{3.18}$$

The solution of the time-dependent Schrödinger equation can then be expressed in the form [104]:

$$\begin{aligned} \psi_\nu(n,t_{j+1}) &= \sum_l[\sum_m \phi_l^*(m,t_j)\psi_\nu(m,t_j)] \\ &\quad \times e^{-i\epsilon_l\Delta t/\hbar}\phi_l(n,t_j) \end{aligned} \tag{3.19}$$

where $\{\phi_l\}$ and $\{\varepsilon_l\}$ are the eigenfunctions and the eigenvalues of the electronic part of the Hamiltonian $H(t)$ at a given time t_j and $\Delta t = t_{j+1}-t_j$.

The motion of the the lattice displacement is given classically by the equation:

$$M\ddot{u}_n(t) = F_n(t) \tag{3.20}$$

where

$$\begin{aligned} F_n(t) &= -K(2u_n(t)-u_{n+1}(t)-u_{n-1}(t)) \\ &\quad +\alpha{\sum_\nu}' e^{-i\gamma A}[\psi_\nu^*(n,t)\psi_\nu(n+1,t)-\psi_\nu^*(n-1,t)\psi_\nu(n,t)] \\ &\quad +\alpha{\sum_\nu}' e^{i\gamma A}[\psi_\nu^*(n+1,t)\psi_\nu(n,t)-\psi_\nu^*(n,t)\psi_\nu(n-1,t)]. \end{aligned} \tag{3.21}$$

The first term on the right hand side of Eq. (3.21) represents the elastic force that neighboring CH units exert on each other. The second and third terms correspond to

the average force with which the whole electron system acts on the atoms on n^{th} site. The prime indicates that the summations are restricted to the occupied electronic states.

The solution to the lattice equations can be written as,

$$\begin{aligned} u_n(t_{j+1}) &= u_n(t_j) + \dot{u}_n(t_j)\Delta t \\ \dot{u}_n(t_{j+1}) &= \dot{u}_n(t_j) + \frac{F(t_j)}{M}\Delta t. \end{aligned} \tag{3.22}$$

Hence, the electronic wave functions and the displacement coordinates at the $(j+1)^{\text{th}}$ time step are obtained from the j^{th} time step. Periodic boundary conditions are assumed for the electronic wave functions, ψ_ν, and the lattice displacements, u_n.

This process of getting u (and $\dot{u}$), as shown in Eq. 3.22, is known as Euler method for solving ordinary differential equations. For the Euler method, the global truncation error is proportional to Δt. To test the accuracy of this method, we have performed a couple calculations (one for $E = 2.6 \times 10^5$ V/cm and the other for $E = 5.0 \times 10^6$ V/cm) using second-order Runge-Kutta method which has a global truncation error proportional to Δt^2. The same results for charge densities and energies have been obtained in both cases.

The total number of lattice points on the chain in all simulations is $N = 100$ and the total number of electrons on the chain N_e is 98 resulting in a positive bipolaron. The motion of the bipolaron is studied with the help of smoothed charge density [104]:

$$\bar{\rho}_n = \frac{1}{4}(\rho_{n-1} + 2\rho_n + \rho_{n+1}) \tag{3.23}$$

where ρ_n is calculated from the electronic wave functions as follows,

$$\rho_n = 1 - \sum_{\nu}{}' \psi_\nu^*(n,t)\psi_\nu(n,t). \tag{3.24}$$

A time step of $\Delta t = 0.036$ femtosecond (fs) is used. For most systems, we follow their dynamics up to 54 fs, that is, 1500 time steps. It is recognized that 54 fs is a relatively short time. A simple calculation shows that the period (T) of a stretching mode of the double bond can be approximately estimated as 20 fs (that is obtained by assuming that if the energy of mode is roughly 0.2 eV, then $T = 1/f = h/E \approx 20$ fs). [35] However, we have found that charge density and energy trends do not change when the time is increased (we have performed calculations up to 72 fs or more to verify this in a few cases). This is also illustrated in Fig. 4.7 where the energies are plotted and the dynamic is followed up to 288 fs. Other cases, where we follow the dynamics for longer times, are: in Fig. 4.3 up to 288 fs in order to estimate the velocity of a bipolaron (for a moderate E) and in Fig. 4.4 up to 180 fs to illustrate the net charge polarization and oscillations in the presence of a very strong E .

It should be noted that the above model Hamiltonian does not include the electron-electron repulsive Coulomb interactions. This will be addressed in the next part of this work.

3.3 Extended SSH Model with e-e Interactions

We apply extended SSH model with e-e interactions to PT. The structure of PT also can be viewed as consisting of a backbone of sp^2 hybridized carbon atoms that is stabilized by S covalently bonded to carbon atoms. [71] The Hamiltonian [38, 49, 51, 52] used to describe the PT has the following form:

$$\begin{aligned} H &= -\sum_n [t_0 - \alpha(u_{n+1} - u_n) - t_1 \cos\frac{n\pi}{2}] \\ &\times (e^{-i\gamma A} c^+_{n+1,s} c_{n,s} + e^{i\gamma A} c^+_{n,s} c_{n+1,s}) \end{aligned}$$

$$
\begin{aligned}
&+U\sum_n(n_{n\uparrow}-\frac{1}{2})(n_{n\downarrow}-\frac{1}{2}) \\
&+V\sum_n(n_n-1)(n_{n+1}-1) \\
&+\frac{1}{2}K\sum_n(u_{n+1}-u_n)^2+\frac{M}{2}\sum_n\dot{u}_n^2
\end{aligned} \tag{3.25}
$$

where U and V are the on-site and the nearest-neighbour Coulomb repulsion strengths, respectively. For PT the following parameters were selected: $a = 1.22$ Å, $t_0 = 2.5$ eV, $t_1 = 0.39t_0$, $K = 26$ eVÅ^{-2}, $\alpha = 3.5$ eVÅ^{-1}, $U = 0.9t_0$ and $V = 0.8U$. These parameters give good agreement between theoretical and experimental values for the bond lengths and the band gap in PT's ground state and for its static bipolaron energy levels. For example, the experimentally determined bond lengths of PT are: $r_{c=c} = 1.357$ Å, $r_{c-c} = 1.433$ Å and $r_{c-c} = 1.48$ Å (between rings). [70] Our corresponding values are 1.356 Å, 1.430 Å and 1.486 Å. The experimental value for the band gap is 2.0 eV [70] and our value is 2.01 eV. In the presence of a bipolaron, our energies above the top of the valance band edge are 0.68 eV and 1.39 eV, which compare well with the experimental values of 0.65 eV and 1.45 eV. [41]

The time-dependent unrestricted Hartree-Fock equations for one-particle wave functions are given in reference [49]:

$$
\begin{aligned}
i\hbar\dot{\psi}_{\nu,s}(n,t) &= -[t_{n,n+1}+V\tau_s(n,t)]\psi_{\nu,s}(n+1,t) \\
&\quad -[t^*_{n-1,n}+V\tau^*_s(n-1,t)]\psi_{\nu,s}(n-1,t) \\
&\quad +\{U[\rho_{-s}(n,t)-\frac{1}{2}]+V\sum_{s'}[\rho_{s'}(n+1,t) \\
&\quad +\rho_{s'}(n-1,t)-1]\}\psi_{\nu,s}(n,t)
\end{aligned} \tag{3.26}
$$

where

$$
\begin{aligned}
t_{n,n+1} &= e^{-i\gamma A}[t_0-\alpha(u_{n+1}-u_n)-t_1\cos\frac{n\pi}{2}] \\
\rho_s(n,t) &= \sum_\nu{}' \psi^*_{\nu,s}(n,t)\psi_{\nu,s}(n,t)
\end{aligned}
$$

$$\tau_s(n,t) = \sum_{\nu}{}' \psi^*_{\nu,s}(n+1,t)\psi_{\nu,s}(n,t).$$

The time-dependent Hartree-Fock equation is integrated by introducing single-electron eigenstates at a given time t_j. The solution can then be expressed in the form [104]:

$$\begin{aligned}\psi_{\nu,s}(n,t_{j+1}) &= \sum_l [\sum_m \phi^*_{l,s}(m,t_j)\psi_{\nu,s}(m,t_j)] \\ &\quad \times e^{-i\varepsilon_l \Delta t/\hbar}\phi_{l,s}(n,t_j) \end{aligned} \tag{3.27}$$

where$\{\phi_l\}$ and $\{\varepsilon_l\}$ are the eigenfunctions and the eigenvalues of the electronic part of the Hamiltonian $H(t)$ at a given time t_j.

The motion of the the lattice displacement is given classically by the equation:

$$M\ddot{u}_n(t) = F_n(t) \tag{3.28}$$

where

$$\begin{aligned} F_n(t) &= -K(2u_n(t) - u_{n+1}(t) - u_{n-1}(t)) \\ &\quad +\alpha \sum_{\nu,s}{}' e^{-i\gamma A}[\psi^*_{\nu,s}(n,t)\psi_{\nu,s}(n+1,t) \\ &\quad -\psi^*_{\nu,s}(n-1,t)\psi_{\nu,s}(n,t)] \\ &\quad +\alpha \sum_{\nu,s}{}' e^{i\gamma A}[\psi^*_{\nu,s}(n+1,t)\psi_{\nu,s}(n,t) \\ &\quad -\psi^*_{\nu,s}(n,t)\psi_{\nu,s}(n-1,t)]. \end{aligned} \tag{3.29}$$

The lattice equations also can be written as,

$$\begin{aligned} u_n(t_{j+1}) &= u_n(t_j) + \dot{u}_n(t_j)\Delta t \\ \dot{u}_n(t_{j+1}) &= \dot{u}_n(t_j) + \frac{F_n(t_j)}{M}\Delta t. \end{aligned} \tag{3.30}$$

Hence, the electronic wave functions and the displacement coordinates at the $(j+1)^{\text{th}}$ time step are obtained from the j^{th} time step. Periodic boundary conditions are assumed for the electronic wave functions, $\psi_{\nu,s}$, and the lattice displacements, u_n.

The total number of lattice points on the chain in all simulations is $N = 104$ and the total number of electrons on the chain N_e is 102 resulting in a positive bipolaron. The motion of the bipolaron is studied with the help of smoothed charge density [104]:

$$\bar{\rho}_n = \frac{1}{4}(\rho_{n-1} + 2\rho_n + \rho_{n+1}) \tag{3.31}$$

where ρ_n is calculated from the electronic wave functions as follows,

$$\rho_n = 1 - \sum_{\nu,s}{}' \psi^*_{\nu,s}(n,t)\psi_{\nu,s}(n,t). \tag{3.32}$$

A time step of $\Delta t = 0.036$ femtosecond (fs) is used. We follow the dynamics of the system up to 54 fs, that is, 1500 time steps for most of our calculations.

Chapter 4

Results and Conclusions

4.1 Part A: Extended SSH Model (no e-e Interactions)

4.1.1 Bipolaron and Polarons (no Electric Field Present)

First, we consider the charge densities and energetics of a bipolaron and two polarons in the heterocyclic polymer. In their lowest state, both excitations (bipolaron and two polarons) introduce localized energy levels: 0.83 eV and 1.54 eV above the top of the valence band in the case of bipolaron and 0.34 eV and 2.03 eV in the case of two polarons. It should be noted that with increasing numbers of polarons and bipolarons on a single chain, the corresponding polaron and bipolaron bands begin to form. For example for two polarons, there are two nearly degenerate bottom and top energy levels in the intraband region. For two bipolarons the localized bipolaron energy levels do not spread either. However, when three bipolarons are placed on 100 lattice points, the bipolaron bands begin to form; energy levels (in eVs) are -1.1839 (top of valence), -0.3580, -0.3559, -0.3513, 0.3513, 0.3559, 0.3580, 1.1839 (bottom

Table 4.1: Total energies and their differences (ΔE) of systems containing a bipolaron (E_{bi}) and two polarons (E_{po}) that are computed with a Hamiltonian that includes electron-electron interactions (which in turned are described by the parameter U) for $\alpha = 4.5$ eV/Å.

U(eV)	E_{bi}(eV)	E_{po}(eV)	ΔE(eV)
0	-323.5200	-323.0484	-0.47
1.25	-354.5571	-354.2243	-0.33
1.5	-360.8392	-360.5305	-0.30
2.5	-386.2056	-385.9868	-0.22
2.8	-393.8882	-393.7012	-0.18
3.0	-399.0283	-398.8669	-0.16
3.6	-414.5365	-414.4903	-0.05
3.8	-419.7532	-419.7436	0.01
4.0	-424.9487	-425.0191	0.07
4.6	-440.6791	-441.2557	0.58
5.5	-463.4211	-464.8232	1.4

of conduction). In Fig. 4.1 (a) and (b), the respective charge densities for a bipolaron and two polarons are plotted (at t=0 fs using Eqs. (3.23) and (3.31) for cases without and with e-e interactions respectively). The width, at the base, of a bipolaron and a polaron is very similar (approximately 24 sites or 6 rings). The charge of a bipolaron is twice that of a polaron as can be seen from Fig. 4.1 (a) and (b).

For the parameters as given in the section 2 of Chapter 3, the comparison of the total energies indicates that the bipolaron is more stable than the two polarons by

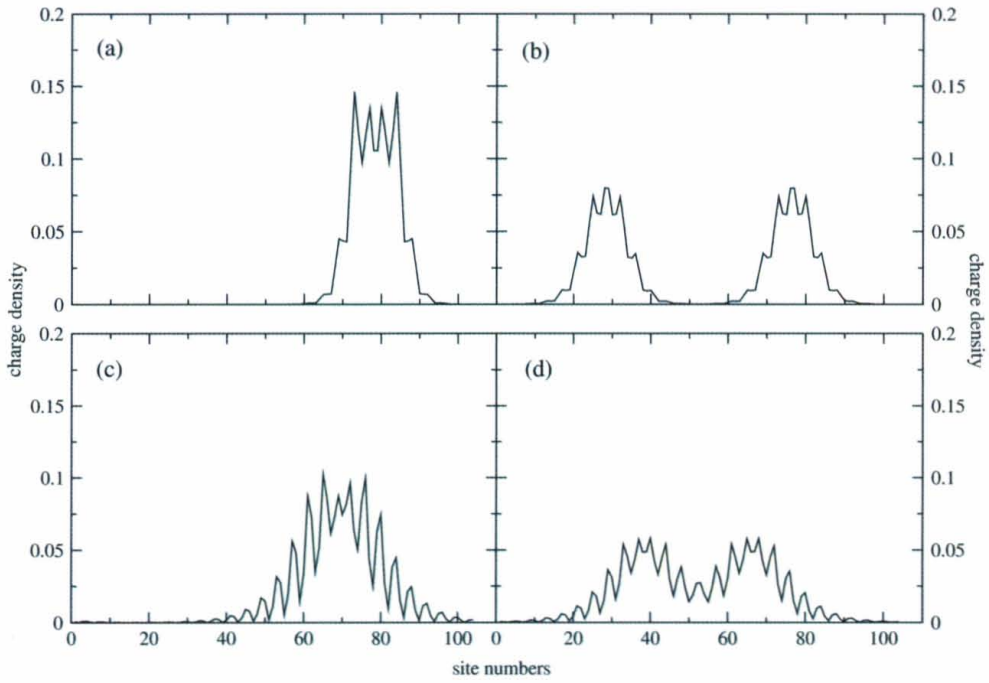

Figure 4.1: Excess charge densities (defined as number of holes per site), $\rho(n)$, of bipolaron (a) and two polarons (b) without e-e interactions and of bipolaron (c) and two polarons (d) with e-e interactions ($U = 2.25$ eV and $V = 1.8$ eV) plotted as a function of site number, n. The site numbers correspond to the projected positions of ions along the chain backbone. The integral of excess charge density over the whole length of the chain is 2e.

approximately 0.5 eV (see Table 4.1). Another way of estimating the binding energy of the bipolaron versus two polarons involves the intra band energy levels. [113] If we assume that the lattice distortion energy due to formation of one bipolaron is roughly the same as that required to form two polarons [113], then once again the bipolaron is more stable than two polarons by approximately 0.5 eV (=(0.83-0.34) eV). Other studies estimate the binding energy of a bipolaron to be somewhere in the range 0.2-0.5 eV. [94] In fact, the stability of the bipolaron versus two polarons continues to be a controversial subject as discussed in Chapter 2. In this thesis, the main focus is on the effect of an electric field once bipolaron is formed (and there is some evidence that it is formed under certain circumstances). Two calculations with $E = 2.6 \times 10^5$V/cm and $E = 2.0 \times 10^4$V/cm were performed up to 180 fs to illustrate what happens when electric field is applied to a positively charge polymer without first forming a bipolaron. No bipolaron is formed when $E = 2.6 \times 10^5$V/cm, charge density is delocalized along the chain and oscillates from positive to negative every two sites (the net charge remains 2e). When $E = 2.0 \times 10^4$V/cm, charge density is still delocalized over the whole chain but some charge polarization begins to emerge and charge density oscillates with larger amplitude. These calculations show that bipolaron does not form even in the presence of very weak electric field such as $E = 2.0 \times 10^4$V/cm, hence the bipolaron must be formed before the electric field is applied.

The strengths of the e-ph coupling (α) and e-e interactions (U) play an important role in the formation of stable bipolaron versus two polarons. As a precursor to Part B, we briefly consider the effect of e-e interactions in the static case (i.e. $t = 0$ when $E = 0$) and summarize our results in Table 4.1, where we vary U from 0 to 5.5 eV while keeping $\alpha = 4.5$ eV/Å. Up to $U = 3.6$ eV the bipolaron remains more stable than the two polarons, then the two polarons become more stable, eventually the

bipolaron (around $U = 5.5$ eV) can not be formed and only polarons exist. Typically $U \sim 2$ eV for physical systems such as PT.

4.1.2 Charge Density

In the presence of an electric field, the bipolaron will move along the chain which can be considered as a quasi one-dimensional system. We study the effect of the electric field on the bipolaron motion as the magnitude of the electric field varies from weak (2.6×10^5 V/cm), moderate (2×10^6 V/cm), strong (5×10^6 V/cm), and to very strong (7×10^6 V/cm). In Fig. 4.2 we plot charge densities as well as the lattice displacements at a time of 54 fs (1500 time steps). First we consider the cases of weak and moderate fields as shown in Fig. 4.2 (a) and (b). In both cases, the charge carriers are tightly trapped by the lattice, forming a bipolaron which is localized to 24 sites. Relative to the initial bipolaron position (near 80th site), the bipolaron in a weak electric field (see Fig. 4.2 (a)) moves to $\sim$ 60th site after 54 fs. As the strength of an electric field is increased to 2×10^6 V/cm, the bipolaron moves (faster) to 50th site (see Fig. 4.2 (b)). After the initial acceleration, we estimate that the charges (two holes) and the lattice displacement move with an approximate velocity of 3×10^6 cm/s when $E = 2 \times 10^6$ V/cm. To show this more clearly we plot the movement of the bipolaron (to the left) at various times (36 fs (1000th time step), 180 fs (5000th) and 288 fs (8000th)) in Fig. 4.3 (which also illustrates the use of periodic boundary condition that was implemented in all simulations). At all times the total charge of the system remains 2e.

It can also be seen from Fig. 4.3 that the width of the bipolaron appears to change as function of time. M. Kuwabara et al. [114] showed that the width of a moving charged soliton in PA exhibits oscillations. In their work, the width is estimated from

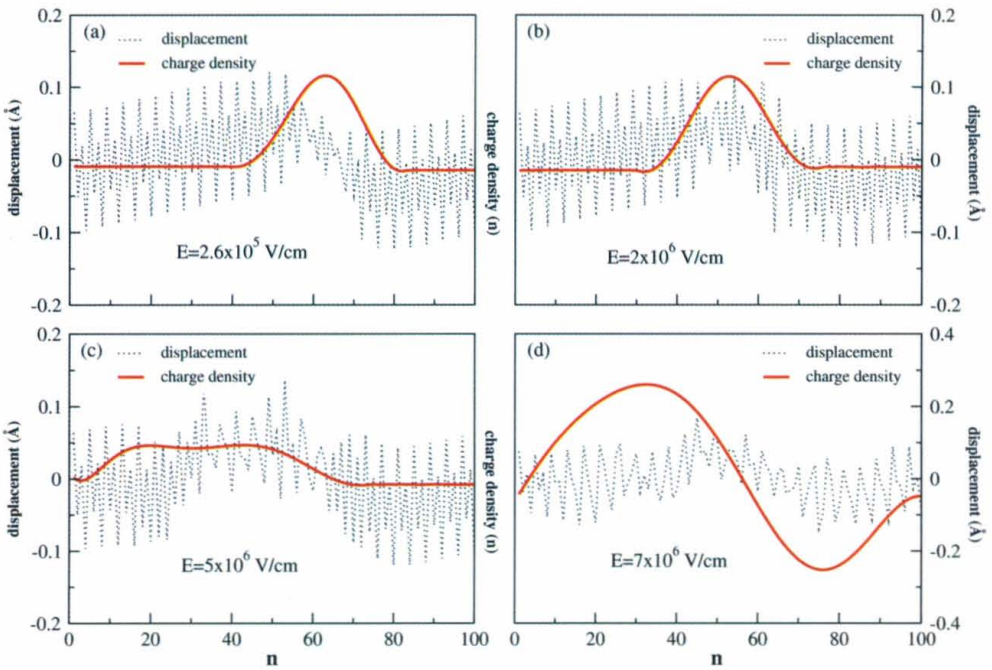

Figure 4.2: Displacements of ions from equilibrium positions, u (in Å) and excess charge densities, $\rho(n)$ (number of holes per site) plotted as a function of site number, n, and determined at $t = 54$ fs (1500th time step), in the presence of electric fields: (a) 2.6×10^5 V/cm, (b) 2×10^6 V/cm, (c) 5×10^6 V/cm, and (d) 7×10^6 V/cm (the shape of the bipolaron is smoothed out to avoid unnecessary details).

the excess charge density profile and the distortion in the lattice displacements. Both methods suggested that the width of the charged soliton decreases with increasing velocity. In our work, we use primarily the excess charge densities to estimate the width of the moving bipolaron (although it should be noted from Fig. 4.2 (a) and (b) that the extent of the lattice distortion closely matches the width of the excess charge density in the case of the weak and moderate electric fields). In order to discuss the finer details regarding the width of the bipolaron we also include the original excess charge densities in Fig. 4.3 (in addition to the fitted curves). We calculate (but not show in the figure) the excess charge densities and their fits for times steps from 0 to 10000th in units of 1000 time steps. We note that the excess charge density profiles for bipolarons have rather complicated shapes (in contrast to polarons or solitons). One way to assess their widths is to consider the distances (expressed in units of Δn =n(peak#2) -n(peak#1) where n is the site number) between the two peaks corresponding to approximate locations of constituent charges in the bipolarons. It appears that after the 1000th time step this distance (Δn) decreases to 7 (from 11) and stays 7 for the remaining time. A more informative way is to model the excess charge density profiles with fitted curves as shown in Fig. 4.3. That is, we estimate the width for the bipolaron by calculating the width at the half full length (w) for fitted excess charge density. The complicated superposition of the charge densities in the center of the bipolaron combined with the height and the symmetry variations of the peaks give rise to different widths of the fitted charge densities. The results ($(w - w_0)/w_0$ where w_0 is the width at 0th time step) are plotted in the Fig. 4.3 as an inset. The main conclusion of this analysis is that bipolaron width as modeled by the fitted data increases initially after the electric field is switched on and decreases till 7000th time step and then begins to increase again relative to w_0 (hence it appear to be exhibiting oscillatory behaviour).

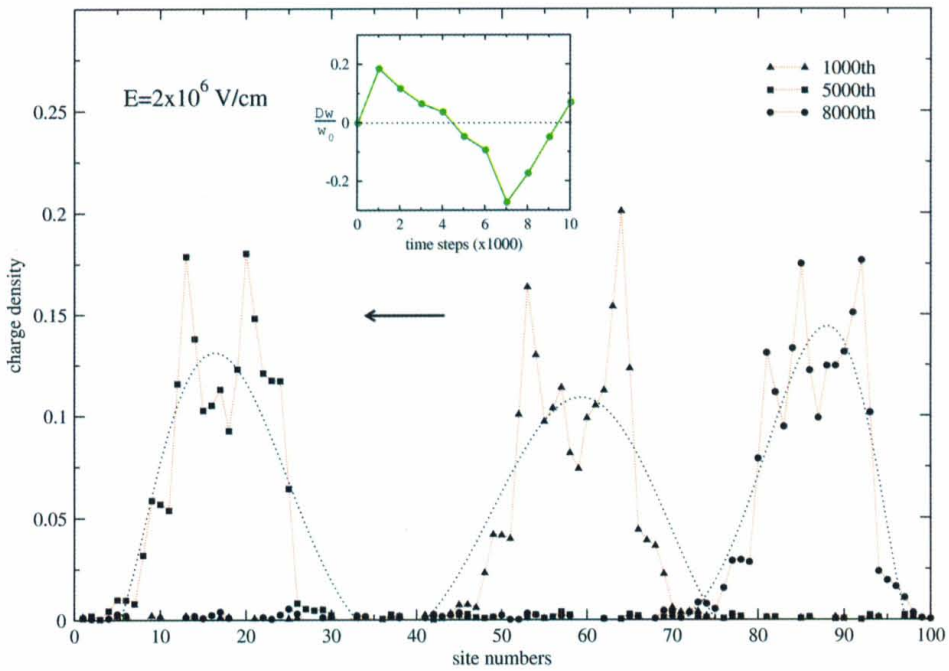

Figure 4.3: The positions of a bipolaron when $E = 2 \times 10^6$ V/cm are shown at various times: $t = 36$ fs (1000th time step), 180 fs (5000th) and 288 fs (8000th) (the shape of the bipolaron is smoothed out to avoid unnecessary details). The inset shows the variation of the relative width difference, Dw/w_0=(w-w_0)/w_0, of bipolaron with time steps where w is the taken as the measure of the bipolaron width and is calculated at the half full length of the fitted excess charge density and w_0 is the width at 0th time step.

In Fig. 4.2, it can be seen that for each ring in a heterocyclic polymer, there are four different values for u corresponding to four bond lengths as discussed in section 2. Without a bipolaron, there would be no drifting of u values. The presence of a bipolaron, with or without the electric field, makes the u values more positive as the location of a bipolaron is approached, i.e. the u values drift upwards. However, the bond lengths do not change. In the region where the bipolaron is located the upward drift pattern of u's is disrupted. In this region bond lengths change, i.e. the aromatic structure of the polymer is replaced with the quinoid like structure which involves the lengthening of "double" bonds and shortening of "single" bonds. Similar behavior for u's has been observed for a polaron. [115]

In the strong electric field of 5×10^6 V/cm (see Fig. 4.2 (c)), the "bipolaron" spreads out, most of the charge density oscillates over a range of 50 sites: negative charge is formed and the total positive and negative charge are 2.1307e and -0.1307e respectively (the net charge is always 2e). In this case, the motion of the lattice can not keep up with the charged particles such as holes (see Fig. 4.2 (c)). For example, we estimate that at 54 fs, the center of the charge density moves with a speed of approximately 1×10^7 cm/s and the lattice displacement with a speed of approximately 7×10^6 cm/s when $E = 5 \times 10^6$ V/cm. The value of the calculated lattice displacement velocity should be compared with the maximum sound velocity of PT. It has been deduced from experimental measurements that the sound velocity in PT is about 1×10^6 cm/s. [116] A quick estimation, using the formula $v = \omega/k = 4a/T$ where $\omega = 2\pi/T$ and $k = \pi/2a$ with $T = 20 \times 10^{-15}$ s and $a \approx 1$ Å or 10^{-8} cm gives maximum phonon velocity (with maximum phonon energy of 0.2 eV) for PT as 2×10^6 cm/s. [35] This shows that the calculated lattice displacement velocity is three or more times larger than the experimentally determined maximum sound velocity in PT. Since lattice can not move faster than its maximum sound velocity, it follows that

charge density must decouple from the lattice when its sound speed reaches maximum value. In the very strong electric field of 7×10^6 V/cm (see Fig. 4.2 (d)), the charge density is greatly polarized, i.e. half of the polymer is predominantly positive and the other half predominantly negative (the net respective charges are 9.0946e and -7.0946e). This large polarization is in part due to the model that we are using since Coulomb interactions are not explicitly included in the model Hamiltonian (see Eq. (1)).

The other contributing factor is the fact that charges (the two holes) are free to move along the chain especially for the electric field strengths of the order of 7×10^6 V/cm. This results in a positive and negative charge accumulations that evolve as a function of time as is shown in Fig. 4.4 (a) where the net negative charge is plotted as a function of time steps. The largest negative charge (approximately -7e) occurs around 1500 time steps. The net negative charge decreases to approximately -5.5e at later times: 1750 and 2000 time steps and then beginning at approximately 2500 time steps it oscillates with a relatively shallow amplitude around -2e value (representative charge densities at various time steps are shown as insets in Fig. 4.4 (a)). Similar behavior is observed for the net positive charge (not shown in this paper) since the net charge must remain 2e. That is, the charge density is continuously changing as long as electric field is applied (the polymer is not in a stable equilibrium state). It should be pointed out that as an additional check, we have performed a calculation of the ground state without the bipolaron at the same electric field strength and observed no chain polarization in that case. Hence we believe that the observed polarization phenomena is due to the presence of the net non-zero charge. In summary, the strength of an electric field plays an important role in the charge transport in heterocyclic polymers.

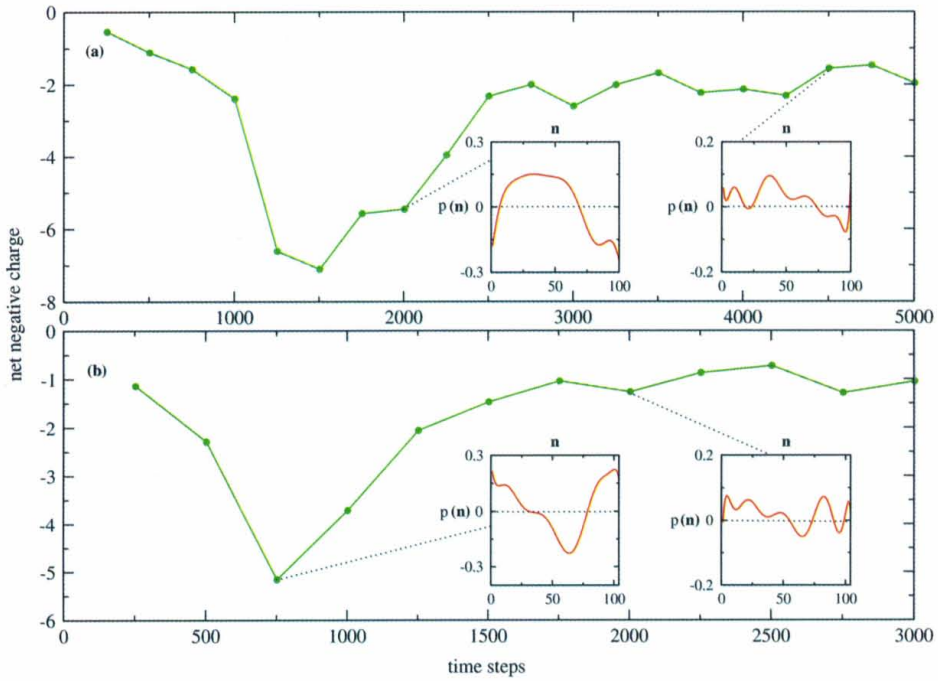

Figure 4.4: Net negative charge density as a function of time steps for electric field equal to 7×10^6 V/cm. (a) without e-e interactions; (b) with e-e interactions.

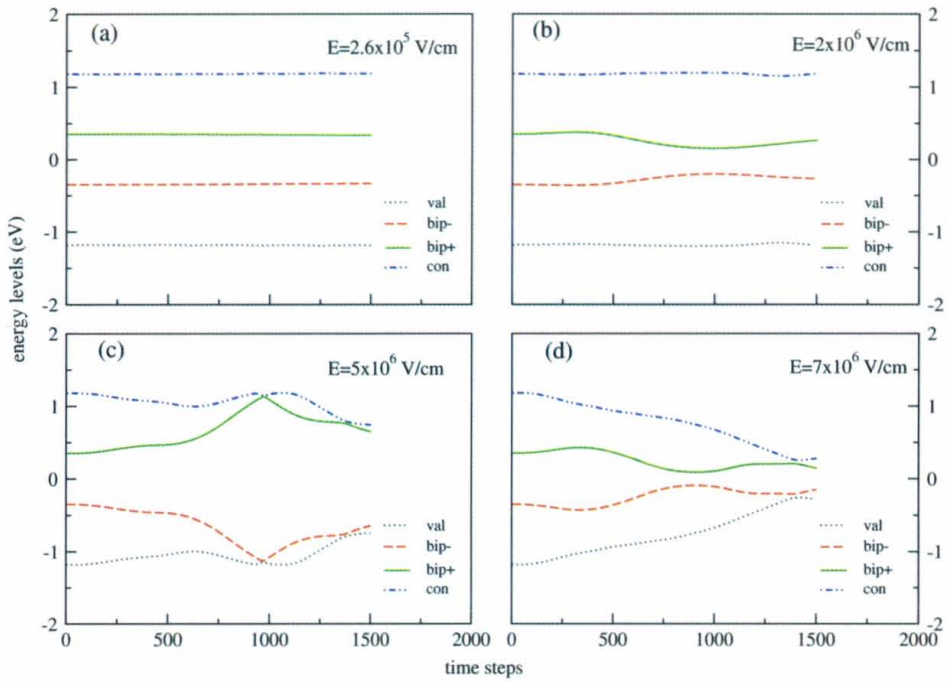

Figure 4.5: Energy levels in the presence of electric fields: (a) 2.6×10^5 V/cm, (b) 2×10^6 V/cm, (c) 5×10^6 V/cm, and (d) 7×10^6 V/cm.

4.1.3 Top Eigenvalues

The behavior of the charge densities is reflected in that of the electronic energy levels. The top electronic band structure of a perfectly dimerized (having all 'single' bonds of the same length and all 'double' bonds of the same length) neutral heterocyclic chain consists of a valence band and a conduction band. In the ground state, the valence band is completely filled, and the conduction band is empty. When a (charged) bipolaron is formed, the band structure of the SSH model is symmetric about the middle of the gap and two energy levels appear in the gap (bip- and bip+ in Fig.

4.5), which correspond to the bipolaron state. For the weak and moderate electric field (see Fig. 4.5 (a) and (b)), the energy levels change little, which means that the bipolaron is affected by the electric field to some degree, but its main character remains unchanged. However, in a strong electric field 5×10^6 V/cm (see Fig. 4.5 (c)), the energy levels change significantly. In fact, bipolaron as such ceases to exist after certain time and its energy levels merge with the valence and conduction band of the polymer. In this process, the band gap decreases somewhat from over 2 eV to 1.5 eV. When the electric field is very strong (see Fig. 4.5 (d)), the process of the bipolaron levels merging with the valence and conduction bands continues and band gap decreases further to approximately 0.5 eV. At this point, the main charge storage species are predominantly free charge carriers such as holes and electrons. However, the material remains a semiconductor.

4.1.4 Total Energy Analysis

In order to increase our understanding of the above results even further, we also calculate the total electronic, lattice potential and lattice kinetic energies as a function of time. They are defined as follows [101],

$$\varepsilon_{ele}(t) = \sum_s \sum_\nu{}' \sum_l \varepsilon_l (\sum_n \phi^*_{l,s}(n,t)\Psi_{\nu,s}(n,t))^2 \tag{4.1}$$

$$\varepsilon_{pot}(t) = K/2 \sum_n (u_{n+1}(t) - u_n(t))^2 \tag{4.2}$$

$$\varepsilon_{kin}(t) = M/2 \sum_n \dot{u}_n^2(t) \tag{4.3}$$

and

$$\varepsilon_{tot}(t) = \varepsilon_{ele}(t) + \varepsilon_{pot}(t) + \varepsilon_{kin}(t). \tag{4.4}$$

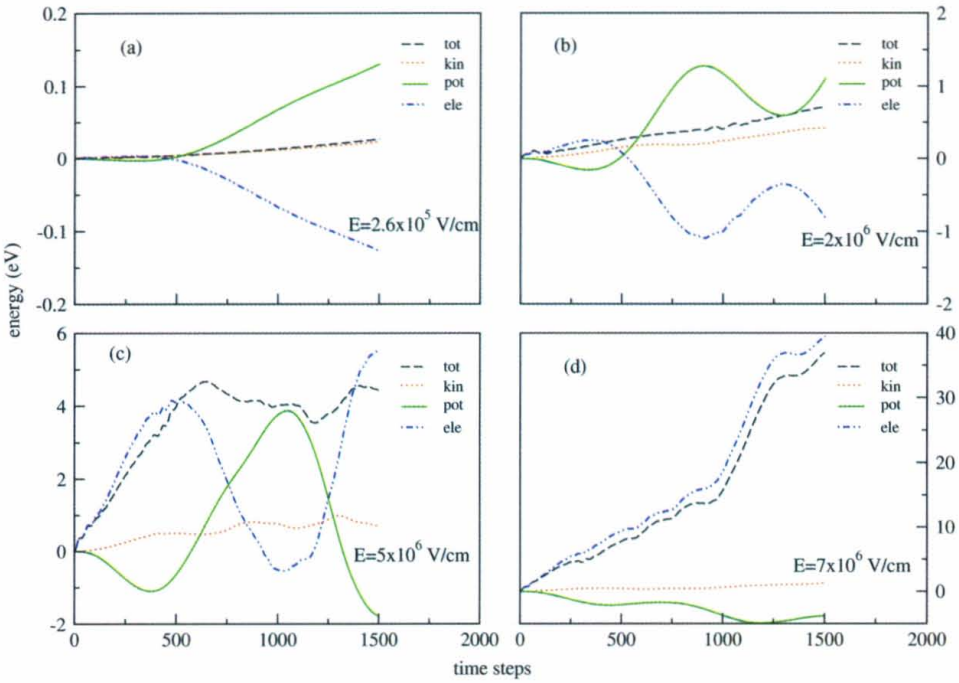

Figure 4.6: Electronic, potential, kinetic and total energies (see Eqs. 4.1 - 4.4 and text below) in the presence of electric fields: (a) 2.6×10^5 V/cm, (b) 2×10^6 V/cm, (c) 5×10^6 V/cm, and (d) 7×10^6 V/cm.

Again the prime attached to the summation symbol denotes the sum over occupied states. In Fig. 4.6, $\varepsilon_{ele}(t) - \varepsilon_{ele}(0)$, $\varepsilon_{pot}(t) - \varepsilon_{pot}(0)$ and $\varepsilon_{tot}(t) - \varepsilon_{tot}(0)$ are depicted instead of $\varepsilon_{ele}(t)$, $\varepsilon_{pot}(t)$, $\varepsilon_{tot}(t)$.

It can be seen that the lattice potential energy and the electronic energy are out of phase with each other for the weak and moderate electric fields as is shown in Fig. 4.6 (a) and (b). This suggests strong correlation between the electrons and the lattice. That is, the lattice must play an important role in the motion of excess

charge. This is illustrated in Fig. 4.6 (a) where in the presence of a weak electric field the potential energy increases almost linearly with time as the electronic energy decreases also nearly linearly with time. As an aside, we can estimate the velocity, v, of the bipolaron as 7×10^6cm/s (which is approximately twice as large as obtained for the moderate electric field) using an expression $\frac{\Delta E}{\Delta t} = Fv = qEv$ where $q = 2e$ and $\frac{\Delta E}{\Delta t} = 3.7 \times 10^{12}$eV/s from Fig. 4.6 (a). [35] This means that the intrachain mobility can be estimated to be $\mu = v/E = 25$ cm^2/sV which suggests that, if the speed of the bipolaron remains constant, then the mobility will increase as E decreases. [35] To check this, we calculate the mobility of the bipolaron at lower electric fields such as $E = 1.0 \times 10^5$V/cm and $E = 2.0 \times 10^4$V/cm. We obtain $\frac{\Delta E}{\Delta t} = 5.6 \times 10^{11}$eV/s, $v = 2.8 \times 10^6$cm/s and $\mu = 28$ cm^2/sV for $E = 1.0 \times 10^5$V/cm, and $\frac{\Delta E}{\Delta t} = 2.0 \times 10^{10}$eV/s, $v = 5 \times 10^5$cm/s and $\mu = 25$ cm^2/sV for $E = 2.0 \times 10^4$V/cm. The main conclusion is that as the electric field decreases the velocity of the bipolaron also decreases (i.e. it does not remain constant), hence the intrachain mobility remains relatively constant (it first increases to 28 cm^2/sV and then decreases to 25 cm^2/sV for the two electric fields respectively).

When the electric field is 2×10^6 V/cm as indicated in Fig. 4.6 (b), the corresponding increase in potential energy and decrease in electronic energy show similar overall trends. However in this case the potential and electronic energies also display out of phase oscillations in their respective curves. To show that this behaviour persists as a function of time in the presence of a moderate field (2×10^6 V/cm) we plot the total energies up to 288 fs (8000 time steps) in Fig. 4.7. In addition, using the above classical formula (i.e. $\Delta E = Fv\Delta t = qEv\Delta t$) potential energy increase can be estimated during the time interval of 288 fs as 3.5 eV which agrees fairly well with what is shown on Fig. 4.7. The two cases, Fig. 4.6 (a) and (b), clearly show that the lattice deformation couples with the charge carriers to form a bipolaron. Their total

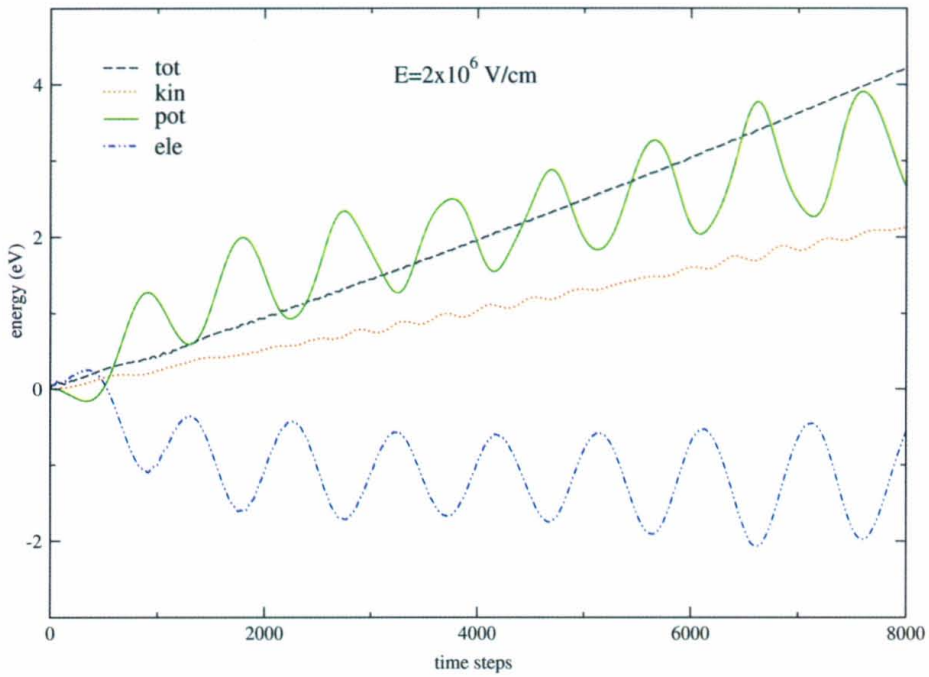

Figure 4.7: Electronic, potential, kinetic and total energies plotted as a function of time for $E = 2 \times 10^6$ V/cm.

and kinetic energies are increasing relatively slowly with time. In the Fig. 4.6 (c), the lattice potential and electric energy are also out of phase, but the oscillations in the electronic energy are larger than those of the potential energy and can be positive indicating that charges are less bound to the lattice in comparison to the two previous cases with weaker electric fields. Consequently, the total energy is no longer close to zero. Kinetic energy contribution due to ions remains small. From Fig. 4.6 (d), we see that the total energy of the system nearly equals to the positive electronic energy which clearly suggests that the presence of free charge carriers. That is, the main

charge carriers are holes and electrons when the electric field is very strong, although some lattice deformation still exists.

4.2 Part B: Extended SSH Model with e-e Interactions

4.2.1 Charge Density

As in Part A we first plot charge densities of a static (the electric field is zero) bipolaron and two polarons (see Fig. 4.1 (c) and (d)). In both cases the e-e interactions (U = 2.25 eV) broaden the shape of their charge densities. For example, the half-height width of a bipolaron spreads over approximately 25 sites as opposed to 15 sites for the bipolaron without the e-e interactions and the height of the bipolaron with e-e interactions in comparison to the one without is reduced from 0.15 to 0.1. This broadening of the charge density shapes is easily accounted for by the fact that e-e interactions are predominantly repulsive causing charges to separate further apart, however, the net charge (corresponding to the area under the ρ curve) remains 2e resulting in the wider and flatter bipolaron (and polaron) shape. The total energy of a static bipolaron is -423.9798 eV which is 0.40 eV lower than the total energy of two static polarons (-423.5831 eV) showing that within the current theoretical model a bipolaron is more stable than two polarons when e-e interactions are included. As in Part A we can also estimate the stability of the bipolaron versus two polarons using their intra band energy levels and the same assumptions. [113] These show that the bipolarons are more stable than two polarons by approximately 0.65 (~0.68-0.04) eV to 0.35 (~0.44-0.07) eV. The two values arise because alpha and beta electrons have different energy levels in the case of two polarons and intra band energies are

no longer symmetric about the middle of the band for both bipolarons and polarons.

When an electric field is present, bipolaron propagates along the quasi-one dimensional PT chain and similar results are obtained for the excess charge density as in Part A. To illustrate some of the differences we consider what happens to net negative charge in the presence of the very strong electric field. We plot the net negative charge for $E = 7 \times 10^6$ V/cm as a function of time in Fig. 4.4 (b). Without the e-e interactions (see Part A) the chain becomes highly polarized (i.e. positive charge accumulates at one end of the chain and negative at another) and then oscillates around -2e value (see Fig. 4.4 (a)). With the e-e interactions the large accumulation of negative (and positive) charge occurs initially as is shown by the insets in Fig. 4.4 (b). The minimum in the net negative charge occurs at 750 time step (where the net negative and positive charges are -5.146e and 7.146e) which is earlier than 1500 time step when no e-e interactions were included. Similarly, the onset of the shallow oscillations observed in the case of no e-e interactions also begins at earlier time (at approximately 1750 time steps) and the oscillations are around -1e value (instead of -2e). In both cases, these oscillations are attributed to smaller (alternating) domains of positive and negative regions of charge that are formed along the chain (and can be seen in the insets in Fig. 4.4). The earlier times for the minimum and the onset of the shallow oscillations and the shift to higher (negative) value around which the oscillations occur in the net negative charge when e-e interactions are included is another consequence of stronger repulsive interactions between electrons. That is, the net negative (and by inference net positive) charge accumulations are smaller in the case when e-e interactions are present. In summary, the strength of an electric field has a significant effect and e-e interactions have a more subtle effect on the charge transport in PT.

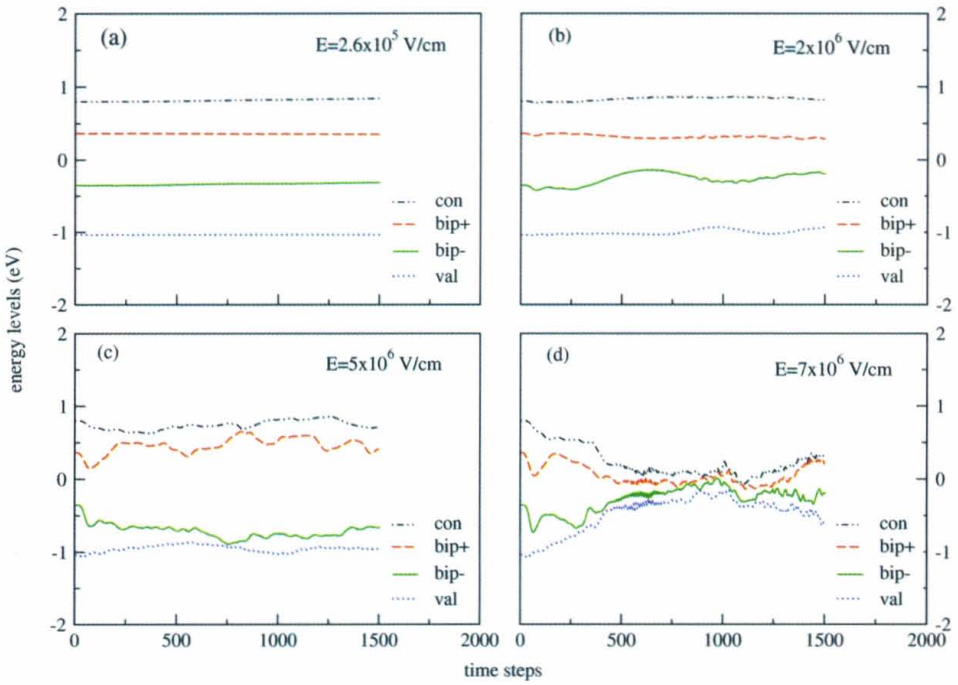

Figure 4.8: Top energy levels of positively charged (+2e) PT in the presence of an electric field: (a) 2.6×10^5 V/cm, (b) 2×10^6 V/cm, (c) 5×10^6 V/cm, and (d) 7×10^6 V/cm.

4.2.2 Top Eigenvalues

In Fig. 4.8, we plot the four top eigenvalues as a function of time for PT under the influence of an electric field. When PT is doped and a (positive) bipolaron is formed, the band gap decreases (in our case from 2.01 to 1.83 eV) and, as in Part A, two intra band energy levels appear in the gap. For the weak and moderate electric field (see Fig. 4.8 (a) and (b)), the results are very similar to what was observed when no e-e interactions were included (see Fig. 4.5 (a) and (b) in Part A).

In a strong electric field 5×10^6 V/cm (see Fig. 4.8 (c)), the energy levels change significantly. The gap between the bipolaron energy levels increases from 0.71 eV ($t = 0$) to 1.06 eV ($t = 54$ fs) and the gap between valance and conduction bands decreases from 1.83 to 1.67 eV ($t = 54$ fs). That is, the bipolaron levels merge with the valence and conduction band of PT (again similar to what was observed in Part A). This indicates the disappearance of a bipolaron and formation of free charges, a behaviour similar to charged inorganic semiconductor. When the electric field is very strong (see Fig. 4.8 (d)), the merging process continues, however in this case both band gap and gap between bipolaron levels decrease significantly (they are 0.91 eV and 0.40 eV respectively at $t = 54$ fs) forming an energy band of four almost overlaping levels at some points. At these points, the system nearly becomes a conductor, however as it evolves in time the gap grows again and PT remains a semiconductor with a very small energy gap. The main charge storage species are predominantly free charge carriers such as holes and electrons. This behaviour is again very similar to what was observed when no e-e interactions were included in Part A.

4.2.3 Total Energy Analysis

As in Part A we also calculate the total electronic, lattice potential and lattice kinetic energies and plot them as a function of time in Fig. 4.9. They are defined as in Part A of this section. Figs. 4.9 (a) and 4.9 (b) have similar features as observed in Fig. 4.6 (a) and (b). That indicates that, in all these cases, the lattice must play an important role in the motion of excess charge since as the lattice potential energy grows, the electric energy decreases. Figs. 4.9 (c) and 4.9 (d) are quite similar in appearance (and resemble Fig. 4.6 (d) in Part A). To understand what causes the

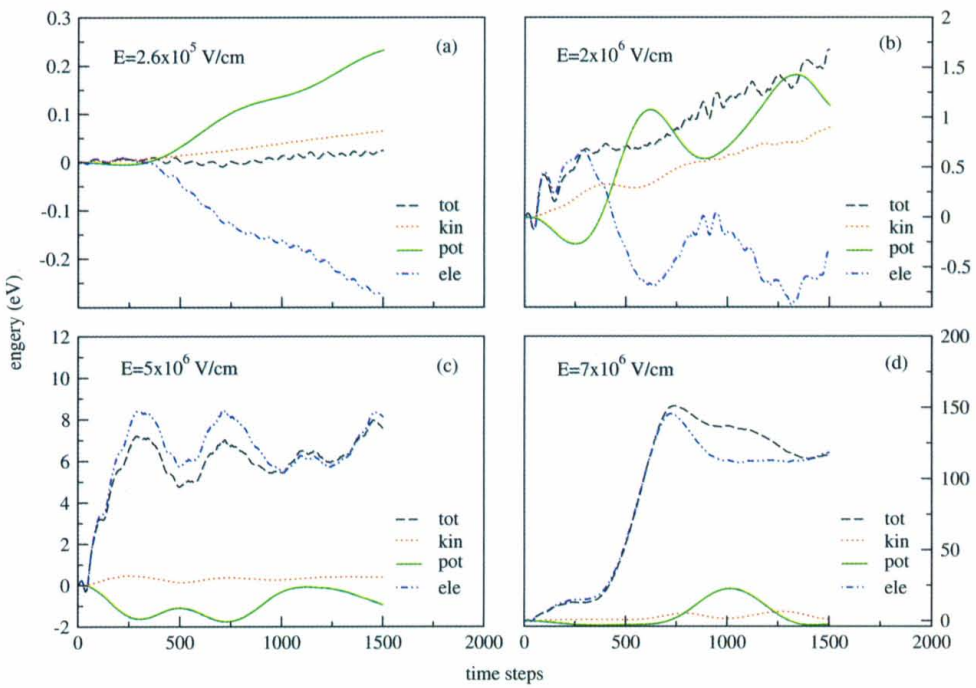

Figure 4.9: Electronic, potential, kinetic and total energies (see Eqs. 11–14) of positively charged (+2e) PT in the presence of an electric field: (a) 2.6×10^5 V/cm, (b) 2×10^6 V/cm, (c) 5×10^6 V/cm, and (d) 7×10^6 V/cm.

change in the (total and electronic) energy slopes, Figs. 4.6 (d) and 4.9 (d) should be compared with Figs. 4.4 (a) and (b) respectively. This comparison shows that the slope changes occur when the charge density of the polymer becomes highly polarized (corresponding to the minima in Fig. 4.4). Figs. 4.9 (d) and 4.4 (b) also show that the energies level off when the charge density begins to oscillate along the chain. In each case, the total energy of the system is nearly equal to the positive electronic energy which clearly suggests that the presence of free charge carriers. It should be noted that there is large variation in energy scales for different fields (for example, in Fig. 4.9 (a) the energies are of the order of 0.1 eV, in (b) of 1 eV, in (c) of 10 eV and in (d) of 100 eV).

4.3 Conclusions

Numerical simulations indicate that in the absence of an electric field and within the SSH model without the e-e interactions, in heterocyclic conjugated polymers (as described by the generic parameters used in Part A), a bipolaron is more stable than two polarons. When e-e interactions are included in the SSH Hamiltonian and the model is applied to PT, we still obtain the result that a bipolaron is more stable than two polarons. However, this conclusion is clearly dependent on the strength of the e-e interactions (which are appear to be relatively weak in PT) in comparison to the e-ph coupling. It is possible that in other heterocyclic conjugated polymers, the e-e interactions play a more significant role and the bipolaron is no longer stable compared to separated two-polaron state. Hence, for PT, the extended SSH model (with and without e-e interactions) suggests that the electric field has important effect on the motion of the bipolaron: in a weak (2.6×10^5 V/cm) or moderate (2×10^6 V/cm) electric field, bipolaron propagates with some shape change, but continues to

remain strongly coupled to the lattice; in strong (5×10^6 V/cm) or very strong (7×10^6 V/cm) electric field, bipolaron dissolves and free charge carriers determine the charge transport. A strong or very strong electric field may initially lead to a polarized charge density with positive and negative charges occupying different regions of the polymer. At later times, in the presence of a very strong field, the charge density forms alternating negative and positive regions along the chain backbone, with the net negative charge oscillating around -2e (no e-e interactions) or -1e value (with e-e interactions). The charges are essentially free electrons and holes. The energy analysis reveals that strong interactions between lattice and charge carriers predominate in a weak or moderate electric field; free charge carriers play an important role in strong or very strong electric field. In summary, in PT, e-e interactions widen bipolaron in comparison to one without e-e interactions, but they do not significantly affect the nature of its transport.

Part II

Charge Mobility in Conjugated Polymers with Application to Solar Cells

Chapter 5

Introduction

As stated in the Chapter 1 materials made of organic conjugated polymers have found many uses in devices such as OLEDs, OFETs, solar cells (OPVCs) and so on. In particular, organic solar cells will become important devices to solve the world environment and energy needs. Many energy experts estimate that the world will need 30 terawatts (TW) of energy by the year 2050 which should be compared to today's 13 TW of energy usage. The new energy resources should not damage our environment. To satisfy growing energy demands without destroying the environment, the sun is proposed as the source of energy. [117] Solar cell is the device that converts the energy of sunlight directly into electricity. In majority commercial applications silicon-based photovoltaic cells are used. However, in the past decade, OPVCs have become increasingly important for many reasons. They offer low cost and easy of processability. [119] OPVCs also operate better at low light levels (i.e. indoor applications) compared with most inorganic PVCs. [118, 119] The silicon-based PVCs have efficiencies in excess of 20% and operational lifetimes of more than 25 years. In the 1980s and early 1990s, the OPVCs because of their low efficiency were not able to compete with silicon-based devices. The OPVCs' performance has improved in

recent years, their efficiencies can be as high as 7% and their estimated operational lifetimes are of the order of 20,000 h. [118, 119] For example, thus far, the best power conversion efficiency (PCE), of the order of 6-7% [120, 121, 122], has been reported for polymer bulk heterojunction (BHJ) OPVCs involving electron-donating alternating conjugated co-polymers and electron-accepting fullerenes such as C_{70} derivatives. One of the remaining problems with OPVCs is that high efficiency and long lifetime have not been obtained in the same device. However, since these improvements have been shown in separate materials, it is likely that they will be obtained in a future single device.

Current research indicates that there are many factors that determine the efficiency of organic solar cells. [123, 124, 125] Most importantly, the material(s) used in the active layer of OPVCs should have a broad absorption in the solar spectrum, suitable band gaps and energy levels, and high carrier mobilities for the polymer, and the appropriate bulk nanoscale morphology. For example, it has been postulated that for optimal performance of BHJ cells, the conjugated polymers should have a band gap between 1.2 and 1.9 eV, since low-band gap polymers can better harvest the solar spectrum,[119, 126, 127] with the highest occupied molecular orbital (HOMO) energy in the range -5.2 to -5.8 eV, the lowest unoccupied molecular orbital (LUMO) in the range -3.7 to -4.0 eV, and a hole mobility higher than 10^{-3} $cm^2V^{-1}s^{-1}$. [128, 129]

Historically, the best performing polymer solar cells were made with regioregular poly(3-hexylthiophene) (P3HT) as donor materials, they achieved an efficiency surpassing 5%. [130] However, the relatively large band gap (around 1.9 eV) of P3HT limits its absorbance from the solar cell spectrum to below a wavelength of 650 nm. [127] Poly[2-methoxy-5-(3',7'-dimethyloctyloxy)-p-phenylenevinylene] (MDMO-PPV) [131] and other conjugated (thiophene based (e.g. [132]) and otherwise) polymers [119, 127] suffer from similar problems. Another group, alternating co-polymers

containing cyclopentadithiopene and benzothiadiazole (BT) units [133, 134, 135] displayed high charge carrier mobilities (and low band gaps) and hence a promise (as yet not realized) of potentially significantly increased PCE values.

Recently, the use of carbazole (see Fig. 5.1) as one of the units in the alternating co-polymers led to the development of many low band gap materials.[127] Initially, the improvements were made with the use of thiophene(s) as co-monomers in these alternating co-polymers.[136] Later, BT, as well as thiophene and cabazole units were used.[126, 128] These three units (BT (or similar N based cyclic unit), thiophene and carbazole, see Fig. 5.2 for the corresponding chemical structures) were used as co-monomers in a number of alternating co-polymers which, in turn, were used to construct organic BHJ solar cells.[128] The properties of these conjugated polymers and corresponding solar cells were then extensively studied. This research indicated that poly(N-9'-heptadecanyl-2-7-carbazole-alt-5,5-(4',7'-di-2-thienyl-2',1',3'-benzothiadiazole)) (PCDTBT) has the highest hole mobility among the poly(2,7-carbazole) (PC) derivatives studied and its corresponding blended material with [6,6]-phenyl C_{61} butyric acid methyl ester ($PC_{61}BM$) gave a relatively good performance in BHJ solar cells. In general, it was also found that symmetric polymers (PCDTBT, PCDTQx) because of higher structural order gave hole mobilities approximately an order of magnitude higher than asymmetric polymers (PCDTPT, PCDTPP) with one exception, both PCDTBX and PCDTPX gave similar mobilities in the pristine state. In addition to the carbazole based polymers which are characterized by their hole mobilities, the electron mobility in poly(9,9-di-n-octylfluorene-alt-benzothiadiazole) (F8BT) (see Fig. 5.3 for its chemical structure) is also studied. [137] The main goal of the Part II of the thesis is to investigate the hole and electron mobilities in the organic conjugated polymers with computational methodology based on their chemical structure and bulk morphology.

Figure 5.1: The chemical structures of fluorene monomer, carbazole monomer and BTT.

First it should be noted that most organic semiconductor devices use polymer films that are relatively amorphous and/or heterogeneous, once formed (e.g. upon doping or through other means) their charges are delocalized within the conjugation length, forming entities such as polarons, that are mostly confined to move along the polymer chain. In the presence of an (external or local) electric field, a hopping model (as oppose to band model), that involves movement of charges (electrons or holes) between polymer chains, is an appropriate mechanism to account for the bulk charge transport in organic semiconductors. [7] Given that the hopping is the main mechanism of charge transport, the computational method implemented in this thesis is similar to the one as proposed by Athanasopoulos et al. [56] for the determination of mobilities in conjugated polymers (PF in their case). The important component of their model for charge transport is that it incorporates explicitly the chemical structure of the polymer. The first step in their approach involved obtaining the relaxed (fully optimized) geometries of the short oligomers corresponding to the spatial extent of charge transporting unit (such as polaron for example) with the use of DFT with the hybrid B3LYP functional. This was followed by calculations of the transfer integrals

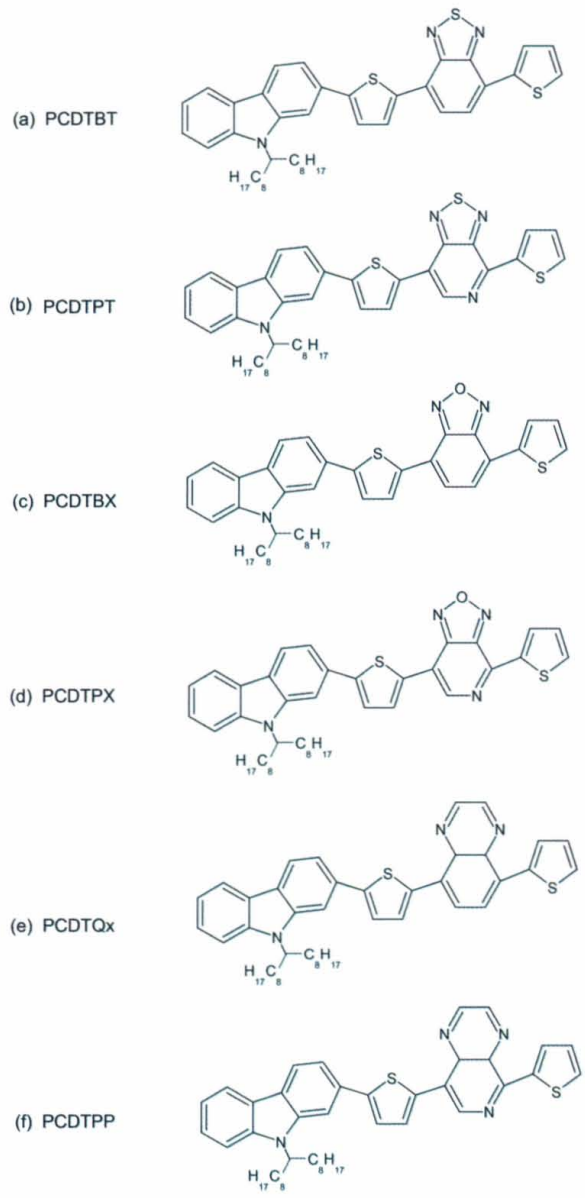

Figure 5.2: The chemical structures of the monomers of carbazole derivatives: (a) PCDTBT, (b) PCDTPT, (c) PCDTBX, (d) PCDTPX, (e) PCDTQx, (f) PCDTPP.

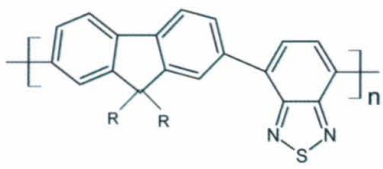

Figure 5.3: The chemical structure of F8BT.

(t's) using the molecular orbital overlap (MOO) method [58] which employed the intermediate neglect of differential overlap Hamiltonian with Zerner's parameterization (ZINDO/S) to obtain atomic overlap (equivalent to molecular orbital overlap) from a single self-consistent field (SCF) calculation on one isolated (DFT geometry optimized) oligomer [58]. The intermolecular transfer rates (Γ's) were then determined using the Marcus-Hush theory [138, 14] which in addition to transfer integrals required the determination of reorganization energies (λ's) (again using DFT method). MC transport simulations of hopping under an applied electric field (a biased random walk) were then performed for given bulk ordered morphologies. These morphologies were based on the observed structures of the crystalline and bulk fluorene polymer material. [56]

In this thesis, the above steps with some variations (details of the proposed computational approach are given in Chapter 6) are applied to known (select few) organic conjugated polymers [119, 128, 137] as discussed above. Namely, in Chapter 7, first pure fluorene and cabazole polymer systems (see Fig. 5.1) are considered and their

transfer rates and mobilities are determined. This is followed by calculations of hole mobilities for more complicated (pristine) polymer (PCDTBT, PCDTPT, PCDTBX, PCDTPX, PCDTQx and PCDTPP, see Fig. 5.2) systems and of electron mobility for F8BT (see Fig. 5.3). The above polymer systems have been primarily chosen to test the proposed computational methodology because the experimental values for their hole [128] and electron [137] mobilities are available for comparison and calibration purposes. It is hoped that greater understanding of the trends in the experimentally determined hole and electron mobilities in organic conjugated polymers can be obtained with the use of the proposed computational methodology. For example, it is expected that it will be possible to establish which polymers (i.e. which chemical structures) and/or, which morphological arrangements (crystalline or disordered etc.) could lead to improved mobilities. In addition, future work will involve computations of mobilities for the heterogeneous systems that include promising conjugated polymers and fullerene derivatives (such as $PC_{61}BM$ or $PC_{71}BM$). The results presented in Chapter 7 have been submitted for publication. [139]

Chapter 6

Multi - Step Computational Approach

6.1 Geometry Optimization

Similar to what was proposed in reference [56], the first step in the proposed approach involves obtaining optimized molecular structures of short oligomers (monomers, dimers, and trimers) with the use of DFT/B3LYP/6-31G* method. [140] This method has proven to be an efficient way for calculating the molecular structures for conjugated organic oligomers (see for example reference [141]). For most conjugated polymers, polarons are the main charge carries. Typically, polarons extend over more than 2 nm (20 Å) along polymer chain. For pure fluorene and carbazole polymers, monomers are too short (typically 7-8 Å long) and trimers should be used to contain the spatial extent of a polaron, however, for the purpose of determining trends in transfer rates we consider monomers and dimers as well as trimers. For carbazole derivatives (see Fig. 5.2), ones that contain, for example, BT, two thiophenes and carbazole units, monomers (typically longer than 2 nm) are long enough to contain

a polaron. For computational expediency, the octyl side chains in carbazole and fluorene units are replaced by H atoms in all calculations (however, it should be noted that side chains are important for the three-dimensional (3D) packing).

6.2 Transfer Integrals

The next step in the proposed procedure involves the calculation of transfer integrals which essentially describe intermolecular overlaps of electronic wave functions and typically are difficult to compute accurately for a number of reasons that will be briefly mentioned below. The description of the actual procedure used in this work will then be given. A method of calculating electron transfer integral using the two-state model and within the Hartree-Fock (HF) approximation was proposed in 1998. [142] Early on it was recognized that even a first-order evaluation of the transfer integral is difficult because many different physical factors (overlap, relaxation and polarization of MO's for example) contribute to t. In reference [143], the authors argue that, the amplitude of the transfer integral which is related to the strength of interaction between two organic oligomers (and is often referred to as an electronic coupling in contract to a electron-phonon coupling) is extremely sensitive to the molecular packing (distance and orientation of oligomers in a cluster) and is inherently related to the HOMO and LUMO energy splitting that occurs when going from an isolated oligomer to interacting oligomers (typically dimers). They determine t using molecular orbital levels within the one-electron picture using semiemperical HF INDO method (as developed by Zerner) for systems such as sexithienyl molecules, oligoacenes etc. and illustrate that cofacial configurations lead to largest t. For another example of this, see also more recent work [144] which shows that for oligofluorenes the increase in the interunit angle leads to a decrease in an electronic coupling between oligomers

and a subsequent decrease in charge mobility. Based on the energy splittings, it is also pointed out [143] that in π-conjugated polymers, electrons as well as holes can give rise to high mobilities. Reference [145] gives a good summary of theory involved in determining t using both the "dimer" method for isolated molecules and the"band width" method (the so called single band approximation) for the extended solid state systems and shows that the value of t depends on the level of theory (semiemperical, HF, DFT, other post HF methods) used in the evaluation of t. One important conclusion relevant to this work is that t should be evaluated using one method when comparing systems' mobilities directly.

More recently, it is pointed out that the "simple" energy dimer splitting method fails when the localized monomer MO's are nonorthogonal. [146] They showed that the correct energy splitting between the dimer's HOMO and HOMO-1 levels for hole mobilities (or LUMO and LUMO+1 levels for electron mobilities) is obtained when a transformation from nonothogonal to orthogonal localized basis set is made. This corrected expression is especially relevant when dealing with two molecules in the dimer that are not symmetrically equivalent since in this case the molecules polarize each other. They carried out their calculations using predominantly DFT with B3LYP functional. This methodology has been used recently to calculate mobilities in disordered C_{60} thin films. [62] The one disadvantage of this approach is that the determination of the energy splitting requires the knowledge of explicit values of matrix elements (overlap and otherwise) that are not readily available from standard computational software.

Yet others pointed out that the value of t can be significantly affected by the thermal motion of molecules. In reference [147] it is shown (with the use of both molecular dynamics (MD) and quantum mechanical (QM) computations) that thermal fluctuations in t can be of the same order as their average over a period of time

due to t's sensitivity to intermolecular distance and orientation. More recently, it is shown, by employing DFT and molecular mechanics (MM) simulations, that the interaction of charge carriers with QM treated lattice vibrations (phonons) plays a key role in the charge-transport properties in organic semiconducting (molecular) crystals [148] and the nonlocal electron-phonon interactions should be included in evaluation of t. Given all these findings we have tried to find a middle ground for evaluating t, a method that is more general than the "dimer" energy splitting but not as complicated as the recent theories that take electron-phonon coupling into account for example. That is, our aim in this work is to develop an approach that is both expedient (from a computational point of view) and accurate enough to provide insight as well as aid in the estimations of mobilities in organic conjugated polymers. We believe the projective method, which will be summarized below, is a good compromise. [58, 149]

As stated above, the (equilibrium) transfer integral can be formally defined as an expectation value of the system Hamiltonian between two multielectron wavefunctions corresponding to two separate molecules involved in the charge transport. [58] Assuming that the multielectron wavefunctions are single Slater determinants and invoking the frozen-core approximation, where it is assumed the determinants differ only by the uppermost MO's (HOMO's in the case of hole transport and LUMO's in the case of electron transport), the above defined integral reduces (using Slater-Condon rules [150]) to a calculation of an expectation value of a Fock matrix between the corresponding HOMO's or LUMO's.

The relative orientation and distance between the two molecules play an important role in determining the value of the transfer integral and hence in the transport properties of a given molecular system. [56] In addition, most of our oligomers are not strictly planar (for example, the dihedral angle between thiophene and carbazole planes is of the order of 30-40^o), hence, we must first establish a common procedure

(i.e. one that can be used for both planar and nonplanar structures) of determining the 'plane' of one oligomer relative to which the second oligomer's orientation can be determined. There is no unique way of doing this. In principle, we can use the locations of all or of a subset of atoms in a given molecule to be fitted to a plane. We have chosen to use all backbone (non hydrogen) atoms in our fits. That is, we fit a plane to a set of points (i.e. coordinates of backbone atoms in a given oligomer) by a least squares plane method (which involves solving a set of simultaneous equations using the eigenvalue-eigenfunction approach [151, 152, 153]). Given a plane, we determine the coordinate system relative to this plane (one axis is perpendicular to the plane, another lies along the line between two farthest points on the plane, the third axis is determined by a cross product with the other two axis). We then transform the original molecular coordinates to new coordinates corresponding to the new set of axis. The position of the second molecule is determined by applying translation (and possibly rotation) operation relative to the first. In our initial study of pure fluorene and carbazole oligomers, we consider three types of orientations (cofacial, CF, (often referred as π-stacking), hexagonal, HX, and side-by-side, SS) between two molecules as shown in Fig. 6.1.

For the carbazole derivatives we primarily consider π-stacking orientation between monomers. The distances (d's) between the planes of the two molecules are initially determined with the use of the experimental values (when available). They are also estimated by fitting our mobilities to the corresponding experimental ones (again when available).

Once the method of determining the orientation and the distance between the molecules is defined, we employ the projective method (instead of MOO which was used in [56]) as described in reference [58] to evaluate the transfer integrals, really the expectation value of the Fock matrix as defined above. The projective method (see

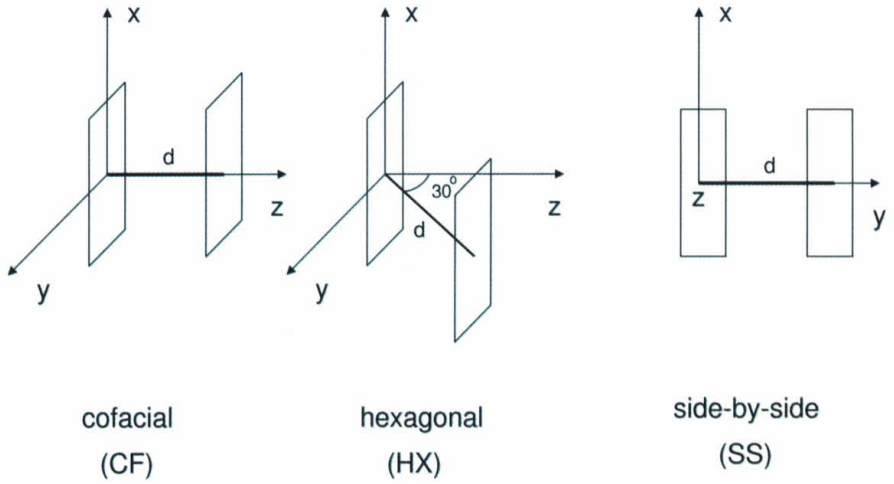

Figure 6.1: The relative orientations of the molecules in the pairs: cofacial (CF) or π-stacking, hexagonal (HX, one molecule is in the center and the other is in front or behind it 30^o off the vertical line) and side-by-side (SS, in the same plane).

also [149]) uses the spectral theorem (which in turn involves a change of basis sets and matrix diagonalization [154]) and requires two (really three) SCF calculations: two for single molecules, one at the origin and another at the required distance and orientation relative to first, and another for a pair of molecules involved in the charge transfer. In this method the orthogonal molecular orbitals (as represented by their coefficients of linear expansion and obtained from the ZINDO calculations using the DFT optimized geometries) of individual molecules are used to build a local basis set (C_{loc}, $N \times N$ Hermitian block diagonal matrix consisting of columns of eigenvectors corresponding to the N occupied eigenstates) which is then projected onto a pair basis set (C_{pair}, also $N \times N$ matrix) consisting of the molecular orbital coefficients of the pair in order to obtain the orbitals of the pair in the localized molecular orbital space, i.e. the localized pair basis set, $C^{loc}_{pair} = C^{t}_{loc} C_{pair}$. A transformed Fock matrix in the new localized basis set of the pair, $F^{loc}_{pair} = C^{loc}_{pair} E_{pair} C^{loc\ t}_{pair}$, is then obtained

where $E_{pair} = C^t_{pair} F_{pair} C_{pair}$ is the diagonal matrix consisting of the eigenvalues of the Fock matrix for the pair and the transfer integral is read off from the appropriate off-diagonal element of the new Fock matrix F^{loc}_{pair}, for a full description see reference [58].

6.3 Reorganization Energies

The reorganization energies, for both the hole and the electron transport, must be determined for the calculations of transfer rates. Physically, the reorganization energy is the energy required to force the reactants to have the same nuclear coordinates as the products without electron transfer (in the reactions involving electron transfer). [138] If molecular vibrations and polarizations due to the surrounding medium are neglected (i.e. the external contributions to reorganization energies are ignored as is the current practice in most of the simulations of mobilities), then the reorganization energy for the hole transfer in the reaction that involves acceptor (A) and donor (D) molecules, i.e. $D + A^{\bullet +} \longrightarrow D^{\bullet +} + A$ can be approximated by a sum of differences between the vertical and adiabatic ionization potentials (IP's) (vertical IP is defined as the process involving electron removal for which the nuclear coordinates in both neutral and positive ions are the same, corresponding to the ground state of neutral molecule; adiabatic IP is defined as the process in which the nuclear coordinates of neutral and positive ions are optimized, both neutral and positive ions are in their relaxed ground states) of the neutral donor (D) and between the vertical and adiabatic electron affinities (EA's) of radical cation acceptor ($A^{\bullet +}$). [14, 155] That is, the hole reorganization energy (λ_h) is given by $\lambda_h = (E_{neut}(D^{\bullet +}) - E_{opt}(D^{\bullet +})) + (E_{radc}(A) - E_{opt}(A))$ where $E_{neut}(D^{\bullet +})$ and $E_{opt}(D^{\bullet +})$ are the energies of the $D^{\bullet +}$ calculated at the neutral (neut) and optimal (opt) cation geometries respectively (their subtraction cor-

responds to the difference between the vertical and adiabatic IP's of the neutral D), and $E_{radc}(A)$ and $E_{opt}(A)$ are the energies of A at the radical cation (radc) and optimal ground-state geometries respectively (corresponding to the difference between the vertical and adiabatic EA's of $A^{\bullet+}$). Similarly, for the electron transfer in the reaction $D^{\bullet-} + A \longrightarrow D + A^{\bullet-}$, the electron reorganization energy (λ_e) can be approximated by a sum of differences between the vertical and adiabatic IP's for the radical anion donor ($D^{\bullet-}$) and between the vertical and adiabatic electron affinities (EA's) (vertical and adiabatic EA's are defined similarly to IP's, see above) of the neutral acceptor (A) and is given by $\lambda_e = (E_{rada}(D) - E_{opt}(D)) + (E_{neut}(A^{\bullet-}) - E_{opt}(A^{\bullet-}))$ where $E_{rada}(D)$ and $E_{opt}(D)$ are energies of the neutral D calculated at the radical anion (rada) and optimal ground-state geometries respectively (this contribution corresponds to the difference between the vertical and adiabatic IP's of the $D^{\bullet-}$), and $E_{neut}(A^{\bullet-})$ and $E_{opt}(A^{\bullet-})$ are the energies of $A^{\bullet-}$ at the neutral and optimal geometries respectively (corresponding to the difference between the vertical and adiabatic EA's of neutral A). All energies are calculated at the level of DFT/B3LYP/6-31G* for consistency and since, as stated above, B3LYP is a functional that is frequently used in electronic structure studies of organic conjugated systems. It should be noted that the actual values the reorganizations energies (similar to transfer integrals) depends to some extent on the ab initio and/or DFT method used to compute the corresponding energies (see for example reference [156]). We feel that for the purpose of this study the B3LYP/6-31G* values are adequate to illustrate the procedure (of determining the mobilities) proposed in this work.

6.4 Transfer Rates and Mobilities

Transfer rate Γ_{ij} is computed using Marcus-Hush theory [138, 14] where Γ_{ij} is given by

$$\Gamma_{ij} = \frac{t_{ij}^2}{\hbar}\sqrt{\frac{\pi}{\lambda k_B T}}\exp\{-\frac{(\Delta G_{ij}-\lambda)^2}{4\lambda k_B T}\} \tag{6.1}$$

Γ_{ij} depends on the electronic transfer integral (t_{ij}), the molecular reorganization energy (λ), and the temperature (T). In Eq. (6.1), k_B is the Boltzmann's constant; $\hbar$ is Planck's constant divided by 2π and $\Delta G_{ij} = e\Delta \mathbf{r}_{ij} \cdot \mathbf{E}$ is the free energy difference between initial and final sites with Δr_{ij} being the distance between sites, e, the magnitude of an electric charge, and E the electric field respectively (since the (torsional) structures of the oligomers do not change after electron transfer, no free energy due to conformational changes is included in ΔG_{ij}). The reorganization energy is determined using the methodology introduced in references [14, 155] and the evaluation of the transfer integral employs the projective method as discussed in reference [58], and in the above respective sections in this chapter.

The mobility is proportional to intermolecular charge (hole or electron) transfer rate Γ_{ij}, We employ the MC method [157] to calculate the mobilities (μ's) of the systems studied.

As an example of calculating 3D mobilities for the ordered (crystalline) polymer system, we model a film of poly(9,9'-dioctylfluorene) (PF) and poly(2,7-carbazole) (PC) as aligned trimers on a hexagonal lattice where the oligomers are parallel both to each other and normal to the substrate (see Chapter 7). The oligomers are arranged coaxially in columns as a model of a continuous chain along the x direction. The electric field is along the y-axis. The oligomer position is determined by the midpoint of the oligomer relative to the (x,y,z) axes (see discussion above for the definition of coordinate system). The 3D simulation system consists of 2000 planes of 20×20

points in the x-z plane (corresponding to the projections of the hexagonal oligomers' positions onto the x and z directions) with periodic boundary conditions applied along these (x and z) directions. Using a similar procedure we also model 3D hole mobilities for carbazole derivatives in crystalline state with tetragonal unit cell and electron mobility for F8BT in a crystalline state with monoclinic unit cell (see Chapter 7). In addition, since most pristine polymer films are amorphous (i.e. they contain certain disordered regions mixed in with crystalline domains) we include some orientational disorder in our 3D mobility simulations for the carbazole derivatives (with tetragonal unit cell). The results of these calculations are discussed in the Chapter 7.

A MC transport simulation is executed on the model system in the following way: for a charge on site i, waiting times τ_{ij}'s are determined for a hop from site i to each of its eight nearest neighbor sites j, using an expression: $\tau_{ij} = -ln(X)/\Gamma_{ij}$, where X is a random number uniformly distributed between 0 and 1, and Γ_{ij} is the transfer rate as given in Eq. (6.1). It should be noted that transfer rates in Tables 7.2, 7.4, 7.6 and 7.7 are calculated with the electric field (and hence ΔG_{ij}) set equal to zero. We have found that for weak or moderate electric fields (of the order of 10^4 V/cm or so that were used in this work) the transfer rates did not change very much when ΔG_{ij} was included in the calculations of Γ_{ij}. In all other cases whenever the transfer rates are used in the mobility calculations, the electric field was not set to zero and was included in the Γ_{ij} computation as given in Eq. 6.1. The hop with the smallest waiting time is chosen and executed and the simulation time (i.e. trajectory time) is increased by τ_{ij}. We follow the trajectory of a hole randomly placed on a monomer in the film and calculate the time for the hole to travel a fixed distance d, (2000 cell widths for 3D simulations that employed in model systems with known symmetry (hexagonal, orthorhombic, tetragonal or monoclinic are used in this thesis) and 20000 lattice sites for 1 dimensional (1D) simulations) in the field direction. A

transit time is averaged over several trajectories (of the order of 10-100 since averaging over larger number of trajectories does not change the result) and $\langle\tau\rangle$ is obtained. The mobility μ is computed using an expression, $\mu = d/(\langle\tau\rangle E)$, where E is the magnitude of an electric field (taken as 4×10^4 V/cm in this work in most cases). It is known experimentally that intrachain mobility of a charge [158] is typically much larger (could be as larger by a factor of 100 or more (e.g. see discussion on page 44)) and will in effect contribute little to the overall 3D bulk mobility which is limited by the charge hopping between the chains. Hence we found that determining 1D mobility (charge moving preferentially in the direction of the electric field) is often sufficient to give realistic (first order) estimate of the bulk mobility. This effect will be discussed in Chapter 7.

Chapter 7

Results

7.1 Transfer Rates: Fluorene and Carbazole Oligomers

First transfer integrals and transfer rates for short fluorene and carbazole oligomers were determined to assess the dependence of the value of the transfer integral and transfer rates on the size of the oligomer and on the orientation of the two molecules in a given pair. We consider fluorene monomer (FM) (repeat unit of fluorene based polymers such as PF, see Fig. 5.1), dimer (FD), and trimer (FT) and carbazole monomer (CM) (repeat unit of carbazole based polymers such as PC, see Fig. 5.1), dimer (CD), and trimer (CT). For each pair of molecules, three types of orientations are investigated: CF, HX and SS as shown in Fig. 6.1. The distances between the centers of the molecules are taken as 4.4 Å (intermolecular distance expected in cofacial orientation [159, 160, 161, 162, 163]), 5.0 Å (an intermediate value) and 6.5 Å (value suggested in [56]) for the CF configuration and 5.0 Å and 6.5 Å for the HX and SS orientations. When possible, reorganization energies are also determined for monomers, dimers and trimers. The results are presented in Tables 7.1 and 7.2 for the hole transport and Tables 7.3 and 7.4 for the electron transport.

Table 7.1: The hole transfer integrals (t's) between pairs of molecules in various orientations. CF, HX and SS correspond to orientations as shown in Fig. 6.1, d is the distance between the centers of the molecules, and λ is the reorganization energy. The distances are in Å's and the energies (transfer integrals and the reorganization) are in meV's.

Oligomer	CF d=4.4	CF d=5.0	CF d=6.5	HX d=5.0	HX d=6.5	SS d=5.0	SS d=6.5	λ
FM	68.698	16.092	0.256	29.403	0.644	22.950	0.545	263.5
FD	70.903	16.637	0.311	31.831	0.719	24.892[a]	0.869[a]	257.6
FT	86.588	21.629	0.370	25.627	0.481	10.733	0.092	211.3
CM	67.674	15.760	0.210	28.424	0.639	18.716	0.382	119.7
CD	68.717	16.018	0.257	29.252	0.612	18.157[a]	0.536[a]	262.4
CT	85.898	21.331	0.407	21.709	0.394	2.596	0.341	211.5

[a]The actual values are 49.783 and 1.737 meV for FD and 36.314 and 1.072 meV for CD, i.e. twice what is given in the table for the reasons given in the text.

From Table 7.1, and in agreement with what is expected, we see that hole transfer integrals decrease when the distance between molecules increases in all cases. For both fluorene and carbazole, for the CF stacking, trimers have the biggest transfer integrals and monomers have the smallest ones, for the HX stacking, all three oligomers have comparable transfer integrals (with trimers somewhat smaller than those for monomers and dimers).

It should be pointed out that for trimers (FT and CT), two degenerate configurations are possible, one leading to the extended linear chain and another to the curved (spiral with large pitch) structure depending on the signs of the dihedral angles between the F (in FT) and C (in CT) units. In Table 7.1 we present results for the linear extended configurations. In addition, for the SS stacking it must be noted that the close contacts (between nearest neighbour atoms) in the FD and CD are approximately twice that in the corresponding monomers, hence the dimer's transfer integrals are approximately twice that of the monomer's. For comparison purposes, for SS stacking the dimers' t values given in the Table 7.1 are half of the actual numbers as noted in the footnote. The transfer integrals for the trimers (FT and CT) are the smallest due to decreased side-by-side interactions in their extended (but twisted since the respective F or C units are not exactly planar as was discussed in Chapter 6) linear structures for the SS stacking. For fluorene oligomers, the reorganization energy decreases from monomer to trimer. For carbazole, monomer has an anomalously small reorganization energy (possibly due to the N atom whose presence is significant in the small oligomer such as CM [164] and which tends to localize the positive charge (hole) near the N atom) whereas its values for the dimer and trimer are comparable to those obtained for fluorene oligomers. These data suggest that for the same distance and orientation between molecules the transfer integrals are approximately of the same order of magnitude for monomers and dimers (but somewhat

different for trimers). This confirms that monomers and dimers are typically too short to obtain accurate estimates for the polymer's transfer integrals and reorganization energies and trimers should be used (although it should be stated that if only rough approximations are needed, both monomers and dimers provide adequate estimates).

In Table 7.2 the corresponding hole transfer rates are given. From Eq. (6.1) it can be seen that Γ is largest when t is large and λ is small. For the CF stacking, all transfer rates are comparable for a given distance with trimers giving slightly larger values for both fluorene and carbazole oligomers with one exception. The one exception is CM and is wholly due to CM's small value of λ. For the HX stacking, the situation is very similar with all fluorene and carbazole oligomers giving very similar values for a given distance with one exception (CM) as discussed above. For the SS stacking, fluorene and carbazole monomers and dimers give comparable values (for comparison purposes the actual values for Γ for FD and CD are now divided by four since $\Gamma \propto t^2$) which in general are larger than those for the trimers for a given distance. The smaller values for the trimers can be accounted for by the smaller t's for trimers as given in Table 7.1. Given the results of Tables 7.1 and 7.2 we can conclude that for CF and HX stacking, monomers and dimers give Γ values that are comparable to those obtained for trimers for a given distance (i.e. in these orientations Γ is not as sensitive to the length of the oligomer). For the SS stacking, because of the various complications with monomers and dimers as discussed above, it is best to use trimers to estimate Γ's for the polymers. Also, as expected smaller reorganization energies can lead to higher transfer rates, especially if they are combined with large transfer integrals (see for example the corresponding values for CM in Tables 7.1 and 7.2). On the average, Γ decreases by four orders of magnitude when distance is increased from 5 to 6.5 Å.

For completeness we also study the electron transport in fluorene and carbazole oligomers. Their transfer integrals, reorganization energies and transfer rates are

Table 7.2: The hole transfer rates between pairs of molecules in various orientations. All the symbols are defined as given in Table 7.1. The unit for transfer rate is s^{-1} and distances (d's) are in Å's. $T = 300$ K.

Oligomer	CF	CF	CF	HX	HX	SS	SS
	$d = 4.4$	$d = 5.0$	$d = 6.5$	$d = 5.0$	$d = 6.5$	$d = 5.0$	$d = 6.5$
	($\times 10^{13}$)	($\times 10^{12}$)	($\times 10^{8}$)	($\times 10^{12}$)	($\times 10^{8}$)	($\times 10^{12}$)	($\times 10^{8}$)
FM	1.2	0.7	1.7	2.2	11	1.3	7.6
FD	1.4	0.8	2.6	1.8	14	1.7[a]	21[a]
FT	3.5	2.2	6.5	3.1	11	0.5	0.4
CM	7.0	3.8	6.7	12	62	5.3	22
CD	1.2	0.7	1.7	2.2	9.7	8.5[a]	7.5[a]
CT	3.5	2.1	7.8	2.2	7.3	0.032	5.5

[a]The actual values are four times those given in the table (see the text and Table 7.1 for an explanation).

Table 7.3: The electron transfer integrals (t's) and reorganization energies (λ's) between pairs of molecules in various orientations. All the symbols and units are the same as given in Table 7.1.

Oligomer	CF $d = 4.4$	CF $d = 5.0$	CF $d = 6.5$	HX $d = 5.0$	HX $d = 6.5$	SS $d = 5.0$	SS $d = 6.5$	λ
FT	32.785	12.200	0.544	38.528	0.613	27.529	3.790	286.3
CT	31.238	10.698	0.390	39.485	1.803	11.092	1.393	259.5

Table 7.4: The electron transfer rates between pairs of molecules in various orientations. All the symbols are defined as given in Table 7.1. The unit for transfer rate is s^{-1} and distances (d's) are in Å's. $T = 300$ K.

Oligomer	CF	CF	CF	HX	HX	SS	SS
	$d = 4.4$	$d = 5.0$	$d = 6.5$	$d = 5.0$	$d = 6.5$	$d = 5.0$	$d = 6.5$
	$(\times 10^{13})$	$(\times 10^{12})$	$(\times 10^{8})$	$(\times 10^{12})$	$(\times 10^{8})$	$(\times 10^{12})$	$(\times 10^{8})$
FT	0.2	0.3	5.8	2.9	7.4	1.5	280
CT	0.3	0.3	4.1	4.2	87	0.33	52

given in Tables 7.3 and 7.4. We have found that for the fluorene and carbazole monomers and dimers (FM, FD, CM and CD) the reorganization energies can not be computed because their monomers and dimers do not form stable negative ions. Hence for the electron transport we consider only trimers: FT and CT. As can be seen from Table 7.3, in most cases, the transfer integrals have comparable values with CT having somewhat smaller values than FT in the CF and SS stacking and somewhat larger than FT in the HX stacking. The reorganization energy for CT is smaller (259 meV) than for FT (286 meV). Because smaller values for λ compensate for smaller values of t in CT, the transfer rates as given in Table 7.4 for CT and FT are very similar in the CF and SS stacking, with CT showing somewhat smaller values especially at larger distances such 6.5 Å. In contrast, for the HX stacking, the larger t's and smaller λ for CT result in higher transfer rates than those for FT. Clearly in the case of electron transport, the transfer rates depend quite strongly on the molecular orientation as well as the distance. For example, for CT, HX stacking give the highest transfer rate, followed by SS and then CF stackings at $d = 6.5$ Å. On the other hand for FT, SS stacking gives the highest transfer rate followed by HX and CF stacking at $d = 6.5$ Å. Also at $d = 6.5$ Å, for CT, in HX and SS stackings, the transfer rates for electron are higher than those for hole transfer rates by one order of magnitude and for FT, the hole transfer rates are higher for the CF and HX stacking by small amounts but are considerably smaller (almost four orders of magnitude) for the SS stacking in comparison to its electron transfer rates. Thus, another general tendency is that CF stacking favours hole transport since in both CT and FT hole Γ's are larger than electron Γ's in this orientation, and SS stacking favours electron transport since again in this case in both CT and FT electron Γ's are larger than hole Γ's especially at larger intermolecular distances.

As an aside, we make one additional note regarding the relative position of two

molecules in a cluster. It has been observed [162, 163] that, say in cofacial (π-stacking) orientation it is possible for the polymers to be either "shifted" or "flipped" (rotated 180°) relative to each other to minimize the side chain interactions. Given the short oligomers used in this work, it is difficult to consider the "shifted" orientation. However, we performed some calculations of transfer integrals for the "flipped" configuration for FT and CT. The general observation is that in the CF stacking at both $d = 5.0$ and 6.5 Å the hole transfer integrals increase somewhat (the actual values are 25.960 and 25.760 meV (5.0 Å) and 0.623 and 0.694 meV (6.5Å) for FT and CT respectively and should be compared with the corresponding numbers in Table 7.1) and the electron transfer integrals decrease somewhat (the actual values are 6.943 and 6.493 meV (5.0Å) and 0.275 and 0.398 meV (6.5 Å) for FT and CT respectively and should be compared with the corresponding numbers in Table 7.3) in the "flipped" configurations. Given that the transfer rates have not changed significantly, we have performed most of our calculations without "shifting" or "flipping". In a more exact treatment this fact should probably be considered, however, this does not appear to be dominant factor in mobility determination in homopolymers such as PF and PC.

Finally in Table 7.5, we present results for 3D and 1D hole and electron mobilities obtained from simulations that used trimers (FT and CT) in various orientations. We note that our 3D mobility calculations use 3D hexagonal lattice whose lattice constant equals to 6.5 Å (as in reference [56]). For the hole mobilities there is fairly good agreement with the calculated and the experimental results for PF and PC (time-of-flight experimental hole mobility for poly(9,9'-dioctylfluorene) has been reported to be of the order of 9×10^{-3} $cm^2V^{-1}s^{-1}$ at an electric field of 10^4 V/cm [165]). It can be estimated (from conductivity measurements) that hole mobility for poly(N-substituted-2,7-carbazole) is of the order of 10^{-6} $cm^2V^{-1}s^{-1}$. [164] It is clear that the calculated hole mobility for pure PF is higher than hole mobility for PC,

Table 7.5: The hole and electron 1D and 3D mobilities, μ, (cm^2/Vs) for fluorene and carbazole trimers (FT and CT) for the orientations as indicated in the table. T = 300 K and the electric field, E, is 4×10^4 V/cm unless it is specified otherwise (see footnotes).

		1D		3D	
d	Oligomer	hole	electron	hole(HX)	electron(HX)
6.5 Å	FT	1.0×10^{-4}(CF)	9.2×10^{-5}(CF)	3.6×10^{-4}	2.4×10^{-3}[a]
		6.4×10^{-6}(SS)	4.5×10^{-3}(SS)		
	CT	1.2×10^{-4}(CF)	6.5×10^{-5}(CF)	3.0×10^{-5}[b]	2.5×10^{-3}
		8.7×10^{-5}(SS)	8.3×10^{-4}(SS)		
5.6 Å	FT	1.3×10^{-2}(CF)	3.4×10^{-3}(CF)		
		2.6×10^{-3}(SS)	6.1×10^{-2}(SS)		
	CT	1.1×10^{-2}(CF)	3.5×10^{-3}(CF)		
		1.8×10^{-4}(SS)	1.5×10^{-2}(SS)		

[a] $E = 1.0 \times 10^5$ V/cm.

[b] $E = 1.5 \times 10^6$ V/cm.

especially that in the 3D case we could not obtain finite bulk mobility (as related to hopping) for CT until the electric field was increased to 1.5×10^6 V/cm (two orders of magnitude higher than for FT) agreeing with the experimental trends that indicate that pure PC has rather low hole mobility (less than 10^{-6} cm^2/Vs). The reverse appears to be true for electron mobilities. Table 7.5 indicates that while the magnitudes of electron mobilities are approximately the same for both FT and CT (of the order of $10^{-3}cm^2/Vs$), the finite value for FT was not obtained until the electric field was increased to 1.0×10^5 V/cm from the low value of 4.0×10^4 V/cm. This seems to suggest that electron mobility is somewhat higher in PC versus PF and in general would be comparable to hole mobility in PF. We also show that mobilities (consistent with the above discussion on transfer rates) can be considerably affected by the relative orientation and distance between the molecules. At $d = 6.5$ and 5.6 Å, 1D hole mobilities, for both FT and CT, are higher in the CF orientation relative to electron mobilities. And 1D electron mobilities, for both FT and CT, are higher in the SS orientation relative to hole mobilities.

In summary, we first note that monomers and dimers should be used with caution in mobility simulations of polymers such as PF and PC (longer oligomers such as trimers are better). Second, for a given orientation and distance for different molecular systems (e.g. FT vs. CT in this work) the relative values of transfer integrals and the reorganization energies are equally important factors in determining their relative charge transport rates. In addition, the general rule appears to be that for a given distance both FT and CT have similar mobilities for both holes and electrons in their respective favourable orientations (CF for holes and SS for electrons). This suggests that both fluorene and carbazole molecular systems can serve equally well as either electron or hole transport layers (in various devices).

7.2 Hole Mobilities: Carbazole Derivatives

In the above discussion, we considered pairs of molecules that were made of fluorene or carbazole units only. In most applications (i.e. when constructing solar cells), it is the derivatives of these pristine polymers that are used. In this work we focus on the derivatives of carbazole (PCDTBT, PCDTPT, PCDTBX, PCDTPX, PCDTQx, and PCDTPP) in CF orientation (we consider only one orientation in the initial analysis since we are dealing with a number of polymers and we are looking for simple trends).

Before the transfer integrals and rates are computed for the monomers of these polymers, we compute the transfer integrals, reorganization energies and transfer rates between the various constituent parts of the monomers (i.e. we consider pairs of heterogeneous as well as homogeneous molecules) since as stated above it is possible that there are other overlaps between molecules that may be preferable for greater mobility. We consider the following parings: FM+FM, CM+CM, BTT+BTT, FM+BTT and CM+BTT (see Fig. 5.1 for the structures) for molecules of the "monomer" length, and FT+FT, CT+CT, CDTBT+CDTBT and CDTBT+TBTCD (see Fig. 5.2 for the structures) for molecules of the "trimer" length for the holes, and FT+FT, CT+CT, CDTBT+CDTBT and CDTBT+TBTCD for the electrons. It should be noted that BTT has the similar length as FM or CM. The transfer integrals, reorganization energies, and transfer rates for these pairs are given in Table 7.6 for the holes and in Table 7.7 for the electrons at $d = 5.0$ Å.

From Tables 7.6 and 7.7, we note that heterogeneous pairs have smaller transfer rates than their corresponding homogeneous pairings with one exception (for holes FM+BTT has a slightly higher transfer rate than BTT+BTT (but not FM+FM) due to its low reorganization energy). However, for all carbazole combinations the transfer rates are higher between the same overlapping molecules (CM+CM, CT+CT,

BTT+BTT, CDTBT+CDTBT) than different ones (i.e.CM+BTT or CDTBT+TBTCD). Hence, since in this work we are primarily concerned with carbazole derivatives we will assume that in their stacking the like parts of the monomers will preferentially stack on top of each other.

As stated above, six carbazole derivatives are studied in this work, they are: PCDTBT, PCDTPT, PCDTBX, PCDTPX, PCDTQx, and PCDTPP. Their structures are given in Fig. 5.2. Of the six polymers, four of them have the π-stacking distance determined using the X-ray diffraction measurements. [128] Hence, we use the experimentally determined distances between the molecules: 4.4 Å for PCDTBT, 4.8 Å for PCDTBX , 4.7 Å for PCDTQx and 4.9 Å for PCDTPX in the our initial calculations. That is, the transfer integrals, reorganization energies, transfer rates and hole 1D mobilities are listed in Table 7.8 for all four compounds for different intermolecular distances. As can be seen from the Table 7.8, at the experimental distances as given above, the comparison between the computed and experimental [128] mobilities differs by two orders of magnitude.

We believe that the distances close to 4.5 Å are not representative of the actual (average) distances between molecules in the bulk, especially in an amorphous (disordered) state. That is, the experimental value are affected by many other factors such as different orientations between molecules in the film which are not being taken into account in our simulations since we are considering CF stacking only. Since we are primarily focused on reproducing the trends in mobilities and not their absolute values, it can be said that, in effect, we are looking for an "effective" intermolecular distances that would be able to adequately reproduce the experimental trends in mobilities using their most favourable orientation for hole transport (see also reference [166] that shows that this "1D" approach to estimate hole mobilities gives reasonable values). To determine these "effective" distances we calculate hole mobilites for the

Table 7.6: Comparison of hole transfer integrals (t), reorganization energies (λ) and transfer rates (Γ) for pairs of molecules as indicated in the first column. The distance between the molecules is 5.0 Å for all pairs and the temperature $T = 300$ K.

Polymer Pair	t(meV)	λ(meV)	$\Gamma(s^{-1})(\times 10^{10})$
FM + FM	16.09	263.5	66
CM + CM	15.76	119.7	380
BTT + BTT	13.49	289.6	34
FM + BTT	8.37	187.3	44
CM + BTT	8.43	352.4	6.6
FT + FT	20.31	211.3	190
CT + CT	18.39	215.1	150
CDTBT + CDTBT	11.14	265.0	31
CDTBT+TBTCD	0.90	265.0	0.2

Table 7.7: Comparison of electron transfer integrals (t), reorganization energies (λ) and transfer rates (Γ) for pairs of molecules as indicated in the first column. The distance between the molecules is 5.0 Å for all pairs and the temperature $T = 300$K.

Polymer Pair	t(meV)	λ(meV)	$\Gamma(s^{-1})(\times 10^{10})$
FT + FT	11.58	286.3	26
CT + CT	9.47	260.6	24
CDTBT + CDTBT	8.57	236.6	26
CDTBT + TBTCD	0.82	236.6	0.24

four systems at different values of d (5.0, 5.5 and 6.0 Å) as given in Table 7.8. It is clear from the comparison between the simulated and experimental values for μ's that the effective distance for the four systems lies between 5.5 and 6.0 Å. We have found that an addition of 1.2 Å to the X-ray values gives good agreement between the calculated and experimental mobilities as is shown in Table 7.9. We have estimated the d value for PCDTPT and PCDTPP to be 6.2 and 6.3 Å respectively. These larger values of d make sense since X-ray shows that PCDTPT and PCDTPP do not really π stack. [128]

In most cases, the correction (i.e. addition of 1.2 Å) results in a good agreement with experimental trends, i.e. PCDTBT gives the highest hole mobility, PCDTQx and PCDTBX follow next and the ratios between the mobility of PCDTBT to PCDTQx and PCDTBX is well reproduced. There is one exception, PCDTPX (which is the antisymmetric counterpart of PCDTBX) because of its largest stacking distance and reorganization energy gives the lowest mobility (but still comparable to that of PCDTBX) which does not agree with the experimental trend. We believe that this result is due to the large separation between the PCDTPX molecules (since the larger the distance the smaller transfer integral and consequently smaller mobility). From Table 7.8, it should be noted that at 5.5 and 6.0 Å, as expected the mobilities for PCDTBX and PCDTPX became comparable, however in our calculations because λ for PCDTBX is smaller than for PCDTPX, the μ for PCDTBX will always be somewhat larger than for PCDTPX (contrary to the experimental result).

To clearly illustrate the trends contained in Table 7.9, we plotted the t's and λ's for the six systems for their respective Γ's in Fig.7.1. This figure shows that for systems with small transfer integrals and relatively large reorganization energies (i.e. PCDTPP, PCDTPT, PCDTPX, PCDTBX and PCDTQx) have relatively small transfer rates in comparison to PCDTBT which has large t and small λ. This trend

Table 7.8: Hole transfer integrals (t's), transfer rates (Γ's), and mobilities (μ's) for pristine pairs of carbazole derivatives as indicated in the first column of the table for the various distances (d's) between monomers in the respective pairs in the CF orientation with $T = 323$ K.

Polymer pair	d(Å)	t(meV)	$\Gamma(s^{-1})$ $(\times 10^{11})$	$\mu(\mathrm{cm}^2/\mathrm{Vs})$ $(\times 10^{-3})$	$\mu^{\dagger}(\mathrm{cm}^2/\mathrm{Vs})$ $(\times 10^{-3})$
PCDTBT	4.4	49.795	74	455	1
PCDTBX	4.8	18.939	7.7	57	0.1
PCDTQx	4.7	26.530	13.0	93	0.3
PCDTPX	4.9	14.739	3.8	30	0.5
PCDTBT	5.0	11.138	3.7	30	1
PCDTBX	5.0	11.440	2.8	23	0.1
PCDTQx	5.0	12.490	2.9	24	0.3
PCDTPX	5.0	11.526	2.3	19	0.5

†Experimental mobilities as obtained from reference [128].

Table 7.8: (continued).

Polymer pair	d(Å)	t (meV)	$\Gamma(s^{-1})$ ($\times 10^{11}$)	$\mu(\mathrm{cm}^2/\mathrm{Vs})$ ($\times 10^{-3}$)	$\mu^{\dagger}(\mathrm{cm}^2/\mathrm{Vs})$ ($\times 10^{-3}$)
PCDTBT	5.5	2.989	0.27	2.7	1
PCDTBX	5.5	3.031	0.20	2.0	0.1
PCDTQx	5.5	3.371	0.22	2.1	0.3
PCDTPX	5.5	2.952	0.15	1.5	0.5
PCDTBT	6.0	0.740	0.017	0.20	1
PCDTBX	6.0	0.767	0.013	0.15	0.1
PCDTQx	6.0	0.840	0.013	0.16	0.3
PCDTPX	6.0	0.699	0.0086	0.10	0.5

†Experimental hole mobilities as obtained from reference [128].

Table 7.9: Hole transfer integrals (t's), reorganization energies (λ's), transfer rates (Γ's), and mobilities (μ's) for pristine carbazole derivatives as indicated in the first column of the table in the CF orientation. The distances (d's) for PCDTBT, PCDTBX, PCDTQx and PCDTPX pairs are respectively 4.4, 4.8, 4.7 and 4.9 Å [128] plus 1.2 Å(see discussion in the text) with $T = 323$ K.

Polymer pair	d(Å)	t(meV)	λ(meV)	$\Gamma(s^{-1})$ $(\times 10^8)$	$\mu(cm^2/sV)$ $(\times 10^{-3})$	$\mu^{\dagger}(cm^2/sV)$ $(\times 10^{-3})$
PCDTBT	5.6	2.091	265.0	130	1.4	1
PCDTPT	6.2	0.446	316.6	3.5	0.043	0.04
PCDTQx	5.9	1.075	308.3	22	0.25	0.3
PCDTPP	6.3	0.242	306.2	1.14	0.015	0.02
PCDTBX	6.0	0.767	295.6	13	0.15	0.1
PCDTPX	6.1	0.532	315.5	5.0	0.06	0.5

†Experimental hole mobilities as obtained from reference [128].

Table 7.10: Electron transfer integrals (t's), reorganization energies (λ's), transfer rates (Γ's), and mobilities (μ's) are given for pristine carbazole derivatives as indicated in the first column of the table in the CF orientation. The distances (d's) for PCDTBT, PCDTBX, PCDTQx and PCDTPX pairs are respectively 4.4, 4.8, 4.7 and 4.9 Å [128] plus 1.2 Å (see discussion in the text) with $T = 323$ K.

Polymer pair	d(Å)	t(meV)	λ(meV)	Γ(s^{-1}) ($\times 10^8$)	μ(cm^2/sV) ($\times 10^{-3}$)	$\mu^{\dagger}$(cm^2/sV) ($\times 10^{-3}$)
PCDTBT	5.6	1.988	236.6	160	1.7	1
PCDTPT	6.2	0.418	250.8	6.19	0.076	0.04
PCDTQx	5.9	0.366	269.2	3.9	0.04	0.3
PCDTPP	6.3	0.255	250.2	2.32	0.029	0.02
PCDTBX	6.0	0.464	250.3	7.7	0.09	0.1
PCDTPX	6.1	0.361	261.9	4.1	0.05	0.5

†Experimental hole mobilities as obtained from reference [128].

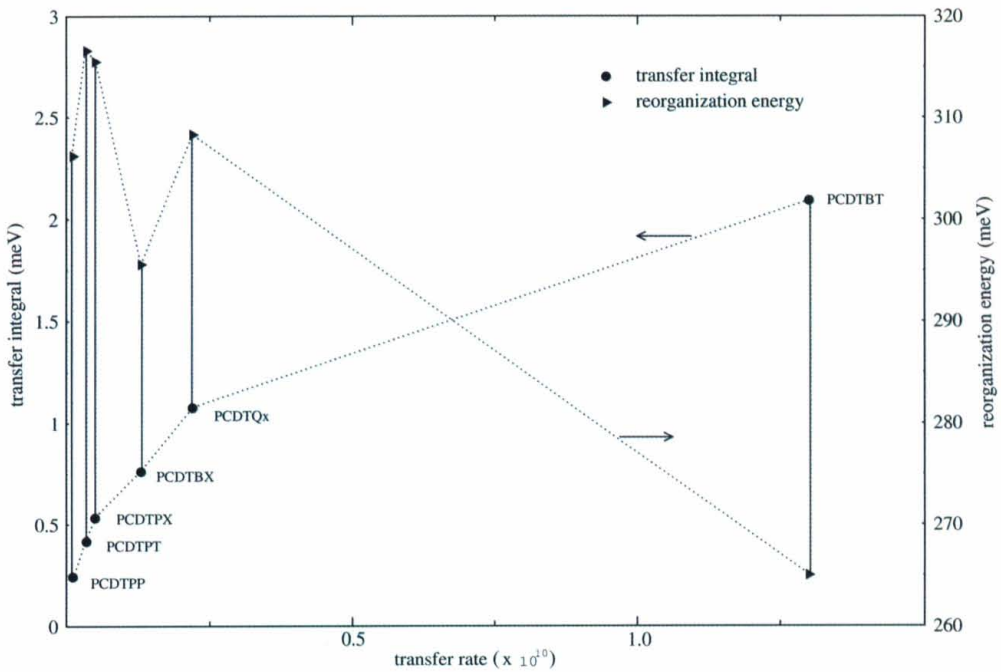

Figure 7.1: Values of transfer integrals and reorganization energies plotted for the various carbazole derivatives as indicated on the figure.

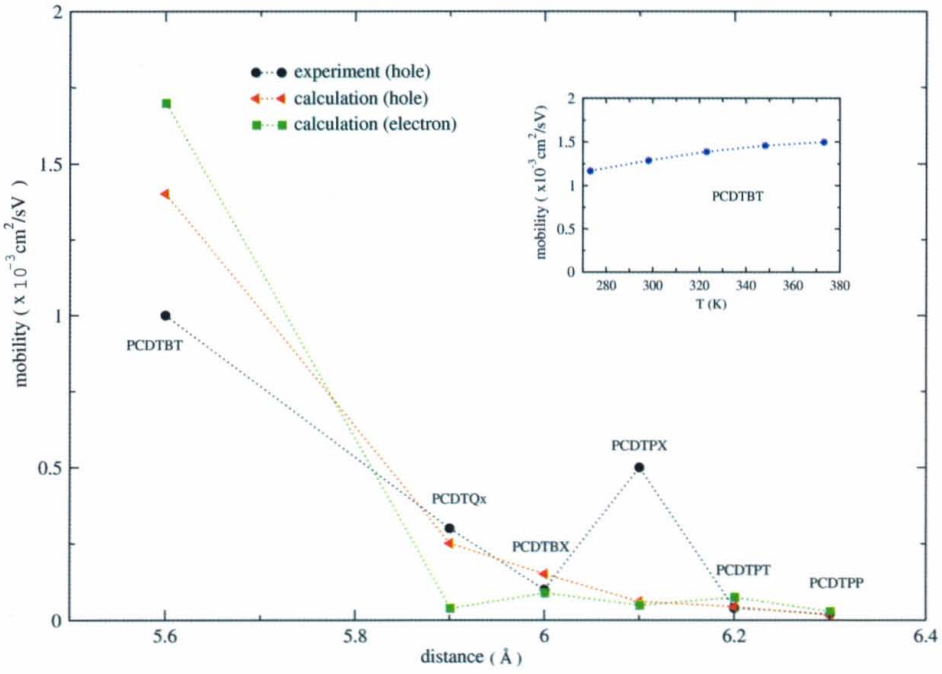

Figure 7.2: Comparison of computationally and experimentally determined values for the hole and electron 1D mobilities for the various carbazole derivatives as indicated on the figure as a function of the intermolecular distance (d). $T = 323$K. The inset shows the plot of μ as a function of T for PCDTBT.

strongly correlates with the intermolecular distance, d, i.e. the closer the polymers are in the π stacking the larger the t's and Γ's and finally μ's as is shown in Fig. 7.2. Of course as discussed above there is one discrepancy (PCDTPX) which does not agree with the experimental result.

We also include an inset in Fig. 7.2 to show the variation of hole mobility with temperature (temperature ranges from 273 K to 373 K). The inset shows that the mobility slightly increases with increasing temperature, but its values are close to experimental value at $T = 323$ K. This behavior is consistent with what is expected in materials that display hopping mechanism for charge transport. [15] Finally, we also computed the electron mobilities (see Table 7.10) for the same distances and CF orientation as employed in Table 7.9. It is clear from these data that once again PCDTBT has the highest electron mobility in addition to having highest hole mobility in comparison to the other systems considered. The remaining systems have very similar electron mobilities which in general are comparable to their corresponding hole mobilities.

In addition to calculations of 1D mobilities for the six carbazole derivatives, we also perform 3D simulations of hole mobilities for the ordered systems (PCDTBT, PCDTBX, PCDTQx and PCDTPX) with orthorhombic unit cells. The results of these simulations are given in Table 7.11. In Table 7.11, a is the unit cell distance along the chain (x-axis) and is determined by the length of the repeat unit, b (along the y-axis) is the distance between the side by side chains which is estimated using the approximate widths of the oligomers and requirement that chains do not overlap and c (along the z-axis) is the π stacking distance between cofacially oriented chains and is taken as given in reference [128] (see Fig. 6.1). The electric field is applied along the z-axis direction and has the same value (4×10^4 V/cm) as is used in the 1D simulations of mobilities. The 3D simulations of mobilites require three values of

Table 7.11: The 3D mobilities in ordered systems (with orthorhombic unit cells with lattice constants as given in the table), PCDTBT, PCDTBX, PCDTQx and PCDTPX. The distances are in Å's, the mobilities are cm^2/Vs and the energies (transfer integrals and the reorganization) are in meV's.

Oligomer	lattice constants			t_a	λ	μ	$\mu^\dagger$
	a	b	c			$(\times 10^{-3})$	$(\times 10^{-3})$
PCDTBT	20.5	7.5	4.4	65.244	265.0	503	1
PCDTBX	20.5	7.5	4.8	71.230	295.6	90	0.1
PCDTQx	20.5	7.5	4.7	72.451	308.3	115	0.3
PCDTPX	20.4	7.5	4.9	61.565	315.5	38	0.5

†Experimental hole mobilities as obtained from reference [128].

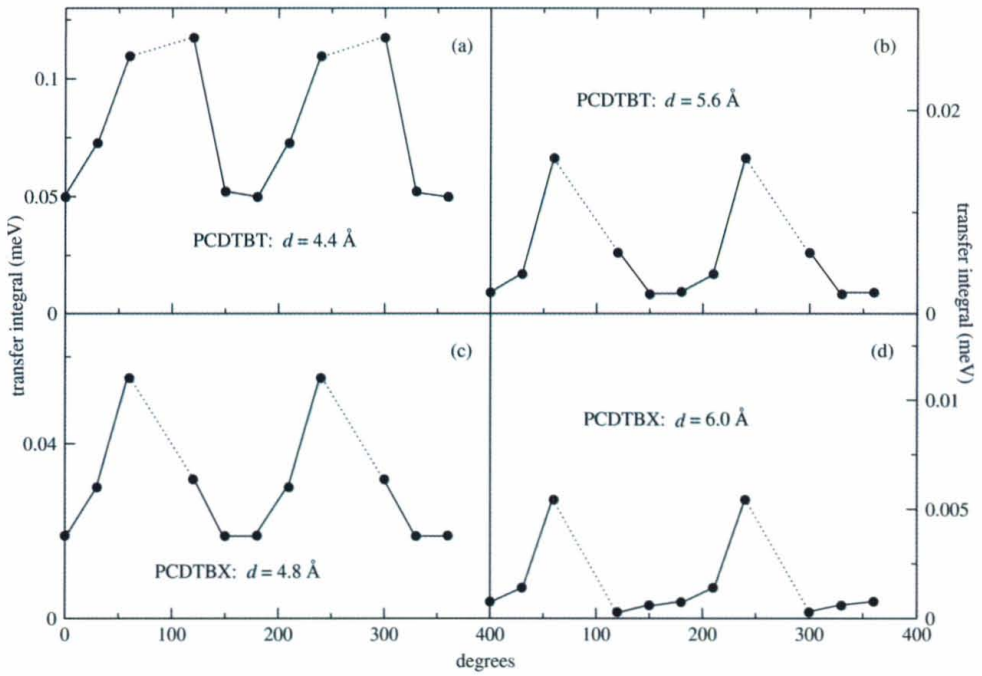

Figure 7.3: Transfer integrals (meV) as a function of rotational angle (degrees) for the pairs of PCDTBT and of PCDTBX with the intermolecular distances as shown in the figure. The solid lines between the discreet points are guides to an eye. The dotted lines correspond to range of angles for which transfer integrals can not be calculated due to molecular overlap as discussed in the text.

Table 7.12: The 3D mobilities in PCDTBT and PCDTBX as a function of orientational disorder (corresponding to the fraction (0, 0.25, 0.50 and 0.75) of the perpendicular orientation between two molecules). The distances are in Å's, the mobilities are cm^2/Vs and the energies (transfer integrals and the reorganization) are in meV's.[†]

Oligomer	$a^{\ddagger}, b, c$	$t_{\parallel}$	$t_{\perp}$	0	0.25	0.50	0.75	λ
	$b = c$			μ				
				$(\times 10^{-3})$	$(\times 10^{-3})$	$(\times 10^{-3})$	$(\times 10^{-3})$	
PCDTBT	4.4	77.511	0.736	1200	780	400	160	265.0
	5.6	5.512	3.850	9.1	6.5	4.8	4.1	
PCDTBX	4.8	29.849	8.488	150	100	70	40	295.6
	6.0	1.608	1.115	1.1	0.16	0.32	0.48	

[†]The electric field is $E = 4 \times 10^5$ V/cm (see discussion in the text).

[‡]a is the same length as given in Table 7.11.

transfer integrals corresponding to the three lattice constants: t_a's (along the chain) are given in Table 7.11, t_b's (for the side by side orientation) are nearly zero, their values are of the order of 10^{-4} and t_c's (for the π stacking) are given in Table 7.8. The values for the 3D mobilities should be compared with the corresponding 1D mobilities as given in Table 7.8. The mobility values are of the same order of magnitude and their trends are the same in both tables. That is, PCDTBT has the highest mobility, followed by PCDTQx, PCDTBX and PCDTPX.

The above results for 1D and 3D hole mobilities are given for pristine ordered polymer films. However, most polymer films are amorphous, that is, they contain certain disordered regions mixed in with crystalline domains. To illustrate the effect of disorder on mobilities, we include some orientational disorder in our 3D mobility simulations for two carbazole derivatives, PCDTBT and PCDTBX as an example. The results of these calculations are given in Table 7.12. In these simulations, the intermolecular distances are fixed as follows: along the y- and z-axis b and c are taken as equal and correspond to the π stacking distance between molecules, along the x-axis a is taken to have same value as given in Table 7.11. In order to simulate the orientational disorder, we focus on two possible (averaged) configurations between polymers chain: one corresponding to parallel ($\parallel$) and another to perpendicular ($\perp$) orientation.

Because b and c are equal and are relatively short (with values of the order of 5 Å as indicated in Table 7.12) this means that in amorphous films (most likely in order to avoid repulsion due to charge overlap) two polymer planes would rotate around (a-b) plane as a parallel unit maintaining their π stacking distance. In Fig. 7.3, the transfer integrals for pairs of rotating molecules are plotted as a function of the rotational angle from 0° to 360°, every 30°. As an example, the distances between molecules for PCDTBT are taken as 4.4 Å and 5.6 Å and for PCDTBX

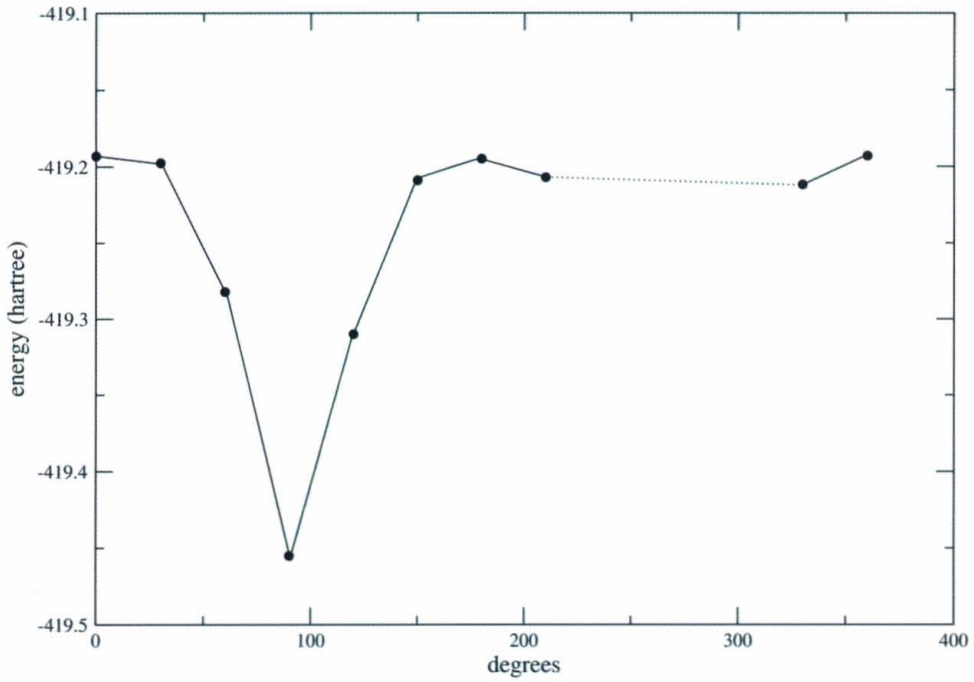

Figure 7.4: Variation of energy as a function of a rotational angle for a pair of PCDTBT monomers separated by 4.4 Å. The rotational angle is the angle between the planes of the two molecules and is determined by having one molecule fixed and another rotated relative to it. (The dotted line corresponds to angles where the two molecules are overlaping which is unphysical and no energies are computed in this region.)

are 4.8 Å and 6.0 Å (corresponding to the experimental π stacking distance and the one estimated in 1D simulations of mobiities). From Fig. 7.3, we can see that the transfer integrals are almost symmetrical about 180°. No transfer integrals can be computed around 90° and 270° (as indicated by dotted lines on Fig. 7.3) since in these orientations molecules are located side by side relative to each other and are overlapping due to the fact that they very close to each other. For the purpose of calculating the mobilities, average values for the parallel transfer integrals ($t_{\parallel}$'s) are determined from Fig. 7.3 data and are given in Table 7.12. The corresponding perpendicular transfer integrals $t_{\perp}$'s are also given in Table 7.12. The perpendicular orientation corresponds to the planes of the two polymer chains being at 90° to each other. The reason why we include the perpendicular (in addition to the parallel) orientation is that our study indicates that the perpendicular orientation is the most stable orientation for an isolated pair of molecules (even though the transfer integrals for perpendicular tend to be small relative to other orientations). To show, as an example, that the perpendicular orientation is the most stable, 1D conformational energy curve (see Fig. 7.4) is obtained with ZINDO method for a pair of PCDTBT molecules separated by 4.4 Å.

The mobilities are then determined for different fractions of the perpendicular orientation between molecules where 0 corresponds to no perpendicular orientation included in the simulation, 0.25 corresponds to 1 out 4 configurations are in the perpendicular orientation etc. It is clear from Table 7.12 that the general trend is, the greater the fraction of perpendicular orientations, the smaller the mobility. Also from Table 7.12, we note that mobility ratios between PCDTBT and PCDTBX are close to 10 which is in good agreement with the experimental result (which is 10) as given in reference [128]. It should be noted that mobility results in Table 7.12 are given for the electric field equal to 4×10^5 V/cm (instead of 4×10^4 V/cm). The

reason for this is the MC simulations for the lower field (4×10^4 V/cm), in most cases when orientational disorder is present, lead to charge being trapped at certain sites with the net effect that charge can not move across the width of the polymer film along the direction of the electric field (charge in the form of a polaron can still move along the polymer chain).

7.3 Electron Mobility: F8BT

Many conjugated polymers such as the carbazole derivatives discussed above have relatively high hole mobilities. Electron transport materials are needed in order to keep carrier balance required for improved device performance. [168] For example, blends of the polyfluorene copolymers poly(9,9′-di-n-octylfluorene-alt-bis-N-N′-(4-butylphenyl)bis-N,N′-phenyl-1,4-phenylene diamine) PFB and F8BT work efficiently in photovoltaic cells. [169, 170] For organic conjugated materials, their charge carrier mobility depends mostly on their packing. [171]

In this section, the electron mobility in F8BT is simulated using the computational approach as described in Chapter 6. As indicated in reference [137], upon annealing the F8BT (in particular F8BT/255K sample as indicated in reference[137]) forms a crystal structure with monoclinic unit cell dimensions: $a = 14.65$ Å, $b = 5.3$ Å, and $c = 16.7$ Å (obtained using wide angle X-rays scattering experiment). The experimental preferential orientation of the unit cell with respect to the substrate was determined to be as follows: the in-plane x-axis lies along the backbone of the polymer chain and a is approximately the length of one F8BT repeat unit, the other in-plane y-axis lies along the side-by-side interchain spacing b and the out-of-plane z-axis points along the π-stacking direction corresponding to the c length which is thought to be equal to four times the π stacking spacing (4.18 Å). The chemical

structure of F8BT (repeat unit) is shown in Fig. 5.3.

The simulation of the electron mobility for F8BT uses the monoclinic unit cells as obtained experimentally. However, some structural details can not be determined from X-ray scattering experiment. One is related to the orientation of the side-by-side planes of the F8BT chains relative to the a-b plane since the distance of 5.3 Å makes interchain spacing unphysically small in the the parallel (in-plane) configuration. The other is related to the orientation of the chains in the π stacking, the work of [137] suggests that in the π stacking the chains are shifted relative to each other in such a way that F8 (fluorene) unit overlaps BT and vice versa. This structured is referred as the alternating structure. It should be noted that two alternating structures are possible, one with BT's pointing in the same direction and one with BT's pointing in the opposite direction. Our calculations show that the two alternating structures are nearly degenerate with the one with BT's pointing in the same direction being slightly more stable. This structure with BT's pointing in the same direction also has larger transfer integral and we have chosen this one to represent alternating structure in the mobility calculations.

F8BT monomer is used in the simulations. The electric field is taken along y-axis (b lattice constant) direction since as shown in section 7.1 and reference [137] the side-by-side orientation gives larger electron mobility. The 2D and 3D mobilities are obtained for F8BT. For completeness, it can be noted that the optimized (DFT/B3LYP) HOMO and LUMO energies for F8BT are 5.5 eV and 2.3 eV giving the estimated bandgap of 3.2 eV which is not a very low bandgap. The reorganization energies are computed using the DFT/B3LYP energies (as discussed in Chapter 6) for neutral molecule in neutral structure, anion molecule in neutral structure, anion molecule in anion structure and neutral molecule in anion structure (see Fig. 7.5). Then the anion (electron) reorganization energy is given by an expression,

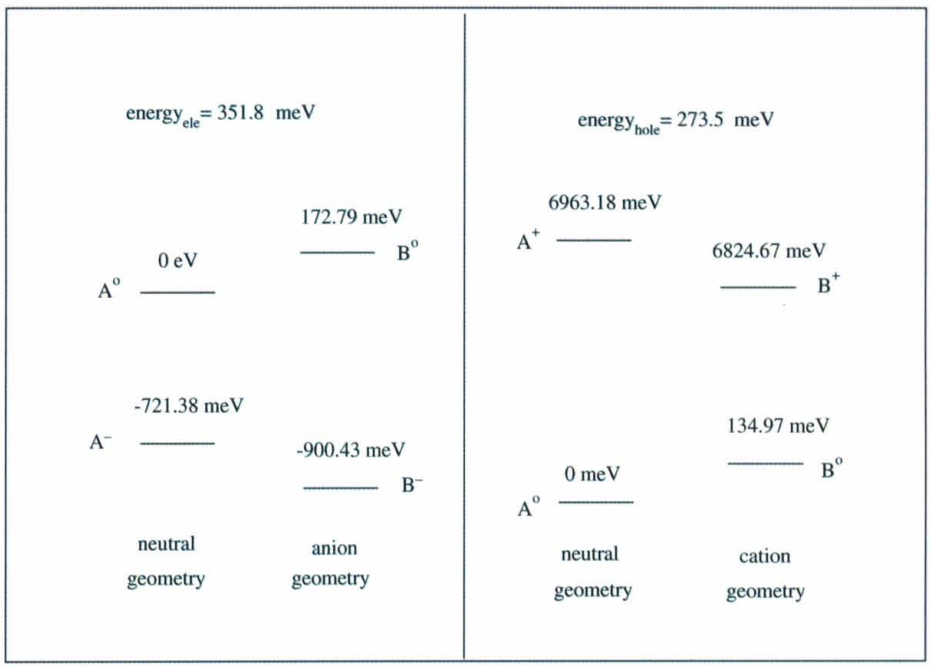

Figure 7.5: The energy levels for the ions and neutral F8BT's and the corresponding electron and hole reorganization energies as indicated on the figure (see text for more discussion and Chapter 6).

$\lambda=(B^0 - B^-) - (A^o - A^-)$ (see also p67), and is 351.8 meV for F8BT. Similarly, the cation (hole) reorganization for F8BT is 273.5 meV.

Next the transfer integrals between molecular pairs are computed. Along the x-axis, the F8BT molecule is translated 14.65 Å and the transfer integral for a pair along the chain is determined to be 0.437 meV. Along the y-axis, as indicated above the parallel in-plane side-by-side arrangement is unphysical and gives very large transfer integral (123.17 meV) which could lead to a very high mobility such as 1.97 cm^2/Vs which is very different from the experimental value of 2.5×10^{-3} cm^2/Vs. This difference is probably due to the fact that the two side-by-side chains are rotated relative to the a-b plane with the interchain spacing being fixed to experimental b value of 5.3 Å. In order to verify this, we determine the optimal angle of rotation by performing 2D mobility simulations. The results of these calculations (variation of mobilities with the rotational angle) are shown in Table 7.13.

From the Table 7.13, it can be noted that rotation angle between 24° and 25° leads to the mobility between 2.8×10^{-3} cm^2/Vs and 1.8×10^{-3} cm^2/Vs which compares well with the experimental value. Hence, these angles will be used for the 3D simulations of mobility. In addition from Table 7.13, it is interesting to observe that, when the transfer integrals 4.627 meV for 24° or 3.773 meV for 25° along the y-axis (between two chains) are compared with the transfer integral of 0.437 meV along x-axis (along the chain), it is clear that the electron transport is occurring predominantly along the y-axis, that is, hopping between tilted side-by-side chains (this observation is consistent with similar conclusion in reference [137]).

For the 3D simulations, the transfer integral corresponding to the two π stacking molecules along the z-axis with the spacing of 4.18 Å is determined to be 26.698 meV and 9.820 meV for the non-alternating and alternating structures respectively. The 3D mobility simulations (with rotational angles of 24^o and 25^o) for F8BT are

Table 7.13: The transfer integrals and 2D mobilities between pairs of molecules. The angle (in degrees) is the angle between the (side-by-side) planes of the two F8BT molecules and the *a*-*b* plane of the unit cell. Transfer integrals are in meV and mobilities are cm^2/Vs.

degree(^{o})	t	μ (simulation)	μ (experiment)[a]
20	10.201	1.35×10^{-2}	2.5×10^{-3}
24	4.627	2.8×10^{-3}	2.5×10^{-3}
25	3.773	1.8×10^{-3}	2.5×10^{-3}
30	1.777	4.0×10^{-4}	2.5×10^{-3}

[a]Experimental value as given in reference [137].

shown in Fig. 7.6 as a function of an electric field. That is, the electric field is varied from 4×10^4 V/cm to 1.0×10^6 V/cm. The details are: 24 (not alternating) stands for 24° tilt relative to *a-b* plane and F8 and BT overlap with F8 and BT in the π stacking; 24 (alternating) stands for 24° tilt and alternating structure along the *z*-axis; 24 (SS alternating) stands for 24° tilt and shifted side-by-side structure (i.e. F8 faces BT and vice versa in the side-by-side configuration), the transfer integral for this structure is 3.932 meV which is slightly smaller than 4.627 meV for the non-shifted structure); 25 (alternating) corresponds to 25° tilt and alternation along the π-stacking direction. All these cases indicate that electric fields have relatively small effect on 3D mobilities. Alternating structures such as (24 (alternating)), 24 (SS alternating) and 25 (alternating) have lower mobilities than not alternating structure (24 (not alternating), which is in agreement with the finding in the reference [137]. At electric fields higher than 2×10^5 V/cm, all the mobilities are of similar magnitude ranging from 2×10^{-3} to 4×10^{-3} cm^2/Vs. At electric field of 4×10^4 V/cm (which corresponds to the value used in the experiment [137]), all alternating structures give mobility in the range 1.6-2.1$\times10^{-3}$ cm^2/Vs which is in fairly good agreement with the experimental (approximate) value of 2.5×10^{-3} cm^2/Vs.

7.4 Conclusions

In this work we test a multi-step method for simulating the hole and electron mobilites in organic semiconducting polymers. The approach is tested, by comparing our predictions with experimental values when available, first on homopolymers such as PF and PC and then on alternating co-polymers such as PCDTBT, PCDTPT, PCDTBX, PCDTPX, PCDTQx, and PCDTPP. We conclude that, the approach as described in this work can, in most cases, be used to determine trends in hole (and

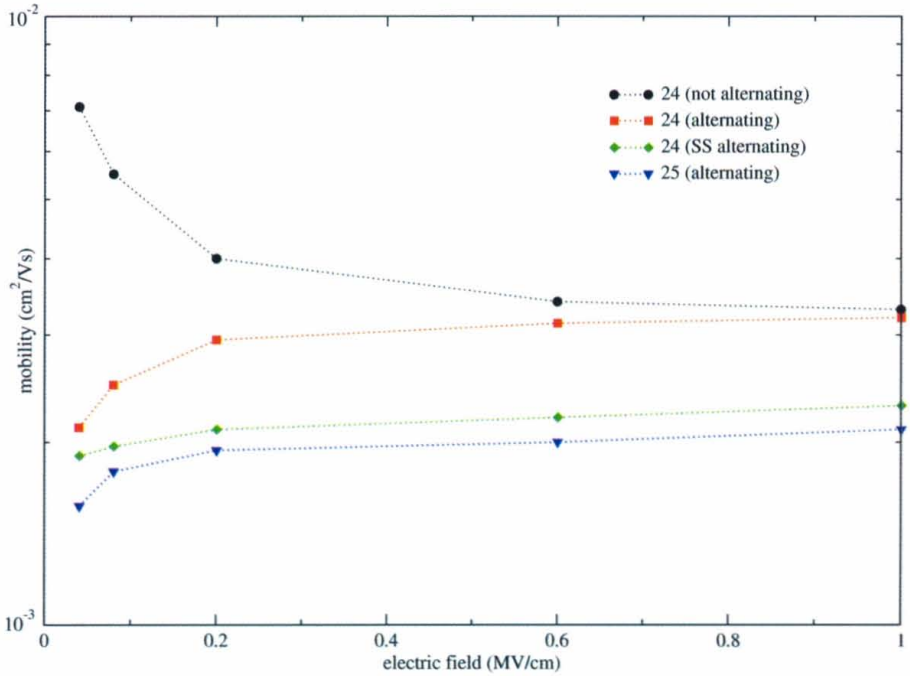

Figure 7.6: Variation of the electron 3D mobility μ with applied electric field E.

possibly electron) mobilities provided certain information is known before the calculations are carried out.

First the oligomers should be of an appropriate length, that is, they should be chosen at least of the order of fluorene or carbazole trimers. For an expedient and efficient screening of systems, 1D simulations of mobilities are adequate to reproduce experimental results provided intermolecular distances between oligomers in, say, π-stacking orientation is known from either X-ray experiments or MD calculations. It should be emphasized that this information (i.e. intermolecular distance) is critical due to the sensitivity of the transfer integral which can change significantly with small variations in distance. In addition the value of reorganization energy plays an important role in determining transfer rate and should be computed with some care. While it is a conventional wisdom based on Marcus-Hush theory [138, 14] that both t and λ play an important role, there are instances when the value of t plays a dominant role in the mobility trends. [167] Further, our simulations indicate that in organic semiconducting polymer, the hole and electron mobilites often have comparable magnitudes even for the same orientation. However, the homopolymer study shows that the hole mobility is somewhat higher in the cofacial orientation and the electron mobility is somewhat higher in the side-by-side orientation.

We also simulate the electron mobility for F8BT using the experimental structure. The computational results show that "alternating structures" decrease the electron mobility of F8BT (but increase the stability of a polymer) which compares relatively well with the experimental value. The calculation also shows that the electron hopping dominates electron transport between the chains. The hopping events along the polymer chain are not important. The electron mobility changes very little with the increasing electric field.

Chapter 8

Summary and Future Work

The main goal of this work is to contribute to the understanding of charge transport in organic conjugated polymers, which will hopefully lead to improved design of organic semiconducting devices such as solar cells.

First, we study the motion of charge species in heterocyclic conjugated polymers as a function of electric field strength. Conducting polymers have an unusual inherent mechanism of electrical conductivity and charge transport along the chains. The charge transfer processes along the chain result in significant local modification of the chain geometry in organic materials and the local geometry modifications of the chain, in turn, markedly affect their electronic structure by inducing localized electronic states in the gap. The formation of inter band states complicates significantly the charge transport phenomena in organic polymers. Hence, the main charge carriers in organic conjugated polymers are solitons, polarons and bipolarons. We employ the extended Su-Schrieffer-Heeger's theoretical model to study the transport property of bipolaron in heterocyclic conjugated polymers. The extended SSH model Hamiltonian includes symmetry-breaking term, e-e interactions and electric field. This model involves the solution of coupled equations which include the time-dependent

Schrödinger equation and the classical motion equation for the lattice displacement which are solved numerically in a self-consistent way. Our numerical simulations indicate that in the absence of an electric field and within the SSH model without the e-e interactions, in heterocyclic conjugated polymers, a bipolaron is more stable than two polarons. The bipolaron (when formed in polymers such as PTs) moves with little change of its shape along the chain backbone in a moderately weak electric field. That is, the charges are localized by the potential energy of the lattice and the main charge carriers are bipolarons (if formed). However, in the presence of a strong electric field, the bipolaron decouples from the lattice potential, that is, the bipolaron dissolves and free charges become the main charge carriers. The same conclusions can be reached from the analysis of the top energy levels and energies such as kinetic energies, lattice potential energies, total energies. Within the extended SSH model, e-e interactions in comparison to e-ph coupling do not significantly affect the nature of bipolaron transport in polymers with weak e-e interactions such as PT.

Second, we concentrate on mobility calculations in organic conjugated polymers employed in devices such as organic solar cells. Organic solar cells are very promising devices that can be used to solve world environment and energy needs in future. The main goal of organic solar cell research is to improve their efficiency. Charge mobility is a very important factor in determining their efficiency. We use multi-step approach to study the mobilities of some promising materials for solar cells. They include fluorene and carbazole derivatives such as PCDTBT, F8BT and so on. The approach includes DFT geometry optimization of short segment of the polymer, calculation of transfer integrals, reorganization energies, transfer rates using Marcus-Hush theory, and simulation of the mobilities with MC method. We obtain mobilities of 1D, 3D ordered and 3D disordered morphological structures. The simulation results point out that the oligomers should be of an appropriate length, that is, they should be

chosen at least the order of fluorene or carbazole trimers. For the carbazole derivatives, 1D simulations of mobilities are adequate to reproduce experimental results provided intermolecular distances between oligomers in, say, π-stacking orientation is known from either X-ray experiments or calculations. 3D ordered and disordered simulations of hole mobilities also agree well with experimental mobility trends for carbazole based polymers. Both transfer integrals and reorganization energies play important roles in charge transfer process, bigger transfer integral and smaller reorganization energy give higher transfer rate and also larger mobility. For fluorene and carbazole oligomers, our study shows that the hole mobility is somewhat higher in the cofacial orientation and the electron mobility is somewhat higher in the side-by-side orientation. For the F8BT material, electron mobility simulation (that uses the experimentally determined crystalline structure) results also agree well with experimental value and charge transport mechanism, that is, electron hopping is dominated by electron transport between the chains and not along the chain (transfer integral along the chain is very small in comparison to transfer integral between chains). The electron mobilities for F8BT increase a little with the increasing electric fields. The relative position of the subunits of repeat unit of polymers is another factor that must be taken into account when calculating mobilities. For example, we find that in F8BT "alternating structures" decrease the mobilities but increase the stability of polymers. The proposed computational approach shows that simulations, based on chemical structure and known morphology of organic semiconductors, produce fairly reliable results, especially when studying the trends in charge mobilities in organic polymers used in devices such as solar cells.

It should be pointed out that, for organic conjugated polymers, there remains many research areas to be further investigated in order to fully understand their charge transport properties and their applications in various devices. In the near

future, we plan to investigate the charge transfers in bulk heterojunction materials since most organic solar cells are made of blended materials. In the current work, we only consider briefly orientationally disordered systems in the mobility simulations. In addition, in the future, we plan to include positional (and energetic) disorder in polymer materials to better illustrate their predominantly amorphous structure. Molecule packing plays a critical role on organic material transport properties. Hence the use of MD simulation should be explored since it could provide valuable information about the structure of the bulk polymer systems. It is also necessary to develop and/or apply more precise methods in the calculations of transfer integrals (see Chapter 6 for discussion) and reorganization energies (e.g., ones that take into account the external contributions in the calculations of reorganization energies). It should also be noted that charge transport in organic solar cells involves other important steps (such as, for example, exciton formation and dissociation) which also needs further investigation.

Bibliography

[1] G. Natta, G. Mazzanti, and P. Corradini, *Stereospecific Polymerization of Acetylene*, Atti. Acad. Naz. Lincei Cl. Sci. Fis. Mat. Nat. Rend., 25 (1958) 3.

[2] M. Hatano, S. Okamaoto and S. Kambara, *Paramagnetic and Electric Properties of Polyacetylene*, J. Polym. Sci. 51 (1961) 26.

[3] C. K. Chiang, C. R. Fincher, Jr, Y. W. Park, A, J. Heeger, H. Shirakawa, E, J. Louis, S. C. Gau and A. G. MacDiarmid, *Electrical Conductivity in Doped Polyacetylene*, Phys. Rev. Lett. 39 (1977) 1098.

[4] H. Naarman, *Synthesis of New Conductive Polymers*, Synth. Met. 17 (1987) 223.

[5] J. H. Burroughs, D. D. C. Bradley, A. R. Brown, R. N. Marks, K. Mackay, R. H. Friend, P. L. Burns and A. B. Holmes. *Light-Emitting Diodes Based on Conjugated Polymers*, Nature 347 (1990) 539.

[6] T. A. Skotheim and J. R. Reynolds (Eds.), *Conjugated Polymers: Theory, Synthesis Properties, and Characterization (Handbook of Conducting Polymers)*, CRC Press, New York (2006).

[7] W. Brütting (Ed.), *Physics of Organic Semiconductors*, Wiley-VCH Verlag, GmbH and Co. KGaA, Weinheim (2005).

[8] A. Dodabalapur, *Organic and Polymer Transistors for Electronics*, Materials Today, 9 (2006) 24

[9] H. Klauk (Ed.), *Organic Electronics*, Wiley-VCH Verlag, GmbH and Co. KGaA, Weinheim (2006).

[10] S. Sun and N. Sariciftci (Eds.), *Organic Photovoltaics* CRC Press, Boca Raton, FL (2004).

[11] J. A. Rogers, Z. Bao, K. Baldwin, A. Dodabalapur, B. Crone, V. R. Raju, V. Kuck, H. Katz, K. Amundson, J. Ewing and P. Drzaic, *Paper-like Electronic Displays: Large-Area Rubber-Stamped Plastic Sheets of Electronics and Microencapsulated Electrophoretic Inks*, Proceedings of the National Academy of Sciences of the United States of America, 98 (2001) 4835.

[12] W. E. Howard, *Better Displays with Organic Films*, Scientific American, 290 (2004) 76.

[13] W. Barford, *Electronic and Optical Properties of Conjugated Polymers*, Oxford University Press Inc., New York (2005).

[14] J. Brédas, D. Beljonne, V. Coropceanu and J. Cornil, *Charge-Transfer and Energy-Transfer Processes in π-Conjugated Oligomers and Polymers: A Molecular Picture*, Chem. Rev. 104 (2004) 4971.

[15] V. Coropceanu, J. Cornil, D. A. da Silva Filho, Y. Olivier, R. Silbey and J. Brédas, *Charge Transport in Organic Semiconductors*, Chem. Rev. 107 (2007) 926.

[16] J. Nelson, J. J. Kwiatkowski, J. Kirkpatrick and J. M. Frost, *Modeling Charge Transport in Organic Photovolaic Materials*, Acc. Chem. Res. 42 (2009) 1768.

[17] N. Karl, *Charge Carrier Transport in Organic Semiconductors*, Synth. Met. 133-134 (2003) 649.

[18] R. G. Kepler, *Charge Carrier Production and Mobility in Anthracene Crystals*, Phys. Rev. 119 (1960) 1226.

[19] N. Karl, in: R. Farchioni and G. Grosso (Eds.), *Organic Electronic Materials*, Spring, Berlin (2001) 283

[20] J. Mort, G. Pfister, in: J. Mort, G. Pfister (Eds.), *Electroni Properties of Polymers*, Wiley, New York (1982) 215.

[21] J. B. Arthur, W. Bardsley, M. A. C. S. Brown and A. F. Gibson, *Carrier Extraction in Germanium*, Proc. Phys. Soc. B 68 (1955) 43

[22] R. Bray, *Minority Carrier Extraction in Germnium*, Phys. Rev. 100 (1955) 1047.

[23] K. Arlauskas, V. Gaidelis, K. Genevicius and G. Juska, *Features of Charge-Carrier Transport in Phthalocyanine Dispersed in Binder Polymer*, Synth. Met. 109 (2000) 101.

[24] G. Juska, K. Arlauskas, R. Österbacka and H. Stubb, *Time-of-Flight Measurements in Thin Films of Regioregular Poly(3-Hexyl Thiophene)*, Synth. Met. 109 (2000) 173.

[25] A. M. van de Craats, J. M. Warman, M. P. de Hass, D. Adam, J. Simerer, D. Haarer and P. Schuhmacher, *The Mobility of Charge Carriers in All Four*

Phases of the Columnar Discotic Material Hexakis(Hexylthio)Triphenylene: Combined TOF and PR-TRMC Results, Adv. Mater. 8 (1996) 823.

[26] G. H. Gelinck and J. M. Warman, *Charge Carrier Dynamics in Pulse-Irradiated Polyphenylenevinylenes: Effects of Broken Conjugation, Temperature, and Accumulated Dose*, J. Phys. Chem. 100 (1996) 20035.

[27] R. J. Hoofman, L. D. Sibbeles, M. P. de Hass, A. Hummel and D. Bloor, *Anisotropy of the Charge-Carrier mobility in Polydiacetylene Crystals*, J. Chem. Phys. 109 (1998) 1885.

[28] M. Pope and C. E. Swenberg, *Electronic Processes in Organic Crystals in Polymers* Oxford University Press, New York (1999).

[29] P. H. Nguyen, G. Paasch, W. Brütting and W. Riess, *Analysis of the DC Conductivity of the Quasi-One-Dimensional Charge-Density-Wave Conductor (Fluoranthene) (2) X*, Phys. Rev. B 49 (1994) 5172.

[30] W. Brütting, P. H. Nguyen, W. Riess and G. Paasch, *DC-Conduction Mechanism and Peierls Gap in Organic and Inorganic Charge-Density-Wave Conductors*, Phys. Rev. B 51 (1995) 9533.

[31] G. Horowitz, R. Hajlaoui, H. Bouchriha, R. Bourguiga and M. Hajlaoui, *The Concept of "Threshold Voltage" in Organic Field-Effect Transistors*, Adv. Mater. 10 (1998) 923.

[32] G. Horowitz, R. Hajlaoui, D. Fichou and A. El Kassmi, *Gate Voltage Dependent Mobility of Oligothiophene Field-Effect Transistors*, J. Appl. Phys. 85 (1999) 3202.

[33] S. Tiwari and N. C. Greenham, *Charge Mobility Measurement Techniques in Organic Semiconductors*, Opt. Quant. Electron 41 (2009) 69.

[34] N. Karl, K. -H. Kraft and J. Marktanner, *Charge Carrier Mobilities in Dark-Conductive Organic Thin Films Determined by the Surface Acoustoelectric Travelling Wave (SAW) Technique*, Synth. Met. 109 (2000) 181.

[35] M. Côte, private communication.

[36] L. Yu, *Solitons and Polarons in Conducting Polymers*, World Scientific Publishing Co Pte Ltd., Singapore (1988).

[37] W. P. Su, J. R. Schriefer and A. J. Heeger, *Solitons in Polyacetylene*, Phys. Rev. Lett. 42 (1979) 1698.

[38] W. P. Su, J. R. Schriefer and A. J. Heeger, *Soliton Excitations in Polyacetylene*, Phys. Rev. B 22 (1980) 2099.

[39] Y. Shimoi and S. Abe, *Competition between Polarons and Bipolarons in Non-degerate Conjugated Polymers*, Phys. Rev. B 50 (1994) 14781.

[40] Denis Fichou (Ed.) *Handbook of Oligo- and Polythiophenes*, Wiley-VCH, New York (1999).

[41] A. J. Heeger, S. Kivelson, J. R. Schrieffer and W. P. Su, *Solitons in Conducting Polymers*, Rev. Mod. Phys. 60 (1988) 781.

[42] S. A. Brazovskii and N. N. Kirova, *Excitons, Polarons, and Bipoalrons in Conducting Polymers*, JETP Letters 33 (1981) 4.

[43] D. Bertho and C. Jouanin, *Polaron and Bipolaron Excitations in Doped Polythiopene*, Phys. Rev. B 35 (1987) 626.

[44] A. Saxena and J. D. Gunton, *Theory of Bipolaron Lattices in Quasi-One-Dimenstional Conducting Polymers*, Phys. Rev. B 35 (1987) 3914.

[45] S. Stafström and J. L. Bredas, *Evolution of the Electronic-Structure of Polyacetylene and Polythiphene as a function of Doping Level and Lattice Conformation*, Phys. Rev. B 38 (1988) 4180.

[46] S. Xie and L. Mei, *Transition beteen Bipolaron and Polaron States in Doped Heterocycle Polymers*, Phys. Rev. B 50 (1994) 13364.

[47] D. Giri and K. Kundu, *Theoretical Study of the Evolution of Electronic Band Structure of Polythiophene due to Bipolaron Doping*, Phys. Rev. B 53 (1996) 4340.

[48] K. Kundu and D. Giri, *Evolution of the Electronic Structure of Cyclic Polythiophene upon Bipolaron Doping*, J. Chem. Phys. 105 (1996) 11075.

[49] G. M. e Silva, *Electric-Field Effects on the Competition between Polarons and Bipolarons in Conjugated Polymers*, Phys. Rev. B 61 (2000) 10777.

[50] D. Liu, L. Wang, S. Xie, S. Han, and L. Mei, *Polaron Tunneling in Copolymers under External Electric Fields*, Opt. Mat. 23 (2003) 479.

[51] L. Wang, D. Liu and S. Xie, *Energy Evolution of Polaron in Poly (P-Phenylene) in the Presence of High Electric Field*, Synth. Met. 135-136 (2003) 501.

[52] L. Wang, D. Liu, S. Xie, S. Han and L. Mei, *Energy Evolution of Bipolaron in Phenylene Ring Polymer under High Electric Field*, Opt. Mat. 23 (2003) 485.

[53] H. Bässler, *Charge Transport in Disordered Organic Photoconductors - A Monte Carlo Simulation Study*, Phys. Stat. Sol. B, 175 (1993) 15.

[54] S.V. Novikov, D. H. Dunlap, V. M. Kenkre, P. E. Parris and A. V. Vannikov, *Essential Role of Correlations in Governing Charge Transport in Disordered Organic Materials*, Phys. Rev. Lett. 81 (1998) 4472.

[55] Z. G. Yu, D. L. Smith, A. Saxena, R. L. Martin and A. R. Bishop, *Molecular Geometry Fluctuaton Model for the Mobility of Conjugated Polymers*, Phys. Rev. Lett. 84 (2000) 721.

[56] S. Athanasopoulos, J. Kirkpatrick, D. Martinez, J. Frost, C. M. Foden, A. B. Walker, and J. Nelson, *Predictive Study of Charge Transport in Disordered Semiconducting Polymers*, Nano. Lett. 7 (2007) 1785.

[57] K. Sakanoue, M. Motoda, M. Sugimoto, and S. Sakaki, *A Molecular Orbital Study on the Hole Transport Property of Organic Amine Compounds*, J. Phys. Chem. A 103 (1999) 5551.

[58] J. Kirkpatrick, *An Approximate Method for Calculating Transfer Integrals Based on the ZINDO Hamiltonian*, Int. J. Quant. Chem. 108 (2008) 51.

[59] J. J. Kwiatkowski, J. Nelson, H. Li, J. L. Brédas, W. Wenzel and C. Lennartz, *Simulating Charge Transport in Tris (8-Hydroxyquinoline) Aluminniu (Alq3)*, Phys. Chem. Chem. Phys. 10 (2008) 1852.

[60] J. Kirkpatrick, V. Marcon, J. Nelson, K. Kremer and D. Andrienko, *Charge Mobility of Discotic Mesophases: A Multiscale Quantum and Classical Study*, Phys. Rev. Lett. 98 (2007) 227402.

[61] A. J. Chatten, A. M. Ballantne, J. M. Frost, Y. Astuti, J. R. Durrant and J. Nelson, 22nd Eur. Photovoltaic Sol. Energy Conf. 40 (2007) 1393.

[62] J. J. Kwiatkowski, J. M. Frost, and J. Nelson, *The Effect of Morphology on Electron Field-Effect Mobility in Disordered C60 Thin Films*, Nano Lett. 9 (2009) 1085.

[63] J. L. Bredas, J. Cornil, F. Meyers, D. Beljonne, in: T. A. Skotheim, R. L. Elesenbaumer, J. R. Reynolds (Eds.), *Handbook of Conducting Polymers*, Marcel Dekker Inc., New York (1998).

[64] H. Takayama, Y. R. Lin-Liu, and K. Maki, *Continuum Model for Solitons in Polyacetylene*, Phys.Rev. B 21 (1980) 2388.

[65] J. Bernasconi and T. Schneider (Eds.), A. J. Heeger and A. G. MacDiarmid, *Physics in One Dimension: Proceedings of an International Conference, Fribourg, Switzerland, August 25-29, 1980*, Springer-Verlag, New York (1981).

[66] E. J. Mele, *Transient Structural Response to Photoexcitation in Polyacetylene*, Phys. Rev. B 26 (1982) 6901.

[67] D. K. Campbell and A. R. Bishop, *Soliton Excitations in Polyacetylene and Relativistic Field Theory Models*, Nucl. Phys. B 200 (1982) 297.

[68] A. J. Epstein, H. Rommelmann, R. Bigelow, H. W. Gibson, D. M. Hoffmann, and D. B. Tanner, *Role of Solitons in Nearly Metallic Polyacetylene*, Phys. Rev. Lett. 50 (1983) 1866.

[69] M. P. Lima and G. M. e Silva, *Dynamical Evolution of Polaron to Bipolaron in Conjugated Polymers*, Phys. Rev. B 74 (2006) 224304.

[70] J. L. Brédas, B. Thémans, J. G. Fripiat, J. M. André and R. R. Chance, *Highly Conducting Polyparaphenylene, Polypyrrole, and Polythiophene Chains: An ab*

initio Study of the Geometry and Electronic-Structure Modifications upon Doping, Phys. Rev. B 29 (1984) 6761.

[71] T. C. Chung, J. H. Kaufman, A. J. Heeger and F. Wudl, *Charge Storage in Doped Poly(thiophene): Optical and Electrochemical Studies*, Phys. Rev. B 30 (1984) 702.

[72] C. H. Evans and J. C. Scaiano, *Photochemical Generation of Radical Cations from .alpha.-terthienyl and Related Thiophenes: Kinetic Behavior and Magnetic Field Effects on Radical-Ion Pairs in Micellar Solution*, J. Am. Chem. Soc. 112 (1990) 2694.

[73] J. V. Caspar, V. Ramamurthy and D. R. Corbin, *Modification of Photochemical Reactivity by Zeolites. Preparation and Spectroscopic Characterization of Polarons and Bipolarons of Thiophene Oligomers within the Channels of Pentasil Zeolites: the Evolution of Organic Radical Ions into Conducting Polymers*, J. Am. Chem. Soc. 113 (1991) 600.

[74] D. Fichou, B. Xu, G. Horowitz, and F. Garnier, *Generation of Stabilized Polarons and Bipolarons on Extended Model Thiophene Oligomers*, Synth. Met. 41 (1991) 463.

[75] T. Bally, K. Roth, W. Tang, R. R. Schrock, K. Knoll, and L. Y. Park, *Stable Polarons in Polyacetylene Oligomers: Optical Spectra of Long Polyene Radical Cations*, J. Am. Chem. Soc. 114 (1992) 2440.

[76] M. G. Hill, K. R. Mann, L. L. Miller, and J.-F. Penneau, *Oligothiophene Cation Radical Dimers. An Alternative To Bipolarons In Oxidized Polythiophene*, J. Am. Chem. Soc. 114 (1992) 2728.

[77] M. G. Hill, J.-F. Penneau, B. Zinger, K. R. Mann, and L. L. Miller, *Oligothiophene Cation Radicals - Pi-Dimers as Alternatives to Bipolarons in Oxidized Polythiophenes*, Chem. Mater. 4 (1992) 1106.

[78] P. Baeuerle, U. Segelbacher, A. Maier, and M. Mehring, *Electronic Structure of Mono- and Dimeric Cation Radicals in End-Capped Oligothiophenes*, J. Am. Chem. Soc. 115 (1993) 10217.

[79] V. Wintgens, P. Valat, and F. Garnier, *Photochemical Generation of Radical Cations from Thiophene Oligomers*, J. Phys. Chem. 98 (1994) 228.

[80] Y. Furukawa, *Reexamination of the Assignments of Electronic Absorption Bands of Polarons and Bipolarons in Conducting Polymers* , Synth. Met. 69 (1995) 629.

[81] J. A. E. H. van Haare, E. E. Havinga, J. L. J. van Dongen, R. A. J. Janssen, J. Cornil, and J. L. Brédas, *Redox States of Long Oligothiophenes: Two Polarons on a Single Chain*, Chem. Europ. J. 4 (1998) 1509.

[82] P. Vogl and C. K. Campbell, *Three-Dimensional Structure and Intrinsic Defects in Trans-Polyacetylene*, Phys. Rev. Lett. 62 (1989) 2012.

[83] P. Vogl and C. K. Campbell, *First-Principles Calculations Of The Three-Dimensional Structure And Intrinsic Defects In Trans-Polyacetylene* , Phys. Rev. B 41 (1990) 12797.

[84] A. J. W. Tol, *The Instability of a Bipolaron versus Two Polarons: Charge Localization in Cyclo-Dodecathiophene*, Synth. Met. 74 (1995) 95.

[85] A. J. W. Tol, *The Electronic and Geometric Structure of Dications of Oligo-Thiophenes*, Chem. Phys. 208 (1996) 73.

[86] G. Brocks, *Polarons and Bipolarons in Oligothiophenes: A First Principles Study*, Synth. Met. 102 (1999) 914.

[87] G. Brocks, *π-Dimers of Oligothiophene Cations*, J. Chem. Phys. 112 (2000) 5353.

[88] G. Moro, G. Scalmani, U. Cosentino, and D. Pitea, *On The Structure Of Polaronic Defects In Thiophene Oligomers: A Combined Hartree-Fock And Density Functional Theory Study*, Synth. Met. 108 (2000) 165.

[89] F. C. Grozema, P. T. van Duijnen, L. D. Siebbeles, A. Goossens, and S. W. Leeuw, *Electronic Structure of Thienylene Vinylene Oligomers: Singlet Excited States, Triplet Excited States, Cations, and Dications*, J. Phys. Chem. B 108 (2004) 16139.

[90] D. A. Scherlis and N. Marzari, *π-Stacking in Charged Thiophene Oligomers*, J. Phys. Chem. B 108 (2004) 17791.

[91] S. S. Zade and M. J. Bendikov, *Theoretical Study of Long Oligothiophene Dications: Bipolaron vs Polaron Pair vs Triplet State*, J. Phys. Chem. B 110 (2006) 15839.

[92] U. Salzner, *Investigation of Charge Carriers in Doped Thiophene Oligomers through Theoretical Modeling of their UV/Vis Spectra*, J. Phys. Chem. A 112 (2008) 5458.

[93] N.S. Sariciftci (Ed.), *Primary Photoexcitations in Conjugated Polymers: Molecular Exciton versus Semiconductor Band Model*, World Scientific Publishing Co. Pte. Ltd., Singapore (1997).

[94] P. A. Lane, X. Wei and Z. V. Vardeny, *Studies of Charged Excitations in π-Conjugated Oligomers and Polymers by Optical Modulation*, Phys. Rev. Lett. 77 (1996) 1544.

[95] G. Zotti, S. Zecchin, B. Vercelli, A. Berlin, S. Grimoldi, M. C. Pasini and M. M. M. Raposo, *Electrochemical, Magnetic, and Electrical Properties of α,ω-Capped Sexithiophene Films. 1. Neutral-Polaron and Polaron-Bipolaron Conductivities*, Chem. Mater. 17 (2005) 6492.

[96] Z. Xie, Y.-M. Kang, Z. An and Y.-C. Li, *Two-Dimensional Localized Vibrational Modes of Polythiophene around A Bipolaron*, Phys. Rev. B 61 (2000) 1096.

[97] S. Brazovskii, N. Kirova, Z. G. Yu, A. R. Bishop and A. Saxena, *Stability of Bipolarons in Conjugated Polymers* , Opt. Mater. 9 (1998) 502.

[98] A. Saxena, S. Brazovskii, N. Kirova, Z. G. Yu, and A. R. Bishop, *Stability of Bipolarons in Conjugated Polymers*, Synth. Met. 101 (1999) 325.

[99] K. Fuks-Janczarek, I. V. Kityk, R. Miedzinski, E. Gondek, A. Dannel, M. Zagorska, Spectrochim, Acta Part A 64 (2006) 264.

[100] Y. Ono and A. Terai, *Motion of Charged Soliton in Polyacetylene Due to Electric Field*, J. Phys. Soc. Jpn. 59 (1990) 2893.

[101] A. Terai and Y. Ono, *Electric Field Induced Depinning of a Charged Soliton from an Impurity Center in Polyacetylene*, J. Phys. Soc. Jpn. 60 (1991) 196.

[102] S. V. Rakhmanova and E. M. Conwell, *Polaron Dissociation in Conducting Polymers by High Electric Fields*, Appl. Phys. Lett. 75 (1999) 1518.

[103] S. V. Rakhmanova and E. M. Conwell, *Nonlinear Dynamics of An Added Carrier in Trans-Polyacetylene in the Presence of An Electric Field* , Synth. Met. 110 (2000) 37.

[104] C. S. Pinheiro and G. M. Silva, *Use of Polarons and Bipolarons in Logical Switches Based on Conjugated Polymers*, Phys. Rev. B 65 (2002) 094304.

[105] A. A. Johansson and S. Stafström, *Nonadiabatic Simulations of Polaron Dynamics*, Phys. Rev. B 69 (2004) 235205.

[106] X. Liu, K. Gao, J. Fu, Y. Li, J. Wei and S. Xie, *Effect of the Electric Field Mode on the Dynamic Process of a Polaron*, Phys. Rev. B 74 (2006) 172301.

[107] H. Chayet, R. Pogreb, and D. Davidov, *Transient UV Electroluminescence from Poly(P-Phenylenevinylene) Conjugated Polymer Induced by Strong Voltage Pulses*, Phys. Rev. B 56 (1997) R12702.

[108] M. Zoli, *Phonon Thermodynamics versus Electron-Phonon Models*, Phys. Rev. B 70 (2004) 184301.

[109] M. Zoli, *Thermodynamics of A Continuum SuSchriefferHeeger Model* , Phys. B: Condesed Matter 344 (2004) 372.

[110] M. Zoli, *Path Integral Computation of Phonon Anharmonicity*, The Eur. Phys. J. B 40 (2004) 79.

[111] Y. Li and J. B. Lagowski, *Electric Field Effects on Bipolaron Transport in Heterocyclic Conjugated Polymers with Application to Polythiophene*, Opt. Mater. 32 (2010) 1177.

[112] Y. Ono, Y. Ohfuti and A. Terai, *Fractionally Charged States in One-Dimensional Electron-Phonon Systems with Commensurability 3*, J. Phys. Soc. Jpn. 54 (1985) 2641.

[113] J. L. Brédas and G. B. Street, *Polarons, Bipolarons, and Solitons in Conducting Polymers*, Acc. Chem. Res. 18 (1985) 309.

[114] M. Kuwabara, Y. Ono. and A. Terai, *Motion of Charged Soliton in Polyacetylene Due to Electric Field. II. Behavior of Width*, J. Phys. Soc. Jpn. 60 (1991) 1286.

[115] A. Terai and Y. Ono, *Phonons around A Soliton and A Polaron in Su-Schriffer-Heeger's Model of trans-(CH)x*, J. Phys. Soc. Jpn. 55 (1986) 213.

[116] G. S. Kanner, X. Wei, B. C. Hess, L. R. Chen and Z. V. Vardeny, *Evolution of Excitons and Polarons in Polythiophene from Femtoseconds to Milliseconds*, Phys. Rev. Lett. 69 (1992) 538.

[117] http://www.azonano.com/Details.asp?ArticleID=1972

[118] R. Gaudiana, R. Echert, J. Cardone, J. Ryan and A. Montello, *Photovoltaic Fibers*, Proc. SPIE 6334 (2006) U6-U9.

[119] E. Bundgaard and F. C. Krebs, *Low Band Gap Polymers for Organic Photovoltaics*, Solar Energy Materials and Solar Cells 91 (2007) 954.

[120] S. Park, A. Roy, S. Beaupre, S. Cho, N. Coates, J. Moon, D. Moses, M. Leclerc, K. Lee and A. Heeger, *Bulk Heterojunction Solar Cells with Internal Quantum Efficiency Approaching 100%*, Nature Photonics 3 (2009) 297.

[121] Y. Liang, D. Feng, Y. Wu, S.-T. Tsai, G. Li, C. Ray, and L. Yu, *Highly Efficient Solar Cell Polymers Developed via Fine-Tuning of Structural and Electronic Properties*, J. Am. Chem. Soc. 131 (2009) 7792.

[122] Y. Liang, Z. Xu, J. Xia, S.-T. Tsai, Y. Wu, G. Li, C. Ray, and L. Yu, *For the Bright Future-Bulk Heterojunction Polymer Solar Cells with Power Conversion Efficiency of 7.4%*, Adv. Mater. 22 (2010) E135.

[123] S. Gunes, H. Neugebauer, and N.S. Sariciftci, *Conjugated Polymer-Based Organic Solar Cells*, Chem. Rev. 107 (2007) 1324.

[124] G. Dennler, M. C. Scharber, and C. J. Brabec, *Polymer-Fullerene Bulk-Heterojunction Solar Cells*, Adv. Mater. 21 (2009) 1323.

[125] J.-L. Bredas and J. R. Durrant (Guest Eds.) Organic Photovoltaics, *Organic Photovoltaics*, Acc. Chem. Res. 42 (2009) 1689-1857.

[126] N. Blouin, A. Michaud, and M. Leclerc, *A Low-Bandgap Poly(2,7-Carbazole) Derivative for Use in High-Performance Solar Cells*, Adv. Mater. 19 (2007) 2295.

[127] R. Kroon, M. Lenes, J. C. Hummelen, P. W. M. Blom, and B. de Boer, *Small Bandgap Polymers for Organic Solar Cells (Polymer Material Development in the Last 5 Years)*, Polym. Rev. 48 (2008) 531.

[128] N. Blouin, A. Michaud, D. Gendron, S. Wakim, E. Blair, R. Neagu-Plesu, M. Belletete, G. Durocher, Y. Tao, and M. Leclerc, *Toward a Rational Design of Poly(2,7-Carbazole) Derivatives for Solar Cells*, J. Am. Chem. Soc. 130 (2008) 732.

[129] Y. Zou, D. Gendron, R. Badrou-Aich, A. Najari, Y. Tao, and M. Leclerc, *A High-Mobility Low-Bandgap Poly(2,7-carbazole) Derivative for Photovoltaic Applications*, Macromolecules 42 (2009) 2891.

[130] M. D. Irwin, D. B. Buchholz, A. W. Hains, R. P. H. Chang, and T. J. Marks, *P-Type Semiconducting Nickel Oxide as An Efficiency-Enhancing Anode Interfacial Layer in Polymer Bulk-Heterojunction Solar cells*, Proc. Natl. Acad. Sci. USA 105 (2008) 2783.

[131] S. E. Shaheen, C. J. Brabec. N. S. Sariciftci, F. Padinger, T. Fromherz, and J. C. Hummelen, *2.5% Efficient Organic Plastic Solar Cells*, Appl. Phys. Lett. 78 (2001) 841.

[132] J. Hou, Z. Tan, Y. Yan, Y. He, C. Yang, and Y. Li, *Synthesis and Photovoltaic Properties of Two-Dimensional Conjugated Polythiophenes with Bi(thienylenevinylene) Side Chains*, J. Am. Chem. Soc. 128 (2006) 4911.

[133] D. Muhlbacher, M. Scharber, M. Morana, Z. Zhu, D. Waller, R. Gaudiana, and C. Brabec, *High Photovoltaic Performance of A Low-Bandgap Polymer*, Adv. Mater. 18 (2006) 2884.

[134] M. Zhang, H. N. Tsao, W. Pisula, C. Yang, A. K. Mishra, and K. Mullen, *Field-Effect Transistors Based on A Benzothiadiazole-Cyclopentadithiophene Copolymer*, J. Am. Chem. Soc. 129 (2007) 3472.

[135] J. Peet, J. Y. Kim, N. E. Coates, W. L. Ma, D. Moses, A. J. Heeger, and G. C. Bazan, *Efficiency Enhancement in Low-Bandgap Polymer Solar Cells by Processing with Alkane Dithiols*, Nat. Mater. 6 (2007) 497.

[136] N. Leclerc, A. Michaud, K. Sirois, J.-F. Morin, and M. Leclerc, *Synthesis of 2,7-Carbazolenevinylene-Based Copolymers and Characterization of Their Photovoltaic Properties*, Adv. Funct. Mater. 16 (2006) 1694.

[137] C. L. Donley, J. Zaumseil, J. W. Andreasen, M. M. Nielsen, H. Sirringhaus, R. H. Friend and J. S. Kim, *Effects of Packing Structure on the Opto-electronic and Charge Transport Properties in Poly(9,9-di-n-octylfluorene-alt-benzothiadiazole)*, J. Am. Chem. Soc. 127 (2005) 12890.

[138] R. A. Marcus, *Electron Transfer Reactions in Chemistry. Theory and Experiment*, Rev. Mod. Phys. 65 (1993) 599.

[139] Y. Li and J. B. Lagowski, *Charge Carrier Mobility in Conjugated Organic Polymers - Case Studies Using Multi-Step Computational Approach*, (2011) submitted for publication.

[140] Gaussian 03, Revision B.05, M. J. Frisch, G. W. Trucks, H. B. Schlegel, G. E. Scuseria, M. A. Robb, J. R. Cheeseman, J. A. Montgomery, Jr., T. Vreven, K. N. Kudin, J. C. Burant, J. M. Millam, S. S. Iyengar, J. Tomasi, V. Barone, B. Mennucci, M. Cossi, G. Scalmani, N. Rega, G. A. Petersson, H. Nakatsuji, M. Hada, M. Ehara, K. Toyota, R. Fukuda, J. Hasegawa, M. Ishida, T. Nakajima, Y. Honda, O. Kitao, H. Nakai, M. Klene, X. Li, J. E. Knox, H. P. Hratchian, J. B. Cross, C. Adamo, J. Jaramillo, R. Gomperts, R. E. Stratmann, O. Yazyev, A. J. Austin, R. Cammi, C. Pomelli, J. W. Ochterski, P. Y. Ayala, K. Morokuma, G. A. Voth, P. Salvador, J. J. Dannenberg, V. G. Zakrzewski, S. Dapprich, A. D. Daniels, M. C. Strain, O. Farkas, D. K. Malick, A. D. Rabuck, K. Raghavachari, J. B. Foresman, J. V. Ortiz, Q. Cui, A. G. Baboul, S. Clifford, J. Cioslowski, B. B. Stefanov, G. Liu, A. Liashenko, P. Piskorz, I. Komaromi, R. L. Martin, D. J. Fox, T. Keith, M. A. Al-Laham, C. Y. Peng, A. Nanayakkara, M. Challacombe, P. M. W. Gill, B. Johnson, W. Chen, M. W. Wong, C. Gonzalez, and J. A. Pople, Gaussian, Inc., Pittsburgh PA, 2003.

[141] M. Belletete, G. Durocher, S. Hamel, M. Cote, S. Wakim, and M. Leclerc, *A First Principles Calculations and Experimental Study of the Ground- and Excited-State Properties of Ladder Oligo(p-aniline)s*, J. Chem. Phys. 122 (2005) 104303.

[142] C. J. Calzado, J.-P. Malrieu, and J. F. Sanz, *Physical Factors Governing the Amplitude of the Electron Transfer Integral in Mixed-Valence Compounds*, J. Phys. Chem. A. 102 (1998) 3659.

[143] J. L. Brédas, J. P. Calbert, D. A. da Silva Filho, and J. Cornil, *Organic Semiconductors: A Theoretical Characterization of the Basic Parameters Governing Charge Transport* , Proc. Natl. Acad. Sci. USA 99 (2002) 5804.

[144] S. Fratiloiu, F. C. Grozema, Y. Koizumi, S. Seki, A. Saeki, S. Tagawa, S. P. Dudek, and L. D. A. Siebbeles, *Electronic Structure and Optical Properties of Charged Oligofluorenes Studied by VIS/NIR Spectroscopy and Time-Dependent Density Functional Theory*, J. Phys. Chem. B 110 (2006) 5984.

[145] J. Huang and M. Kertesz, *Validation of Intermolecular Transfer Integral and Bandwidth Calculations for Organic Molecular M aterials*, J. Chem. Phys. 122 (2005) 234707.

[146] E. F. Valeev, V. Coropceanu, D. A. da Silva Filho, S. Salman, and J. L. Bredas, *Effect of Electronic Polarization on Charge-Transport Parameters in Molecular Organic Semiconductors*, J. Am. Chem. Soc. 128 (2006) 9882.

[147] A. Troisi and G. Orlandi, *Dynamics of the Intermolecular Transfer Integral in Crystalline Organic Semiconductors*, J. Phys. Chem. A 110 (2006) 4065.

[148] V. Coropceanu, R. S. Sanchez-Carrera, P. Paramonov, G. M. Day, and J. L. Bredas, *Interaction of Charge Carriers with Lattice Vibrations in Organic Molecular Semiconductors: Naphthalene as a Case Study*, J. Phys. Chem. C 113 (2009) 4679.

[149] D. Reha, W. Barford, and S. Harris, *A Multi-Scale Method for the Calculation of Charge Transfer Rates through the π-Stack of DNA: Application to DNA Dynamics*, Phys. Chem. Chem. Phys. 10 (2008) 5436.

[150] A. Szabo and N.S. Ostlund, *Modern Quantum Chemistry: Introduction to the Advanced Electronic Structure Theory*, Dover, Mineola, New York (1996), Chapter 2.3.3.

[151] K. Pearson, *On Lines and Planes of Closest Fit to Systems of Points in Space*, Philosophical Magazine 2 (1901) 559.

[152] V. Schomaker, J. Wasser, R.E. Marsh, and G. Bergman, *To Fit a Plane or a Line to a Set of Points by Least Squares*, Acta Cryst. 12 (1959) 600.

[153] D. M. Blow, *To Fit a Plane to a Set of Points by Least Sqaures*, Acta Cryst. 13 (1960) 168.

[154] M. Hazenwinkel (Ed.), *Spectral Theory of Linear Operators*, Encyclopaedia of Mathematics, Springer (2001); S. Axler, *Linear Algebra Done Right*, Springer Verlag (1997).

[155] M. Malagoli and J. L. Bredas, *Density Functional Theory Study of the Geometric Structure and Energetics of Triphenylamine-Based Hole-Transporting Molecules*, Chem. Phys. Lett. 327 (2000) 13.

[156] J. C. Sancho-Garcia and A. J. Perez-Jimenez, *Dependence of Charge-Transport Parameters on Static Correlation and Self-Interaction Energy: The Case of a 1,4-Bis(Phenylethynyl)Benzene Derivative Conjugated Molecule*, J. Phys. Chem. A 112 (2008) 10325.

[157] R. Y. Rubinstein and D. P. Kroese, *Simulation and the Monte Carlo Method (2nd ed.)*, John Wiley & Sons, New York (2007); N. Metropolis and S. Ulam, *The Monte Carlo Method*, J. Am. Stat. Assoc. 44 (1949) 335.

[158] P. Prins, F. C. Grozema, J. M. Schins, S. Patil, U. Scherf, and L. D. A. Siebbeles, *High Intrachain Hole Mobility on Molecular Wires of Ladder-Type Poly(p-Phenylenes)*, Phys. Rev. Lett. 96 (2006) 146601.

[159] S. H. Chen, A. C. Su, C. H. Su, and S. A. Chen, *Crystalline Forms and Emission Behavior of Poly(9,9-di-n-octyl-2,7-fluorene)*, Macromolecules 38 (2005) 379.

[160] S. H. Chen, A. C. Su, and S. A. Chen, *Noncrystalline Phases in Poly(9,9-di-n-octyl-2,7-fluorene)*, J. Phys. Chem. B 109 (2005) 10067.

[161] M. Grell, D. D. C. Bradley, G. Ungar, J. Hill, and K.S. Whitehead, *Interplay of Physical Structure and Photophysics for A Liquid Crystalline Polyfluorene*, Macromolecules 32 (1999) 5810.

[162] M. Surin, E. Hennebicq, C. Ego, D. Marsitzky, A. C. Grimsdale, K. Mullen, J.-L. Bredas, R. Lazzaroni, and P. Leclere, *Correlation between the Microscopic Morphology and the Solid-State Photoluminescence Properties in Fluorene-Based Polymers and Copolymers*, Chem. Mater. 16 (2004) 994.

[163] M. Surin, P. Sonar, A. C. Grimsdale, K. Mullen, R. Lazzaroni, and P. Leclere, *Supramolecular Organization in Fluorene/Indenofluorene Oligothiophene Alternating Conjugated Copolymers*, Adv. Funct. Mater. 15 (2005) 1426.

[164] J.-F. Morin, M. Leclerc, D. Ades, and A. Siove, *Polycarbazoles: 25 Years of Progress*, Macromol. Rapid Commun. 26 (2005) 761.

[165] T. Kreouzis, D. Poplavskyy, S. M. Tuladhar, M. Campoy-Quiles, J. Nelson, A. J. Campbell, and D. D. C. Bredley, *Temperature and Field Dependence of Hole Mobility in Poly(9,9-Dioctylfluorene)*, Phys. Rev. B 73 (2006) 235201.

[166] Y. Olivier, V. Lemaur, J. L. Bredas, and J. Cornil, *Charge Hopping in Organic Semiconductors: Influence of Molecular Parameters on Macroscopic Mobilities in Model One-Dimensional Stacks*, J. Phys. Chem. A 110 (2006) 6356.

[167] S. C. Tse, S. K. So, M.Y. Yeung, C. F. Lo, S. W. Wen, and C. H. Chen, *The Role of Charge-Transfer Integral in Determining and Engineering the Carrier Mobilities of 9,10-di(2-Naphthyl)Anthracene Compounds*, Chem. Phys. Let. 422 (2006) 354.

[168] A. J. Campbell, D. D. C. Bradley and H. Antoniadis, *Dispersive Electron Transport in An electroluminescent Polyfluorene Copolymer Measured by the Current Integration Time-of-Flight Method*, Appl. Phys. Lett. 79 (2001) 2133.

[169] J. J. M. Halls, A. C. Arias, J. D. MacKenzie, W. Wu, M. Inbasekaran, W. P. Woo, R. H. Friend, *Photodiodes Based on Polyfluorene Composites: Influence of Morphology*, Adv. Mater. 12 (2000) 498.

[170] A. C. Morteani, A. S. Dhoot, J. S. Kim, C. Silva, N. C. Greenham, C. Murphy, E. Moons, S. Cina, J. H. Burroughes, R. H. Friend, *Barrier-Free ElectronHole*

Capture in Polymer Blend Heterojunction Light-Emitting Diodes, Adv. Mater. 15 (2003) 1708.

[171] W. Pisula, M. Zorn, J. Chang, K. Mullen, and R. Zentel, *Liquid Crystalline Ordering and Charge Transport in Semiconducting Materials*, Macromol. Rapid Commun. 30 (2009) 1179.